THE FRIES FAULT NEAR RINER, VIRGINIA:
AN EXAMPLE OF A POLYDEFORMED, DUCTILE DEFORMATION ZONE

by

Patti Boyd Kaygi

Thesis submitted to the Graduate Faculty of the

Virginia Polytechnic Institute and State University

in partial fulfillment of the requirements for the degree of

MASTER OF SCIENCE

in

Geological Sciences

APPROVED:

Dr. D. R. Gray, Co-Chairman

Dr. Lynn Glover III, Co-Chairman

Dr. D. A. Hewitt

Dr. R. K. Bambach

May 1979

Blacksburg, Virginia

ACKNOWLEDGMENTS

The author wishes to acknowledge Dr. David Gray and Dr. Lynn Glover, III, co-chairmen, for their constant encouragement and help throughout the study. Appreciation also is expressed to Dr. Mervin J. Bartholomew for many fruitful discussions and to Drs. D. A. Hewitt and R. K. Bambach for critical reading of the preliminary draft.

Financial support was provided through a teaching assistantship from Virginia Polytechnic Institute and State University and Nuclear Regulatory Commission Contract No. to Dr. Lynn Glover, III. Thanks go to , and for drafting of figures and geologic map.

Very special appreciation is extended to or all photographic work and for assistance in the field, as well as encouragement throughout the duration of this study.

For their continual inspiration and moral support the author endearingly thanks her parents.

Finally, to ., thank you for your extreme tolerance during the latter months of this study and for bringing added joy to its completion.

TABLE OF CONTENTS

LIST OF ILLUSTRATIONS

I. Introduction

Mylonites, i.e., rocks that have undergone ductile deformation, have been examined from numerous fault zones around the world (Christie, 1960; Eisbacher, 1970; Stirewalt and Dunn, 1973; Bak, et al, 1975; Jain, 1975; Bell and Etheridge, 1976; Wakefield, 1977; and Mitra, 1978), and, yet, controversial questions still exist as to the nature of the processes involved in their development. These include:

1. Type of operative strain (i.e., shearing vs. flattening),
2. The degree of interaction of chemical and mechanical processes, and
3. The nature of grain-scale deformation mechanisms.

This study analyzes a portion of the Fries Fault Zone in southwestern Virginia with the aim of providing a better understanding of ductile processes, the associated strain, and the operative deformation mechanisms. The Fries Fault represents a major tectonic discontinuity and is possibly one of the most extensive in the central and southern Appalachians, as it extends from northern Virginia to North Carolina, and possibly Alabama (Rankin, 1975; Hatcher, 1978; Bartholomew, in press). Associated with the fault in the study area is an extensive mylonite zone up to 2.5 km in width that provides excellent opportunities for the study of mylonitic fabrics and their development. This zone of deformation is comparable to some of the largest in the world, such as the Moine and the Brevard. However, detailed studies of this fault and its associated fault rocks are virtually lacking.

Both crystalline basement and overlying metasedimentary rocks are

involved in the deformation, each having responded differently to the imposed stresses. The basement rocks exhibit progressive stages of mylonitization, while the metasedimentary rocks show features characteristic of a regional deformation and metamorphic event, although much more intense in their development. Although the entire fault zone underwent ductile deformation, on the microscopic scale both ductile and brittle behavior is recognized. Shearing strain was dominant initially followed by late stage flattening.

Located just one mile from the Blue Ridge structural front, the Fries also provides a link in present studies that will eventually correlate deformational histories across the Valley and Ridge - Blue Ridge transitional zone. Thus, detailed structural analyses of this segment of the Fries and adjacent Blue Ridge rocks are critical to an understanding of regional Appalachian tectonics and especially the possible concurrent involvement of Valley and Ridge and Blue Ridge rocks.

The study herein involves characterization of this fault zone and adjacent rocks within the study area which is located in the southern part of Montgomery County and northern part of Floyd County, southwestern Virginia (Fig. 1). The objectives are threefold:

1. To establish the deformational and metamorphic history of the fault zone and adjacent rocks,
2. To determine which deformation mechanisms were responsible for the development of mylonitic fabrics, and
3. To determine, qualitatively, the degree of interaction of

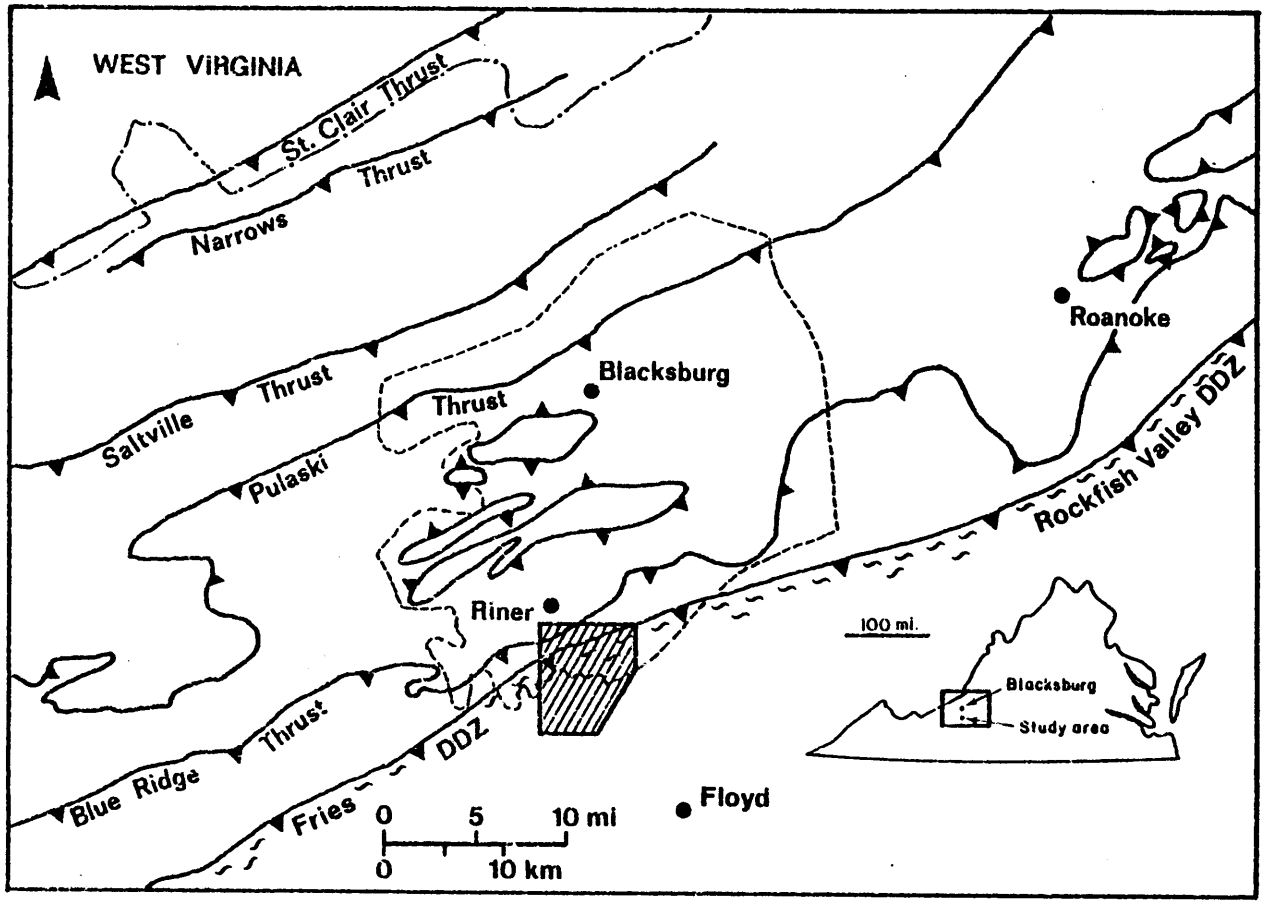

Fig. 1: Location of study area (shaded). Taken from Geologic Map of Virginia, 1963 (modified by Bartholomew, pers. comm.). Dashed line is the outline of Montgomery County.

chemical and mechanical processes during mylonitization.

The work involved in the accomplishment of these objectives included:

1. Detailed field mapping of lithologic and tectonic contacts, gathering of structural data and mapping the distribution of zones representing differing intensities of mylonitization;
2. Structural analyses of individual outcrops;
3. Detailed petrographic and microstructural analyses of over 250 thin sections, and
4. Microprobe analyses of selected samples to determine mineralogic compositions.

Previous Work

The earliest significant work within the area was by Dietrich (1954, 1959). This work recognized basement, named the Little River Gneiss, and attempted to delineate the trace of the Fries Fault, although now located differently. The Fries as mapped by Dietrich was correlated with the Fries Fault of the type locality by Stose and Stose (1957). Metasediments on the hanging wall block, covering a two mile wide zone, were placed within the Alum Phyllite named by Dietrich (1959). However, as the fault is presently mapped, Dietrich's Alum Phyllite is actually part of the Chilhowee Formation and only found on the footwall block of the fault as presently mapped.

The earliest detailed mapping which included the study area was done by Lewis (1975), who informally named the Pilot Gneiss that Dietrich (1959) had described but not differentiated from the Little River Gneiss. Lewis remapped the trace of the Fries Fault, based upon

both a zone of mylonitic rocks and the presence of the Little River and Pilot Gneisses consistently south and north of the fault trace, respectively. She placed metasediments on the hanging wall and some on the footwall within the Ashe Formation.

Truman (1976) also mapped much of the same area, at which time he placed the Pilot Gneiss back within the Little River Formation, but considered all metasediments on the footwall block to be possibly correlative with the Chilhowee Group rocks. He also recognized and differentiated a number of mafic dikes, and mapped two additional faults as splays off of the Fries based upon alternating basement - metasediment lithologies.

This study agrees with previous workers on the differentiation of the Pilot gneiss as a separate unit from the Little River, the placement of metasediments on the footwall block of the fault within the Chilhowee Group, and the trace of the Fries as mapped by Lewis (1975) and Truman (1976).

Terminology

The following terms will be used throughout this study in the sense indicated.

1. Mylonite - A strongly foliated and commonly lineated, fine grained equivalent of adjacent rocks that has been formed by ductile processes (cf. Bell and Etheridge, 1973). The classification used herein (Table 1) is from Sibson (1977), and is based upon the ratio of matrix to relict grains. It refers primarily to quartzo-feldspathic crystalline rocks, as these exhibit grain-size reduction

TABLE 1

Textural Classification of Fault Rocks

(from Sibson, 1976)

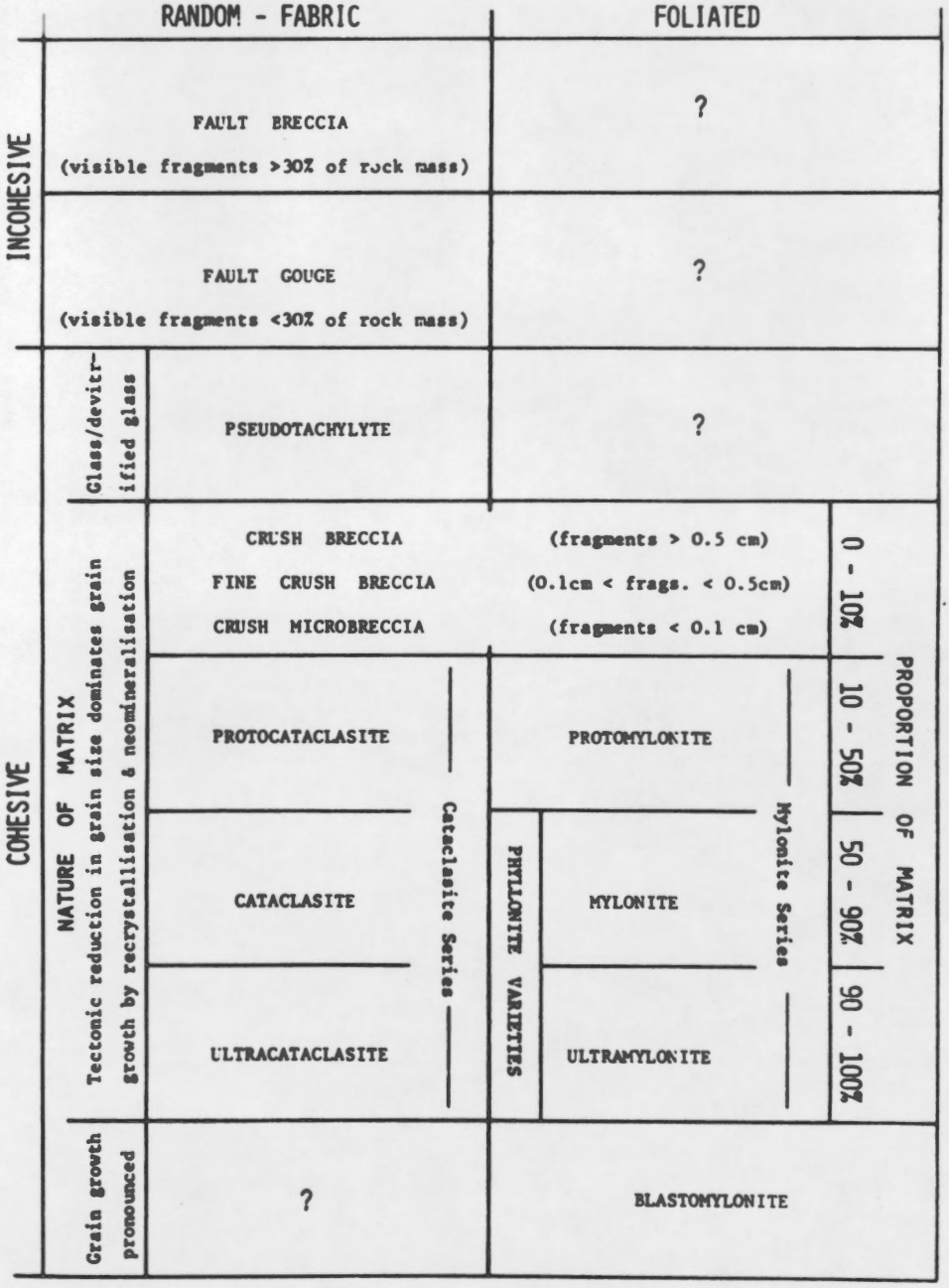

well enough to fit into the classification scheme.

2. Cataclasis - Brittle fragmentation of mineral grains with rotation of grain fragments accompanied by frictional grain boundary sliding and dilatancy (Sibson, 1977; Engelder, 1974).

3. Pressure solution - The solution and removal of mineral substance at a grain contact subjected to pressure and in response to stress gradients (Durney, 1976; cf. Kerrich, et al, 1977; Coble, 1963; Elliott, 1972).

4. Solution Transfer - The dissolution, transport and precipitation of a crystal substance from one part of a rock interior to another via a solution medium (Durney, 1976). It involves concomitant solution, diffusion and crystallization.

5. Recrystallization - refers to development in the solid state of crystals of an already existing phase, by the migration of high-angle tilt grain boundaries through the material (Cahn, 1965, p. 925) resulting in a polycrystalline aggregate forming where once there was a single crystal (Hobbs et al., 1976, p. 107). This is a mechanism of lowering the free energy of the deformed crystal.

6. Ductile Deformation - Deformation during which rock deforms by distributing the strain in a smoothly varying manner throughout the deforming mass (Hobbs et al., 1976, p. 61). It involves the intracrystalline deformation of individual grains, commonly by the motion of lattice dislocations through crystals, including such mechanisms as crystallographic slip and twinning (cf. Verhoogen et al., 1970).

7. Brittle Deformation - Rocks deform by developing marked discontinuities across which there is often a break in cohesion (Hobbs et al., 1976, p. 61). Mechanisms commonly involve faulting, microfracturing and associated cataclastic effects.

8. Ductile Deformation Zone - Zones that have undergone permanent change of shape without gross fracturing (Mitra, 1978).

II. Stratigraphy

Regional Framework

The southern Blue Ridge is bounded by the Brevard Fault Zone and James River Synclinorium on the east and by low angle thrust faults on the northwest (Bryant and Reed, 1970). It is a probable allocthonous mass of Precambrian crystalline rocks that have been transported kilometers to the northwest over unmetamorphosed or weakly metamorphosed Paleozoic sedimentary rocks of the Valley and Ridge Province. The most easterly of these major low angle thrust faults is the Fries, which extends from northern Virginia where it is coextensive with the Rockfish Valley Fault (Bartholomew, in press), at least as far south as the Grandfather Mountain area in North Carolina where it is coextensive with the Fork Ridge Fault (Bartholomew and Gryta, 1979), a distance of over 300 kilometers. It has been suggested that the Fries extends southwestward from the Grandfather Mountain Window into Alabama or Georgia (Rankin, 1975; Hatcher, 1978). This fault zone could possibly be more extensive than the Blue Ridge thrust and tectonically one of the most important in the Appalachians. Interpretations of COCORP seismic reflection data in northeast Georgia indicate that the Blue Ridge - Inner Piedmont thrust sheet is a "6-10 kilometer thick crystalline sheet with at least 200 kilometers of horizontal displacement. The Brevard zone is probably a low angle thrust related to the main Blue Ridge fault" (Cook et al., 1979). The relationship of the Fries ductile fault zone to the brittle Blue Ridge thrust is unclear at this time, but it is unlikely to be similar to that postulated above

for the Brevard. Displacements on the Fries are on the order of 65 kilometers in North Carolina to 32 kilometers near Roanoke, Virginia (Rankin et al., 1973, Bartholomew, in press). Rb-Sr mineral and whole rock analyses performed on mylonitized samples from the Fries Fault Zone in the study area (Dietrich et al., 1969) give an age of 330 ± 15 million years for the timing of movement on the fault.

Stratigraphy

In the study area, the Little River Gneiss and nonconformably overlying Ashe Formation were juxtaposed kilometers to the northwest over the Pilot Gneiss and overlying Chilhowee Group rocks along the Fries Fault (Fig. 2). The latter units are allocthonous as well, and were thrust north over the Lower Cambrian Rome Formation of the Valley and Ridge Province along the Blue Ridge Fault.

Brief lithologic descriptions of nonmylonitized stratigraphic units follow. Other aspects of the stratigraphy are discussed by Lewis (1975) and Truman (1976). The mineralogic and fabric transitions concomitant with faulting will be discussed in a later section.

Little River Gneiss

The Little River Gneiss (Dietrich, 1959) is a massive, medium to fine grained, biotite-rich augen gneiss of granite to granodiorite composition. It consists of irregularly alternating light gray quartzofeldspathic rich and dark gray biotite-rich layers (Fig. 3). White augen with indiscrete boundaries make up about 13% of the rock. These are intergrowths of quartz and feldspar (primarily plagioclase), although quartz and dominantly alkali feldspar augen are present

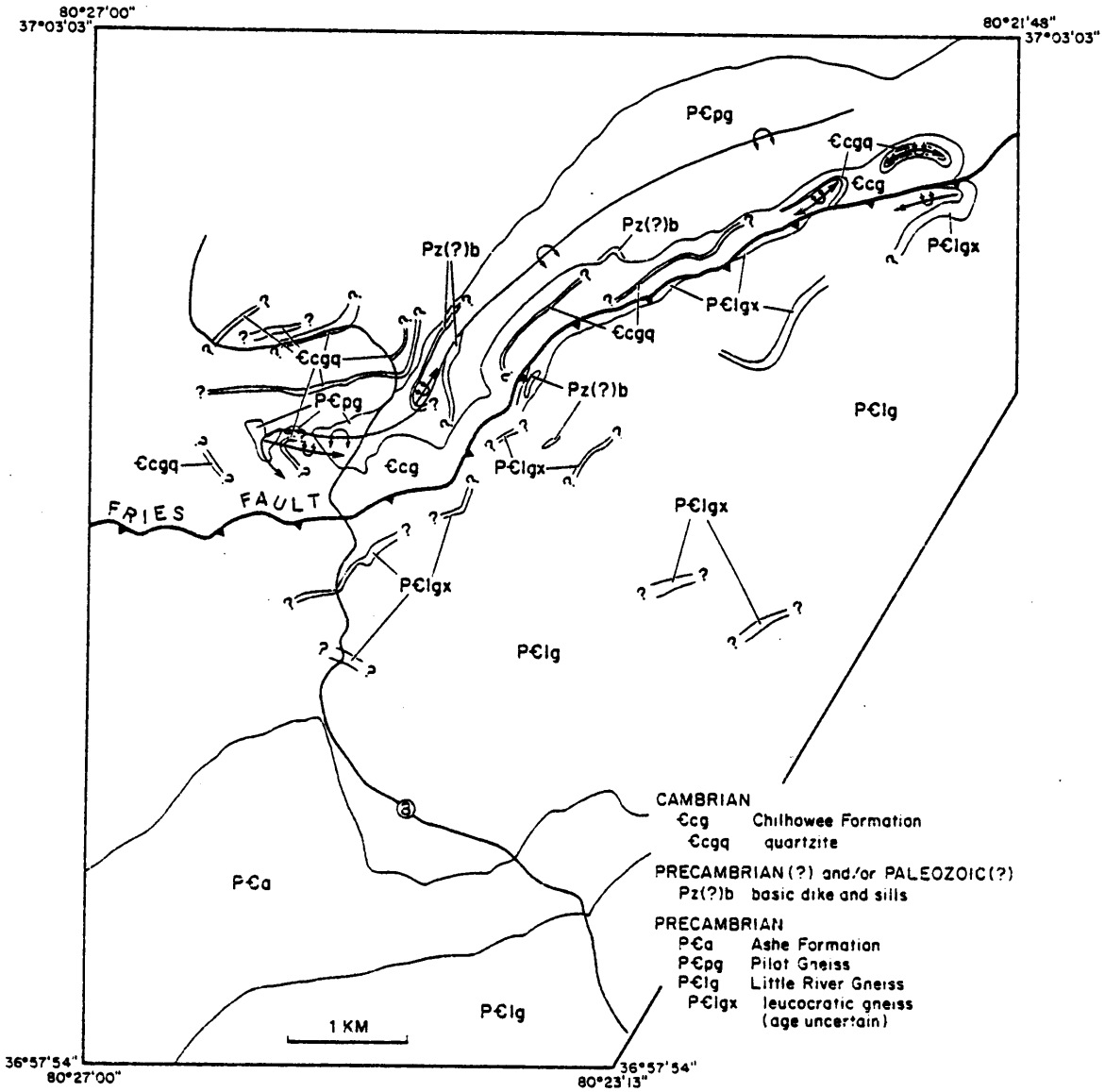

Fig. 2. Generalized Geologic Map of Study Area

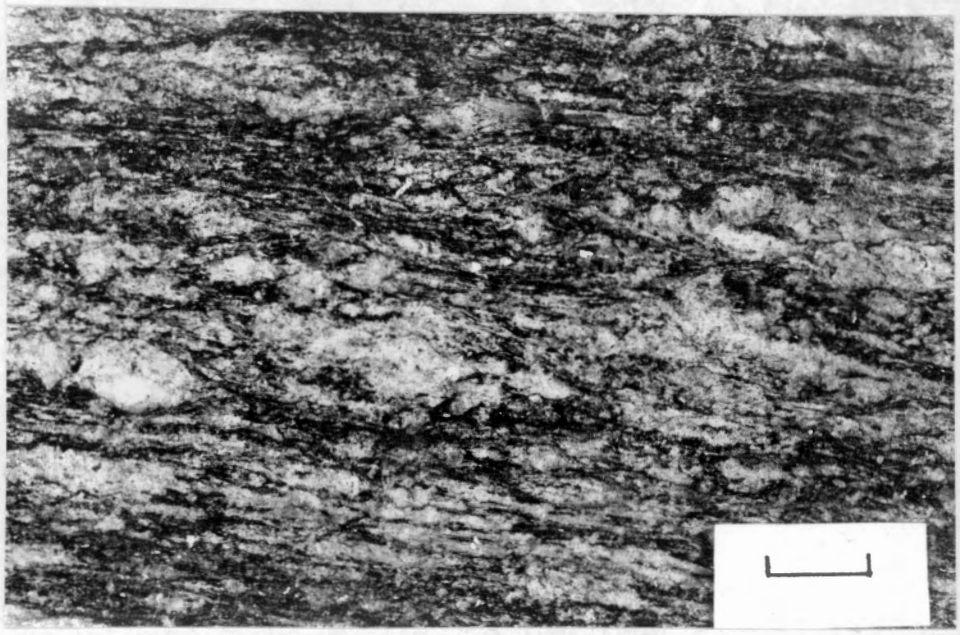

Fig. 3. Slab photo of Little River Gneiss, S_1 gneissosity defined by irregularly alternating light gray, quartzo-feldspathic rich and dark gray, biotite-rich layers, sample #296 (see appendix for location), scale = 1 cm.

locally. The augen are set in a finer grained groundmass of biotite, muscovite, quartz, epidote/clinozoisite and minor feldspar. Accessories are sphene, apatite and zircon with traces of chlorite and calcite. Both, thin zones (one to 15 centimeters wide) of dominantly biotite, and wider zones of finer grained, semi-schistose equivalents of the Little River Gneiss are intercalated locally. Three U/Pb isotopic analyses of zircons on two samples of the Little River augen gneiss yield a concordia upper intercept age of 1128 ± 25 my (Truman, 1976). This was interpreted as the age of igneous emplacement.

Discontinuous, discrete lenses of a leucocratic gneiss occur throughout the Little River augen gneiss and comprise about 5-10% of the unit. Contacts are sharp with the country rock and widths vary from less than a meter to tens of meters. There are at least three phases of this gneiss, each consisting of about 20-30% quartz with variable alkali feldspar and plagioclase contents. Compositionally, these vary from granite to alkali feldspar granite. Textures are porphyroclastic to equigranular or granoblastic, the latter of which contains almandine rich garnets. Accessories present in all include biotite, muscovite, apatite, sphene, zircon and opaques.

Ashe Formation

The Ashe Formation of Late PreCambrian age nonconformably overlies Little River Gneiss in the southern part of the area. The Ashe has been correlated with the Lynchburg to the northeast by Rankin (1970, 1973). The unit consists primarily of phyllites and biotite-muscovite schists of the greenschist facies. Phyllites are of two distinct types;

well-laminated graphite-rich phyllites in which weathering produced millimeter scale color-banding defined by interlayered dark purple and silver-gray to black layers; and light brown to orange-brown phyllites. In thin section, these consist of alternating quartz-rich and mica-rich layers composed of about 30% quartz and 55-60% muscovite and chlorite. Most of the quartz is recrystallized or has undergone normal grain growth/neocrystallization. Graphite comprises 8-10% of the dark phyllites. Plagioclase and alkali feldspar are present in trace amounts along with accessories of sphene and hematite. Interlayered with these dark phyllites and minor in occurrence are thin, black to steel gray, graphite-rich zones that contain up to 55-60% graphite.

Light gray, medium to coarse grained, biotite-muscovite schists comprise most of the unit near the contact with the Little River Gneiss. These consist of alternating fine biotite-muscovite rich and medium to fine grained quartzo-feldspathic rich layers. Quartz comprises about 35% of the rock and has undergone near complete recrystallization accompanying metamorphic grain growth. Anhedral alkali feldspar, .5 - 1 mm in size and usually perthitic, varies from 10-20%, plagioclase ranges up to 10% and biotite and muscovite comprise about 20%. Accessories include apatite, sphene and zircon. Locally interlayered with biotite schists are thin (2-3 cm) zones comprised dominantly of quartz and feldspar with less than 5% mica. Muscovite schists are relatively minor. Bedding within these units is inconspicuous.

Pilot Gneiss

The Pilot Gneiss lithologies were first recognized by Dietrich

(1954), although he did not differentitate them as a separate unit from the Little River Gneiss. Lewis (1975) informally named the unit and described it in exposures along Montgomery County Road 601, about 3 kilometers south-southwest of Pilot. The Pilot Gneiss crops out in a large, anticlinal nappe-like structure flanked by Chilhowee Group metasediments, in the northern part of the study area (Fig. 2). It extends northeastward into the adjacent Pilot quadrangle with the same stratigraphic relationships. The unit crops out again in the northeastern part of the Indian Valley quadrangle, but contacts there have not been established, and it is not clear how far to the southwest the unit extends.

The Pilot Gneiss, granitic in composition, consists of two distinct phases; a hornblende-rich and a hornblende-free phase. Both are mica poor and thus are weakly to non-foliated. An excellent exposure of the hornblende-rich lithology is found along Montgomery Rd. 617, about .3 kilometers south of its junction with 601. Parts of this outcrop seem to be unaffected by the faulting and, thus, the assemblage is considered pre-faulting. This phase is a greenish-white to light pink, medium grained, granoblastic gneiss composed of about 23% pink or pale green, perthitic feldspar, 20% clear to light pink quartz, 13-15% plagioclase, 6-10% hornblende and 30% sericite/sausserite, the latter an alteration of plagioclase (Fig. 4).

A second phase of the unit, and seemingly the more dominant, is a massive, light gray to white or cream, medium grained gneiss. It is fairly equigranular and composed of clear quartz, cream to white

feldspar (perthitic feldspar greater than plagioclase), with minor amounts of chlorite and sericite (Fig. 5). Garnet and pyroxene were observed in one sample of this phase by Lewis (pers. comm., 1979). Accessories in both phases include fine grained epidote, sphene, biotite, chlorite, zircon and opaques.

Within the Pilot Gneiss is an intermixed, coarse grained, porphyroblastic granulite gneiss that has not heen delineated in this study due to poor exposure. However, the unit probably correlates with similar rocks to the northeast in the Stewartsville quadrangle that were intruded by younger PreCambrian plutons (Bartholomew, in press). The rock consists of very large (3-4 cm) perthitic feldspar porphyroblasts, albitic plagioclase and quartz (sometimes intergrown with perthite in augen), deep red-brown biotite, sericite, chlorite and traces of hornblende locally. Almandine garnet and orthopyroxene were observed in one sample.

Chilhowee Group Metasediments

The Lower Cambrian Chilhowee Group nonconformably overlies the Pilot Gneiss in the northern part of the area. This relationship is based upon the outcrop pattern of the Pilot in this area (i.e., a large anticlinal structure), the repetition of stratigraphy on either flank of this fold, the unmylonitized Pilot as one goes to the northeast along the Pilot and Chilhowee contact, and one basement(?) cobble found in the Chilhowee metasediments at Pilot.

The Chilhowee consists of quartzites, metagraywackes, metasiltstones and phyllites. Quartzites are gray, white or pink, massive and

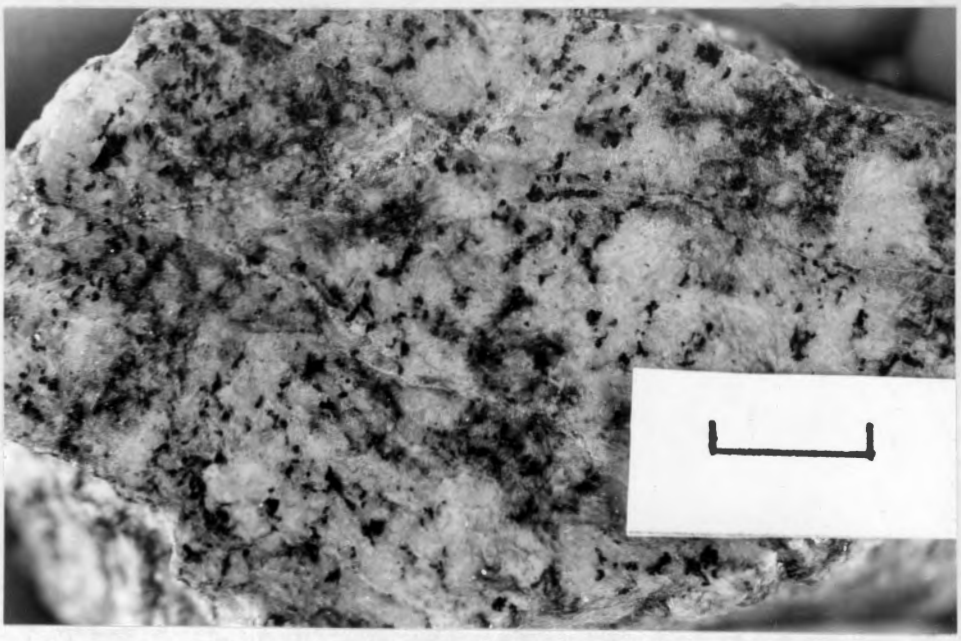

Fig. 4. Slab photo of hornblende-rich phase of Pilot Gneiss, scale is = 1 cm, sample #432 (see appendix).

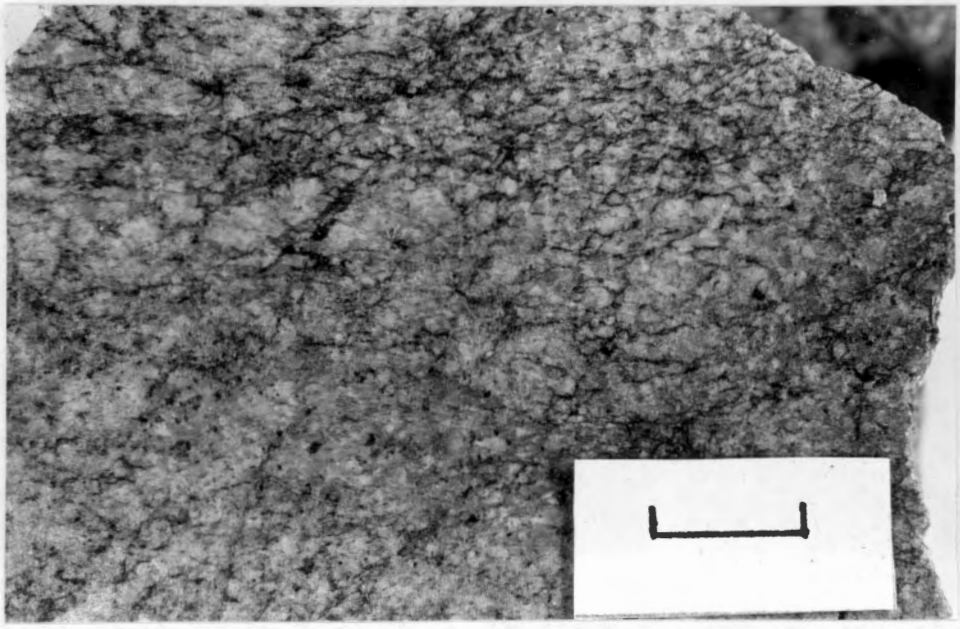

Fig. 5. Slab photo of hornblende-free phase of Pilot Gneiss, scale = 1 cm, Just across from church at Pilot along Rt. 615.

thick to medium-bedded. The white quartzites consist of 90-95% quartz with a matrix of sericite and chlorite and accessory zircon, tourmaline and opaques. Lineations are defined by quartz mineral growth and, in some cases, needle-like opaques. Cross-cutting quartzite veins are quite common as well. Light gray, dirty quartzose sandstones consisting of 65% quartz, 25% sericite, 5% hematite and traces of chlorite are minor in occurrence.

Metagraywackes are dark gray, fine to medium grained and consist of 70-90% quartz in a finer, recrystallized siliceous matrix together with 20-35% sericite. These may contain up to 10-15% feldspar (alkali and plagioclase) and accessories include chlorite, graphite and opaques. Light orange-brown metagraywackes with extensive iron-oxide staining are common as well, composed of 65-70% quartz, 10-20% feldspar (plagioclase and perthitic feldspar) and the remainder as sericite and accessory zircon, opaques and calcite. Metasiltstones are light gray to yellow-brown or brown, generally well-laminated, and consist of about 35-50% quartz, 5-10% plagioclase, less than 5% alkali feldspar, 35-60% sericite/muscovite and minor amounts of chlorite, sphene and opaques.

Silver to dark gray phyllites contain up to 95% micas, primarily sericite with about 5% quartz, and minor opaques. Near the fault, however, phyllonites are recognized that consist of up to 50-55% quartz and 40-45% micas. The latter dominate over the phyllites in the study area.

Mafic Intrusions

Mafic intrusions are common within the basement rocks as dikes

and sills, and are most abundant within the Pilot Gneiss wherein mechanical intermixing of the two is evident. Near the fault, where most were observed, these have undergone extensive chemical alteration producing very fine grained greenschists. Only a few relatively undeformed and unaltered (during faulting) dikes/sills were observed that may give clues as to their original composition. Basically two types are present; a coarse to medium grained amphibolite and a fine grained basalt, the latter only minor in occurrence. These were probably intruded at different times. Some of the undeformed, coarser grained amphibolites consist of up to 85% hornblende, chlorite, minor actinolite and plagioclase with traces of sphene, epidote and calcite. Others, however, have compositions of only 15-35% hornblende, 0-35% actinolite, 35-65% plagioclase, 5-6% biotite and traces of epidote and pyroxene, the latter coring hornblende. The finer grained dikes consist of dominantly to wholly plagioclase, and in one sample contain larger, plagioclase phenocrysts (Truman, 1976). Protoliths for the dikes and sills have had variable composition and, therefore, mineralogy. The coarser grained hornblende bodies were probably associated with a dioritic magma, metamorphosed to amphibolites during the early Paleozoic. The finer grained rock was clearly a basalt. The timing of intrusion is equivocal, but field and textural relations suggest either pre- or syn-faulting. Supportive evidence for this will be discussed in a later section.

III. Structure

The Fries Fault Zone and adjacent rocks have undergone at least four phases of deformation during the Paleozoic (Table 2). The latter two are not necessarily distinct, time-isolated events, but for the sake of clarity have been categorized as D_3 and D_4 deformational events, respectively. Relict mineralogy indicative of earlier Grenville orogenesis will be discussed in the section on metamorphism.

Chronology

Structural features associated with D_1 are regionally dominant outside of the fault zone while those associated with D_2 are dominant only within the fault zone. The latter is correlative with the main movement along the Fries Fault. There are a few problems, however, in establishing this relationship. In the Little River Gneiss outside of the fault zone the dominant foliation could possibly be an S_2 rather than S_1. If this were the case, it would imply that D_2 was regional rather than localized within the fault zone. However, textural relations in adjacent metasediments, and locally within the basement, suggests that S_m(mylonitic foliation)/S_2 within the fault zone is actually the result of near transposition of an S_1 surface. The relations supporting this inference are:

1) The overlying, low grade, Ashe Formation metasediments in the southern part of the study area outside of the fault zone show S_1 to be dominant.

2) In the Ashe Formation to the south, near Floyd, where metamorphic grade increases, S_1 is still dominant with a well developed, cross-cutting, crenulation cleavage (S_2).

TABLE 2: DEFORMATIONAL EVENTS

D_1 EVENT
Foliation (S_1):
Type and Presence: 1) Primary Gneissosity Little River Gneiss; defined by brown to red-brown biotite and muscovite porphyroblasts up to 2 mm in length, these undulate gently around larger feldspar and quartz Pilot Gneiss - generally lacking, granoblastic texture observed primarily 2) Slaty Cleavage Chilhowee - defined by oriented micas; subparallel to parallel to S_o Ashe Formation - Present in phyllites where subparallel or at a slight angle (up to 30^o) to S_o; defined by fine grained muscovite 3) Schistosity - Ashe Formation - Present in metagraywackes; defined by alternating biotite-muscovite and quartz rich layers
Attitude (Fig. 6): N50-55E, 40^oSE
Occurrence: Dominant in Little River Gneiss and Ashe Formation on south side (hanging wall) of fault outside of fault zone; on footwall only recognized as dominant just at northern edge of study area where it is subparallel to S_o.
NOTE: Best recognized in thin section where crenulated and microfolded.
Folding (F_1):
Scale: Megascopic
Type: Overturned, isoclinal, meganappe-type structure
Attitude: NE trend with shallow SE dipping axial plane
Occurrence: Only recognizable in Pilot Gneiss from outcrop pattern; the homogeneity of the Little River Gneiss precludes accurate delineation of fold patterns
Lineation (l_1):
Description and occurrence: Biotite lineation in the Little River Gneiss and in Chilhowee Formation defined by micas primarily, but locally by needlelike opaques
Attitude: S20-25E at $25-30^o$

TABLE 2 continued

D_2 EVENT
Foliation (S_m/S_2):
Type and Presence: 1) S_m, mylonitic foliation Little River Gneiss - Defined by alternating quartzo-feldspathic and mica-rich layers along which quartz is extremely elongated and feldspars are strung out; fine grained epidote-rich layers and tectonic styolites are evident as well (Fig. 11). Pilot Gneiss - Defined by alternating elongate quartz-quartzo-feldspathic and epidote rich or epidote-hornblende/actinolite rich layers Chilhowee Formation - quartzites, defined by elongate quartzose ribbons 2) S_2, crenulation cleavage (Fig. 9, 10, 12) Chilhowee Formation - Dominant foliation across fault zone, nearly transposing S_1; defined by alternating quartz-rich and mica-rich layers or just micas in the more phyllitic phases; metamorphic grain growth (muscovite) is quite pronounced in the most intensely deformed zones; quartzose layers tightly folded with axial planes parallel to S_2; solution offset along S_2 and extensive concentrations of opaques/iron oxides helping define S_2 (i.e. tectonic styolites)(see Fig. 12); axial planar to mesoscopic F_2 folds
Attitude (Fig. 6): $N45^oE$ north of fault (footwall) to about $N65^oE$ south of fault (hanging wall); dips fairly constant across zone between 35^o and 40^o to the southeast
Occurrence: Ubiquitous and dominant across entire fault zone
Folding (F_2):
Scale: Megascopic, Mesoscopic, Microscopic
Type: Overturned to the northwest, tight to isoclinal usually with axial planes parallel to S_m/S_2
Attitude (Fig. 6): $N75^oE$ at 10^o
Occurrence: only locally developed 1) primarily in less competent Chilhowee a) megascopic - defined by outcrop pattern of quartzites; early D_2 (cut off by fault) b) mesoscopic - buckled quartzite veins with axial plane parallel to S_2 (Fig. 14 and 15) and chevron type crenulations at one locality (Fig. 20)

TABLE 2 continued

c) microscopic - microfolds (Fig. 17)

2) Little River Gneiss

observed at one locality in:

Augen gneiss - mesoscopic, formed late in D_2 and actually fold S_m (limbs parallel to S_m); seems to indicate rotation of S_m surface during deformation (Fig. 18a, b); microscopic folds in fine epidote layers as well

Leucocratic Phase - microscopic; quartzbse stringer isoclinally folded with axial plane parallel to S_m (folds S_m) (Fig. 19); may be due to rotation during S_m development as suggested for mesoscopic folds above; this is indicated as well by microfolds in fine grained epidote layers

Lineation (l_m):

Description and occurrence:

Little River Gneiss - mylonitic lineation, defined by elongated quartz and feldspars parallel to the dip of S_m (micas oriented as well)

Chilhowee - "grooves" on highly polished surfaces, elongate quartz in quartzites

Attitude (Fig. 6): S40E at 35-40°

D_3 EVENT

Foliation (S_3):

Type and Presence: Crenulation Cleavage -

Chilhowee Formation - primarily present herein; widely spaced, sometimes forming a "button-like" texture due to intersection with S_2, and in some cases seems to "drag" S_2 indicating possible rotation of earlier surface during D_3 event; minor recrystallization of mica along S_3 surfaces, (Fig. 13)

Little River Gneiss - widely spaced; only visible in outcrop in finer grained or more mylonitized samples; readily recognized on cut surface

Pilot Gneiss - local, only recognized in highly mylonitized samples

Attitude (Fig. 6): N50°E, 25°SE

Occurrence: Fairly ubiquitous in Chilhowee, observed locally in basement (in finer grained samples), see Fig. 8

TABLE 2 continued

Folding (F_3):

Scale: Megascopic, mesoscopic

Type: 1) overturned tight folds on megascale (local)

2) Tight to open asymmetric folds and crenulations on mesoscopic scale; locally developed, (M, S and Z type recognized) (Fig. 21)

Attitude: 1) mesoscopic - N70E with shallow plunge (less than 20^{o}) (Fig. 6), a few have SW plunges

2) megascopic - northeast trends

Occurrence: very local on mesoscopic scale; not recognized in outcrop as extensively in Chilhowee as in Little River Gneiss (Fig. 8)

D_4 EVENT

Foliation: none observed

Folding (F_4 or post F_3):

Scale: megascopic

Type: gentle, open

Attitude (Fig. 6): β = $S50^{o}E$ at $25-35^{o}$; (from S_2 on footwall block and S_3 stereonets)

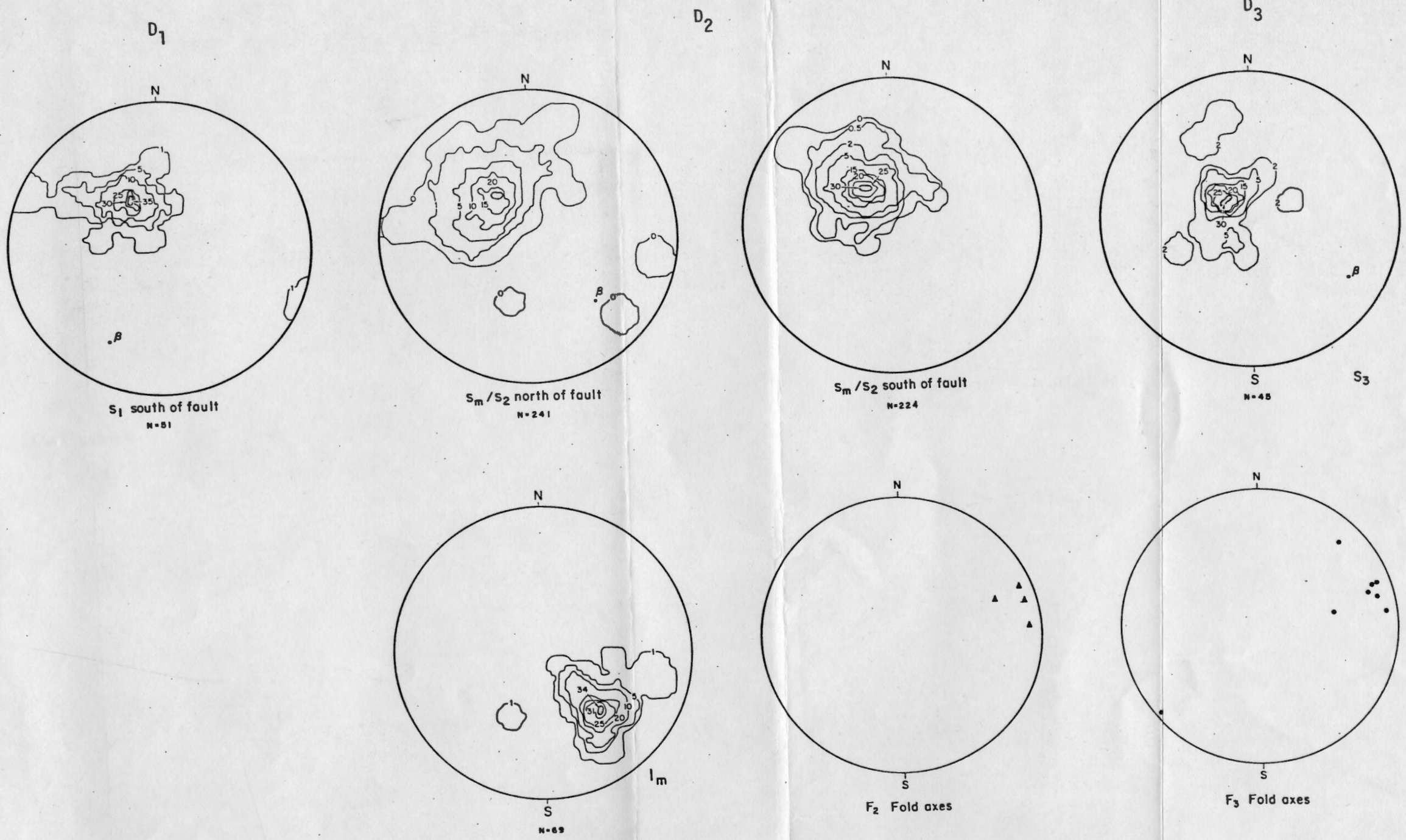

Fig. 6: Stereonet plots of structural data from study area.

cutting, crenulation cleavage.

3) Pre S_m biotites (wrapped by S_m) are recognized in the Little River Gneiss that are similar to those in the unmylonitized samples, i.e., relatively large, brown, platy porphyroblasts. These are unoriented and sometimes kinked and folded with their axial planes parallel to S_m (Fig. 7). Pre S_m muscovites are locally folded as well, but most have undergone recrystallization parallel to S_m.

D_3 and D_4 associated structural features are recognized only locally within the study area (Fig. 8), indicating the intensity of such was much less than the former two deformational events. Later, brittle deformation effects are obvious in the area as well, recognized by fractured and offset quartz layers in the Little River Gneiss and extensive fracturing and quartz-feldspar vein filling in the Pilot Gniess. These may all be related to the same event that is at least post D_3.

Foliations

An S_2, crenulation cleavage, within Chilhowee metasediments and S_m, mylonitic foliation, within the basement rocks is dominant across the entire fault zone. A morphological description of these foliations is given in Table 2. Mylonitization in the metasediments is indicated by the intensity of S_2, by a mylonitic foliation due to quartz elongation in the quartzites, and highly polished, grooved surfaces in the more phyllitic phases that are recognized near the fault trace. S_2 nearly transposes an earlier slaty cleavage (Fig. 9,10) and S_m transposes an earlier S_1 gneissosity in the Little River Gneiss by ductile/brittle

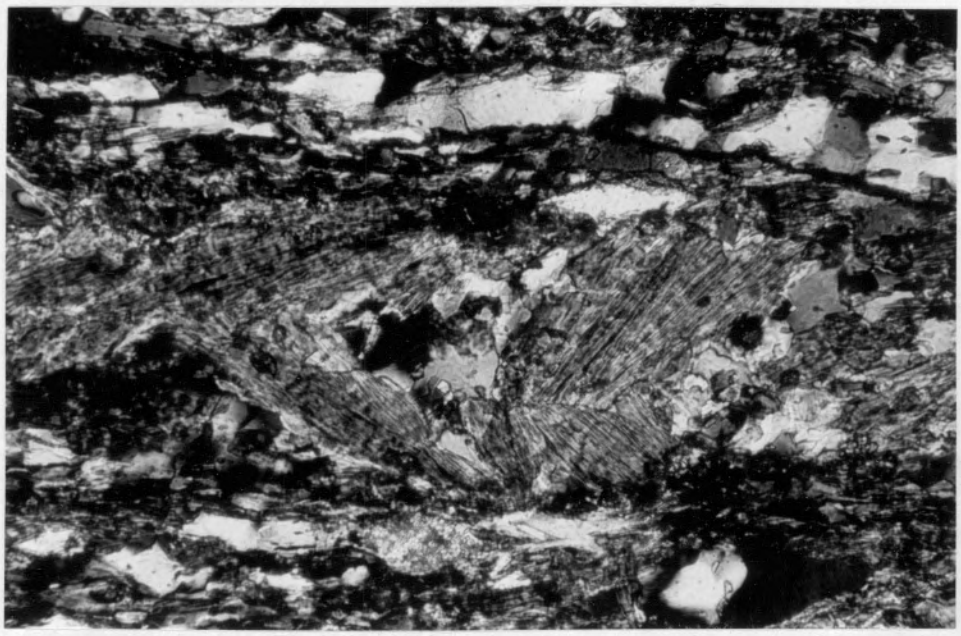

Fig. 7. Pre S_m biotite in Little River Gneiss, kinked with axial plane parallel to S_m, 1 cm = .04 mm, sample #100 (see location map in appendix)

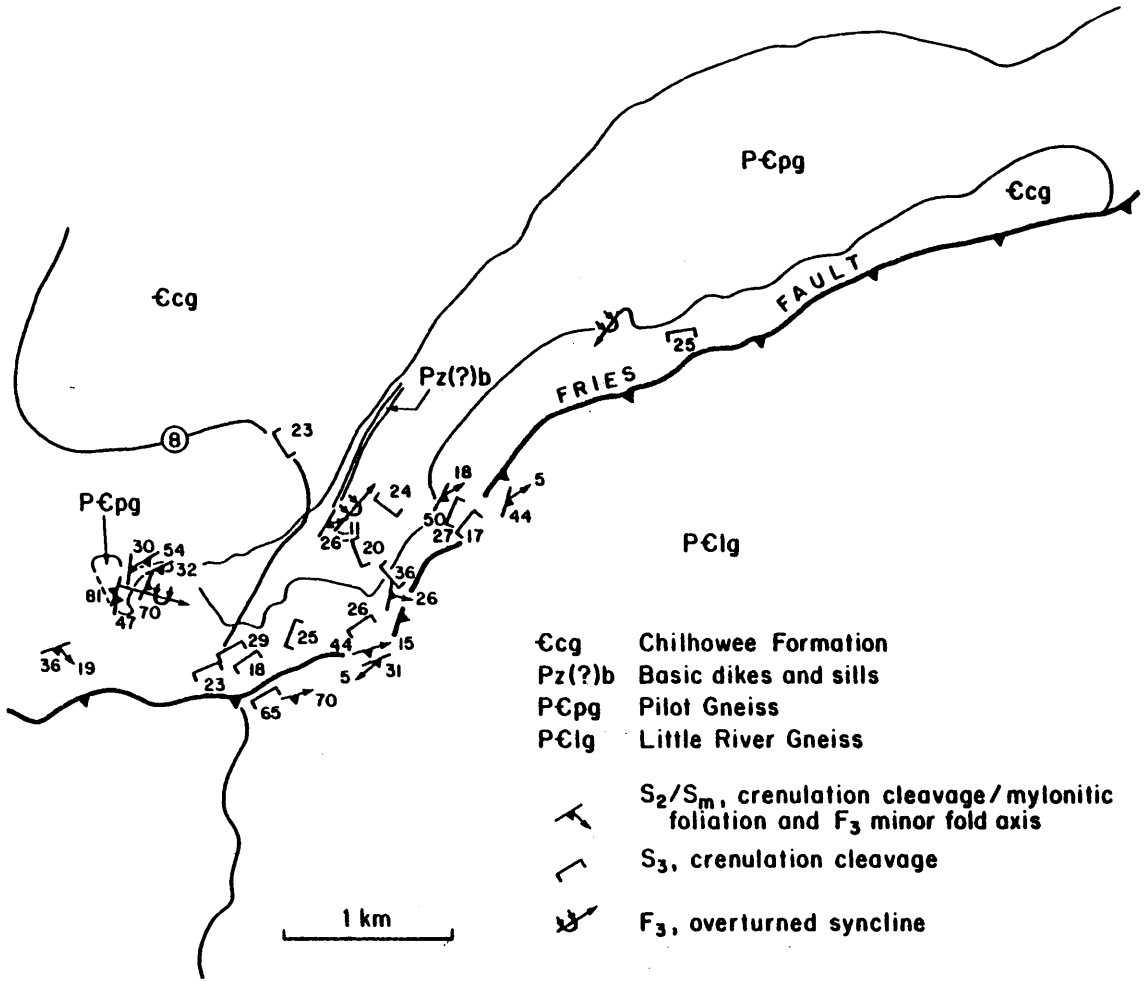

Fig. 8: Development of S_3/F_3 within the Fries Fault Zone

Fig. 9. S_1 (slaty cleavage) X S_2 (crenulation cleavage) in Chilhowee metasediments; 1 cm = .18 mm, sample #C-3 (see appendix).

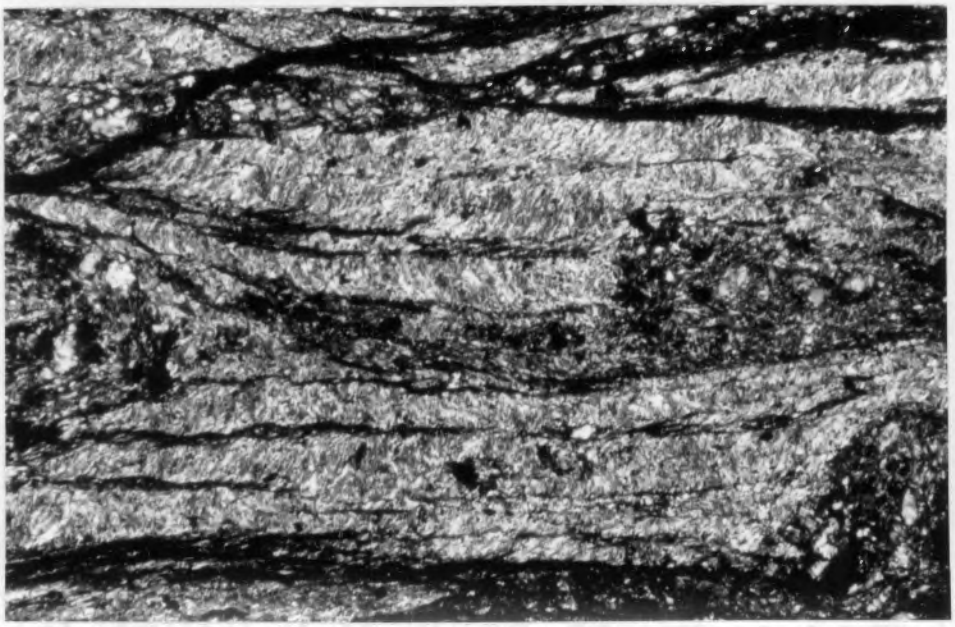

Fig. 10. S_1 (slaty cleavage) X S_2 (crenulation cleavage) in Chilhowee metasediments, S_2 dominant; 1 cm = .29 mm, sample #F-5 (see appendix).

processes in quartz and feldspar accompanied by chemical processes. These processes are discussed in detail in Part II. The orientation of S_m in the Little River Gneiss is controlled by the pre-existing planar fabric. S_m within the Pilot, however, does not refold or transpose any earlier surface as such is generally lacking due to lack of primary micas and original granoblastic texture. The exception to this is the possible mylonitic foliation (S_1?) formed due to shearing on the overturned limb of the large F_1 nappe structure. Near the nose, S_2/S_m is dominant, but may have been superimposed over S_1. This is suggested at one locality. In the northeastern corner of the study area, however, the mylonitic foliation definitely appears to be an S_1, although the original coarse grained nature of the rock precludes accurate determination of this. Brown hornblende, only partially retrograded to actinolite is wrapped by the foliation, while deep red-brown biotites are synchronous with its development. Others retain relict garnets and pyroxene. The pattern of mylonitization around this fold suggests mylonitization due to shearing on the overturned limb as well (Fig. 22). Another possibility to explain this pattern, however, is folding of the fault surface with subsequent erosion, exposing different levels.

S_2 is generally axial planar to small-scale F_2 folds (Figs. 14-16), and can be observed grading into S_m of the Little River Gneiss without a change in orientation (Fig. 23). This indicates that they are coplanar and, thus, their development is inferred to be synchronous. Tectonic styolites are parallel to and help define S_m (Figs. 11 and 12). The orientation of S_2/S_m varies from N45°E north of the fault to N65°E

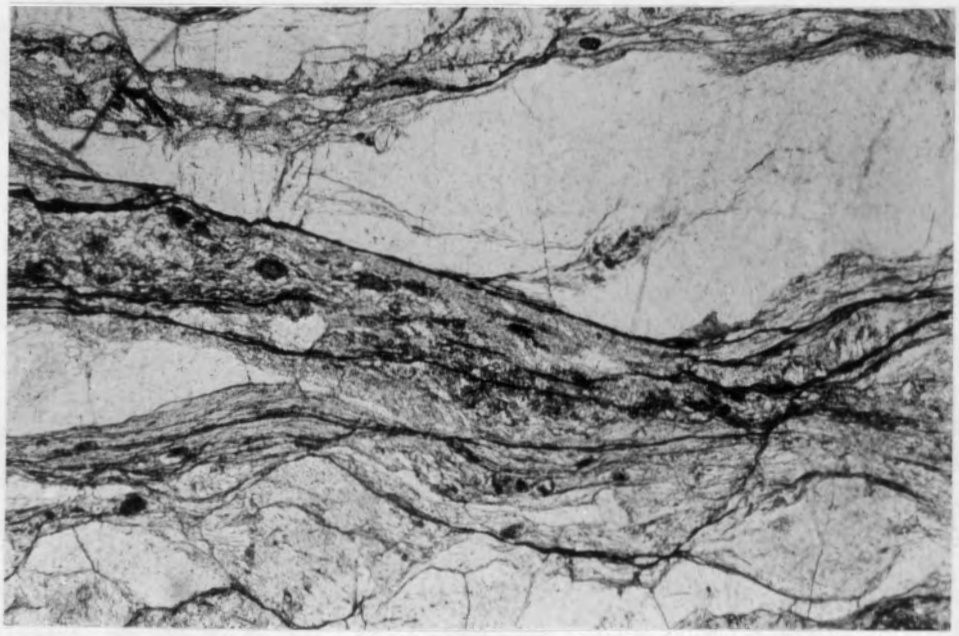

Fig. 11. Tectonic styolites in the Little River Gneiss; S_m dominant (horizontal); 1 cm = .29 mm, sample #B-9 (see appendix).

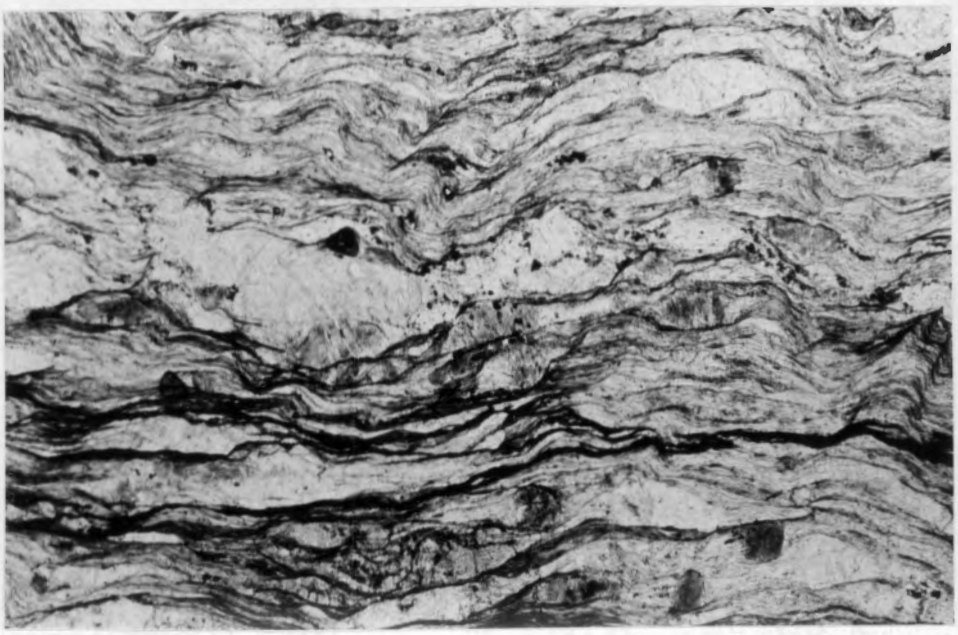

Fig. 12. Tectonic styolites in Chilhowee metasediments that are parallel to and help to define S_2; 1 cm = .3 mm, sample #F-13b (see appendix).

south of the fault with dips fairly constant between 35° and 40° to the southeast (Fig. 6, D_2 event). Different orientations on the hanging and footwall blocks of the fault may be due to different lithologies, original inhomogeneities (i.e., primary fabric), later refolding, or, more probably, a combination of these.

S_3 is a widely spaced, crenulation cleavage (Fig. 13 and Table 2) that is best developed within Chilhowee metasediments, although recognizable in the finer grained mylonitic Little River and Pilot Gneisses. The more competent nature of the latter is responsible for the general lack of S_3 across the area in these units (Fig. 8), although it is a regional event that has been recognized throughout the Blue Ridge. The average orientation of S_3 is N50°E, dipping at about 25° to the southeast (Fig. 6). Stereonets suggest it may be axial planar to F_3 folds. Fig. 8 shows S_3 and F_3 within the study area and its localized development.

Folding

F_1, although undoubtedly present across the entire study area, is most readily distinguishable in the northern part due to the outcrop pattern of the Pilot Gneiss (Fig. 3 and geologic map), defining a large-scale, northeast trending, mega-nappe structure that is overturned to the northwest. Similar structures are also recognized just a few kilometers to the north in the Valley and Ridge province (Bartholomew and Lowry, 1979; Schultz, pers. comm., 1979) and are suggested to be F_1 folds of probable early to middle Paleozoic age. The outcrop pattern of the Ashe Formation in northern Floyd County may

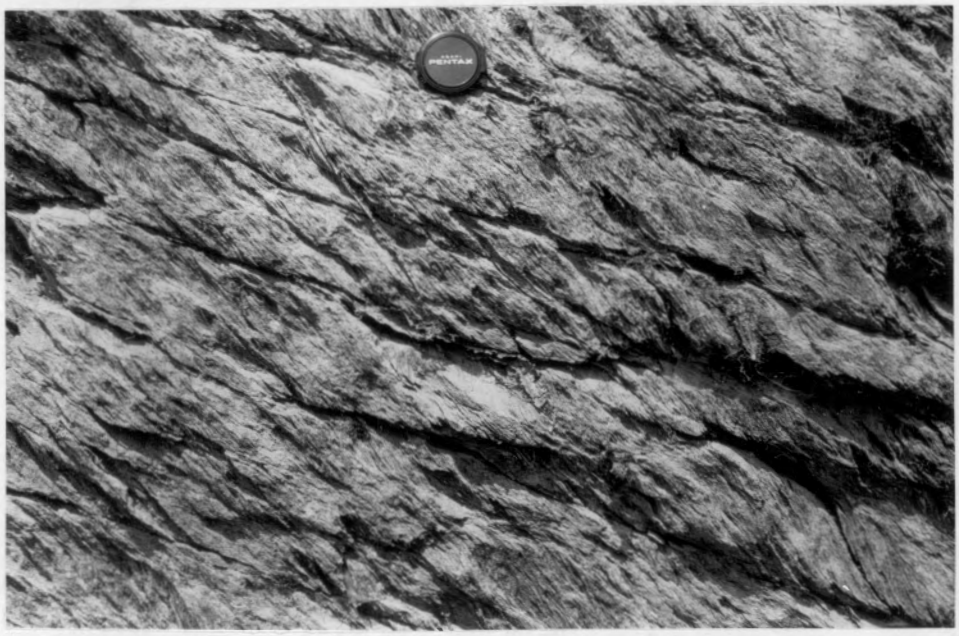

Fig. 13. S_2 (crenulation cleavage) X S_3 (crenulation cleavage) in Chilhowee metasediments very near fault trace; sample #C (see appendix).

define a large scale F_1 syncline (Dietrich, 1959). The outcrop patterns of the leucocratic gneisses within the Little River (Fig. 3 and geologic map) also probably define these large-scale F_1's, but lack of exposure makes accurate delineation difficult. Large areas of homogeneous lithologies, general lack of exposure and polydeformation preclude determination of regional fold patterns across this zone. Small scale (outcrop scale) F_1's have not been recognized.

F_2 folds seem to be only locally developed, primarily within the Chilhowee metasediments, localized at the leading edge of the thrust sheet. These folds are recognized in quartzite units which are truncated by the Fries Fault (Fig. 3 and geologic map), presumably due to late D_2 movement. Others, on an outcrop scale, are buckled quartz veins with axial planes parallel to S_2 (Figs. 14 and 15) or, in the more phyllitic phases where S_o is parallel to S_1, both define the enveloping surface of small-scale F_2's (Fig. 16). In thin section, asymmetric microfolds are recognized as well (Fig. 17). F_2(?) folds in the Little River Gneiss were observed at only one locality that is near the fault trace (Fig. 18a and 18b). These actually fold S_m, but the limbs are parallel to it. Although these may represent refolding of an earlier S_1 gneissosity, as suggested by the development of a crenulation cleavage that is parallel to S_m recognized within the same outcrop, their development was probably due to rotation of the S_m surface late during D_2 (cf. Bell, 1978). This is mirrored on a microscopic scale as well, by an F_2 microfold seen in thin section that has an axial plane subparallel to S_m (Fig. 19). In the northern part of

Fig. 14. F_2 folds in quartz veins of Chilhowee Formation, axial planes parallel to S_2; sample #94a (see appendix).

Fig. 15. F_2 folds in Chilhowee Formation with axial plane parallel to S_2; 1 cm = 3.6 mm, sample #265 (see appendix).

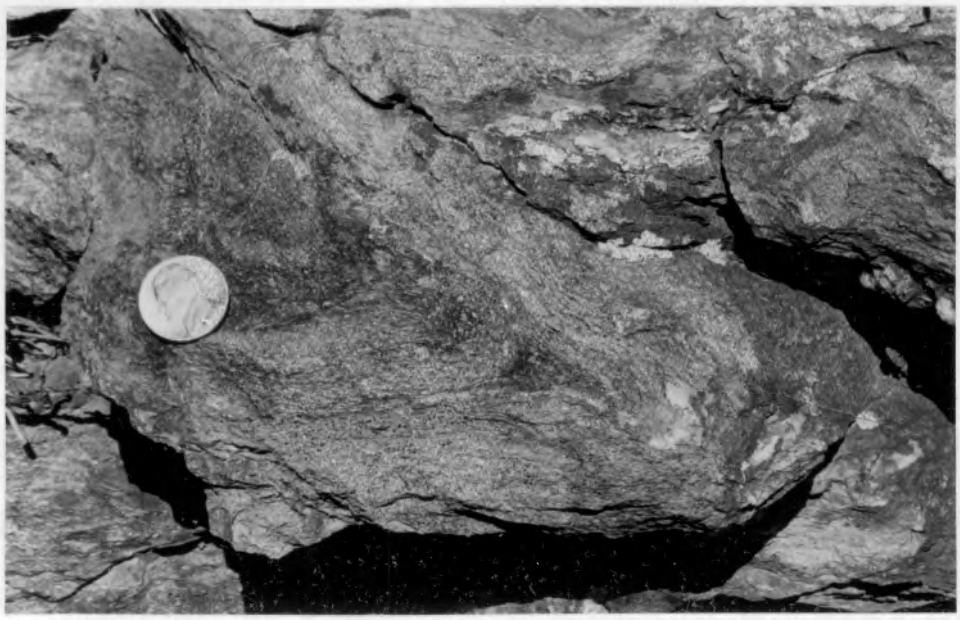

Fig. 16. F_2 fold in Chilhowee metasediments with axial plane parallel to S_2; sample #F-1 (see appendix).

Fig. 17. Assymmetric F_2 microfolds in thin psammitic layer. Note the discrete crenulation cleavage (S_2) in the adjacent pelite (S_2 horizontal); 1 cm^2= .18 mm, sample #C (see appendix).

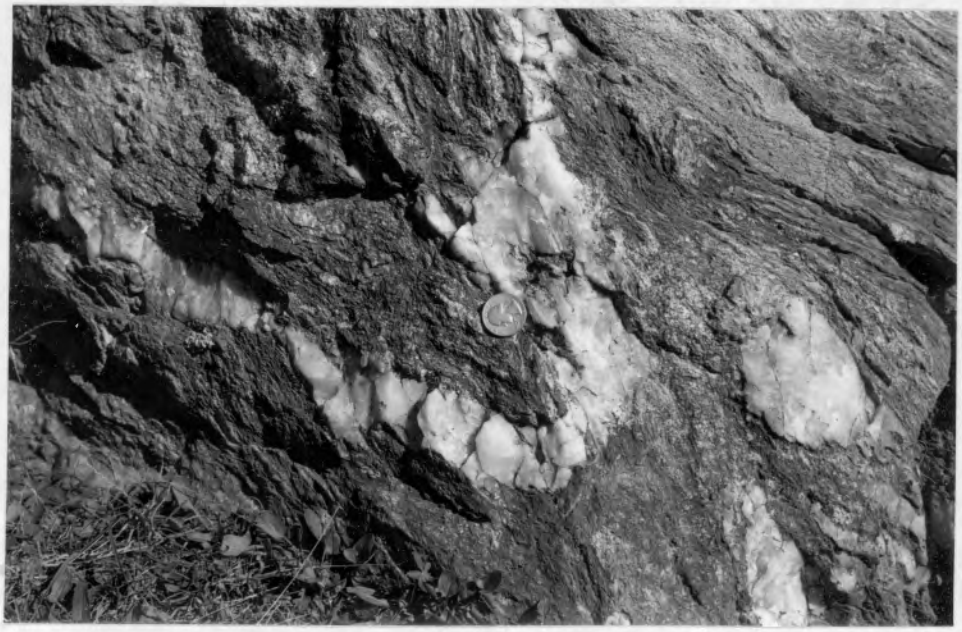

Fig. 18a. see below

Fig. 18b. F_2(?) folds in Little River Gneiss that fold S_m indicating their development was late D_2; sample #431 (see appendix).

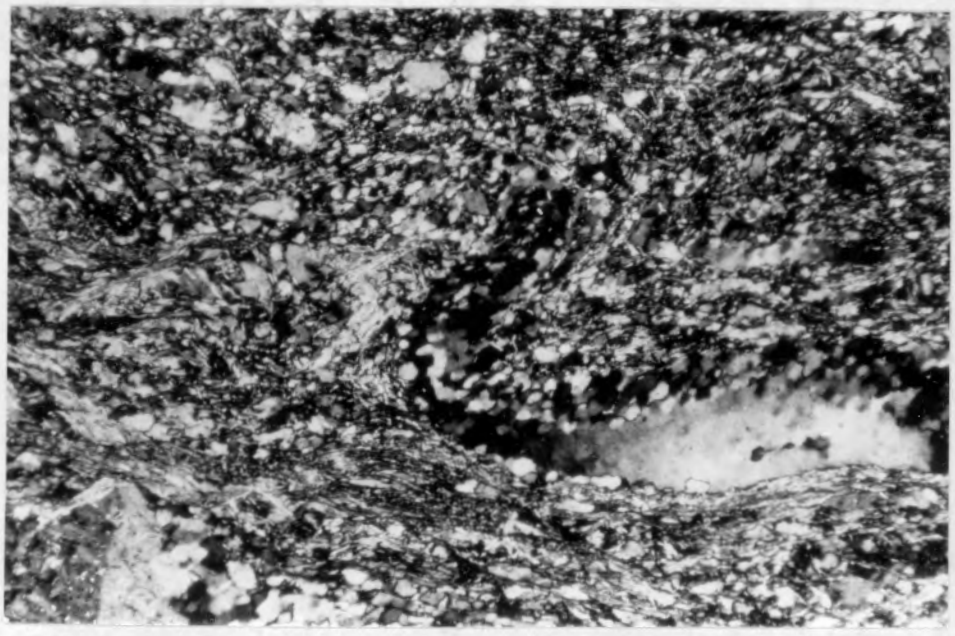

Fig. 19. F_2 microfold in granitic phase of Little River Gneiss; note axial plane and lower limb sub-parallel to S_m; 1 cm = .13 mm, sample #51 (see appendix).

Fig. 20. F_2 crenulation in Chilhowee phyllite; S_2, crenulation cleavage developed locally; 1 cm = 2.1 mm, sample #142 (see appendix).

the study area, in the Chilhowee Formation, an S_2 crenulation cleavage is developed along limbs of small-scale crenulations or kinks (Fig. 20). Chevron-type kinks have been recognized as well just north of the study area (Lewis, 1975), and it is not clear whether these are related to the faulting or whether they correspond to F_3 folds within the fault zone. The average orientation of F_2's within the study area is N75°E at 10° (Fig. 6).

Small-scale, F_3 folds are recognized locally within the Little River Gneiss and Chilhowee Formation (Fig. 21). Their average orientation is N70°E with a shallow plunge, generally less than 10° (Fig. 6). The basement rocks seem to have responded to this later deformational event moreso by folding, whereas the metasediments responded by the development of a crenulation cleavage. These may represent parasitic folds on larger structures, as S, Z and M types have been recognized. Larger scale F_3 folds have refolded S_2/S_m locally across the area and these are shown on Figure 8 and the geologic map (see pocket). These are most evident in the most intensely deformed parts of the fault zone and variations in the plunge of the mylonitic lineation is attribute to this event. The large F_1 fold of the Pilot Gneiss is refolded about an F_3(?) inasmuch as the S_2/S_m is actually wrapped about the nose (geologic map). F_2 may not have developed in this area or was coaxial with F_1.

D_4 (includes all post D_3 deformation) folding is best seen by the stereonets of S_2/S_m north of the fault and of S_3. These show a gentle folding about a β (i.e., fold axis) with a NW-SE trend.

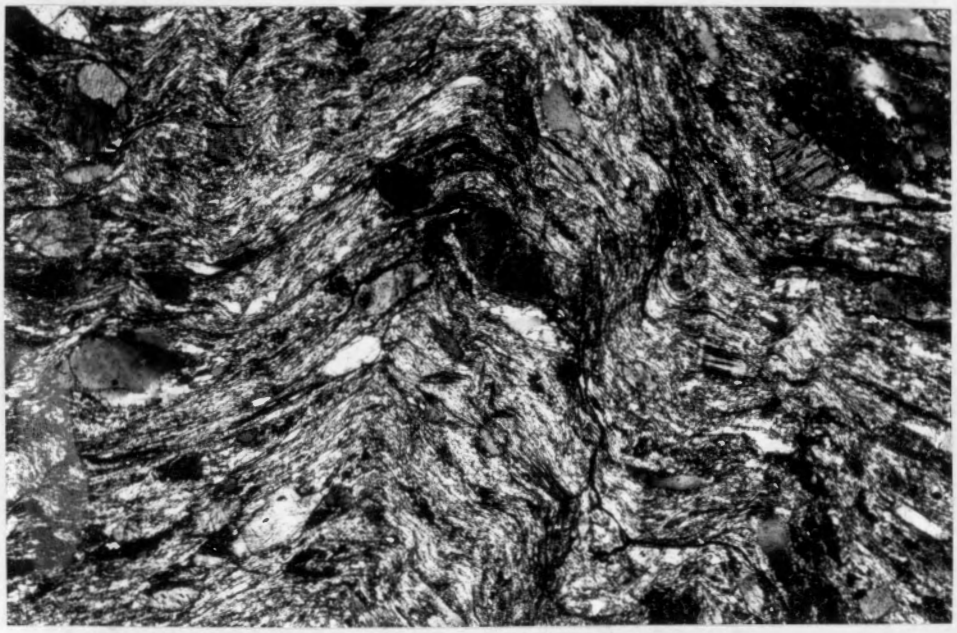

Fig. 21. F_3 m-type folds in Chilhowee metagraywacke just at fault contact with Little River Gneiss; 1 cm = .18 mm, sample #F-13b (see appendix).

Stereonets of S_1 south of the fault zone (Fig. 6) give a SW trending β, which may represent the regional D_2 (F_2 outside of the fault zone = F_3 within). The latter, as well as the open, northwest trending warp within the study area (F_4), correspond to folds of similar orientation recognized near Floyd which also represent the latest deformation.

Lineations

An L_1, biotite lineation, is recognized outside of the fault zone in the Little River Gneiss. Within the fault zone, however, L_m, a stretching lineation, is defined by elongated quartz and feldspars and is ubiquitous. Only in the less intensely deformed zones is the L_1 still observed. Grooves along S_2 surfaces of the Chilhowee Formation in the most intense zones very near the fault trace are considered "tectonic lineations" associated with the faulting as well.

IV. Metamorphism

The basement rocks underwent at least two metamorphic events and the overlying metasediments at least one, prior to faulting. The assemblages associated with each event for the different units are given in Table 3. Granulite facies metamorphism is indicated in the Pilot Gneiss by the assemblage: hypersthene + almandine garnet + perthitic feldspar + plagioclase + quartz ± biotite; and upper amphibolite or lower granulite facies in the Little River Gneiss and associated granitic phases by: almandine-rich garnets + perthitic feldspar + plagioclase (antiperthite comprises a large percentage) + quartz + biotite. It is not clear whether there was primary muscovite, and, therefore, accurate determination of the facies is difficult. These mineralogies are probably indicative of the Grenville metamorphic event (850-900 my) (M_{1preC}) that has been recognized throughout the Blue Ridge. The juxtaposition of relatively lower grade (upper amphibolite to lower granulite) rocks on the south over upper granulite facies rocks on the north side of the fault is consistent with similar relationships recognized along strike (Bartholomew and Lewis, 1977). This suggests a high grade Blue Ridge core that gradually decreased in metamorphic intensity to the southeast.

A second regional metamorphic event (M_2) that dominates the entire area outside of the fault zone retrograded basement rocks to lower amphibolite or ab-epidote amphibolite facies while prograding overlying metasediments to lower to upper greenschist facies (Table 3). The peak of regional metamorphism in the Blue Ridge is considered to be at least 430 my (Butler, 1972). This study shows the early metamorphism to

TABLE 3: MINERAL ASSEMBLAGES FOR M_1-m_3 METAMORPHIC EVENTS

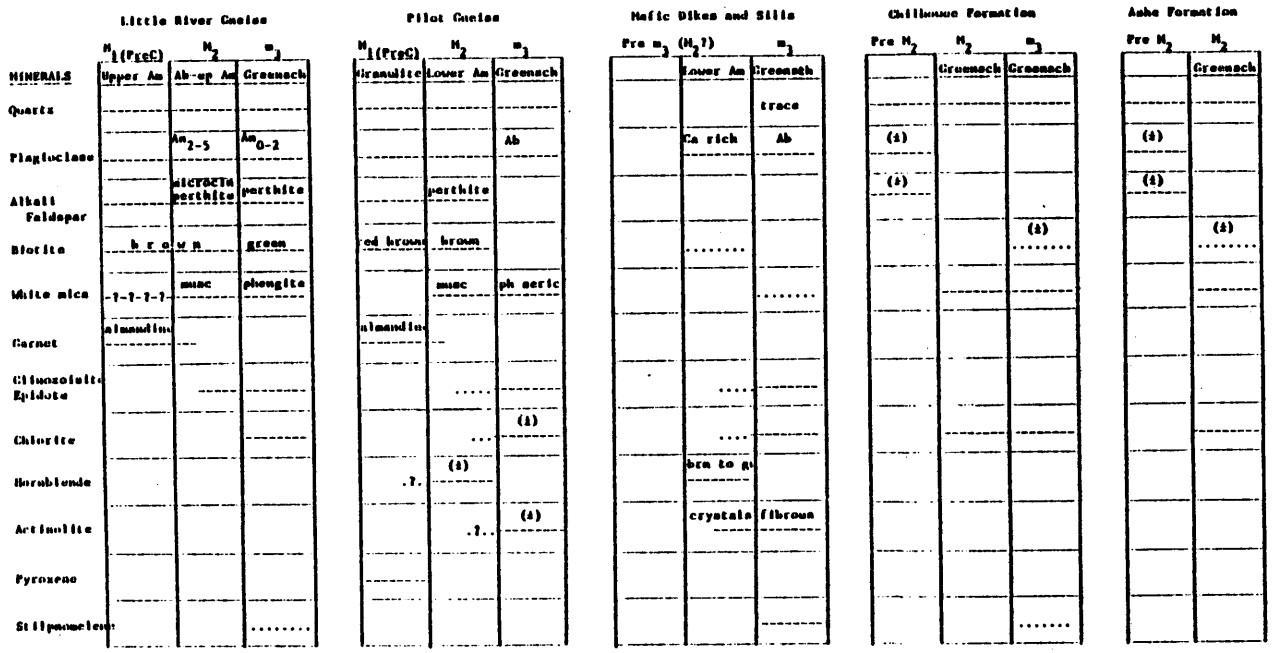

-------- presence of mineral in assemblage

..... mineral present in trace amounts

-?--.?.. textural relations make presence questionable

Am - Amphibolite

Greensch - Greenschist

musc - muscovite

ph - phengite

represent the peak of regional metamorphism in this area as well, and dates obtained by Dietrich and others (1969) agree well with the 430 my episode. However, the reliability of these dates is questionable.

m_3, a local retrogressive event associated with faulting, retrogressed basement rocks and mafic dikes and sills within the study area to the greenschist facies. Aspects of mineral chemistry and mineralogic transformations concomitant with this event are discussed in a later section. The Chilhowee metasediments remained at lower greenschist facies during faulting (chlorite zone), although at two localities very near the fault trace syn S_m biotite is observed. These are probably the result of elevated temperatures at the fault contact due to an inverted thermal gradient or to aseismic shear. An inverted thermal gradient could be developed by thrusting warmer rocks rapidly over colder, wetter rocks. This is discussed by Cliff, 1971 (Beach and Fyfe, 1972). Steady aseismic shearing can give rise to temperature increases due to shear resistance (friction) (Sibson, 1977). Ashe metasediments were not involved in the m_3 metamorphic event, as they are only present outside of the fault zone.

Table 4 graphically depicts metamorphic intensity versus deformation. It suggests that metamorphic intensity declined to zero between M_{1preC} and M_2, and m_3 is a retrogressive phase associated with faulting, but as temperatures were declining from the regional M_2 event. There was probably some elevation of temperatures, however, due to friction (as suggested above) and overburden pressure.

A biotite zone boundary associated with the M_2 event is coincident with the trace of the Fries Fault, and indicates that the peak of

metamorphism was reached prior to movement, or at least last movement, along the fault.

TABLE 4:- Deformation and Metamorphism within the study area.

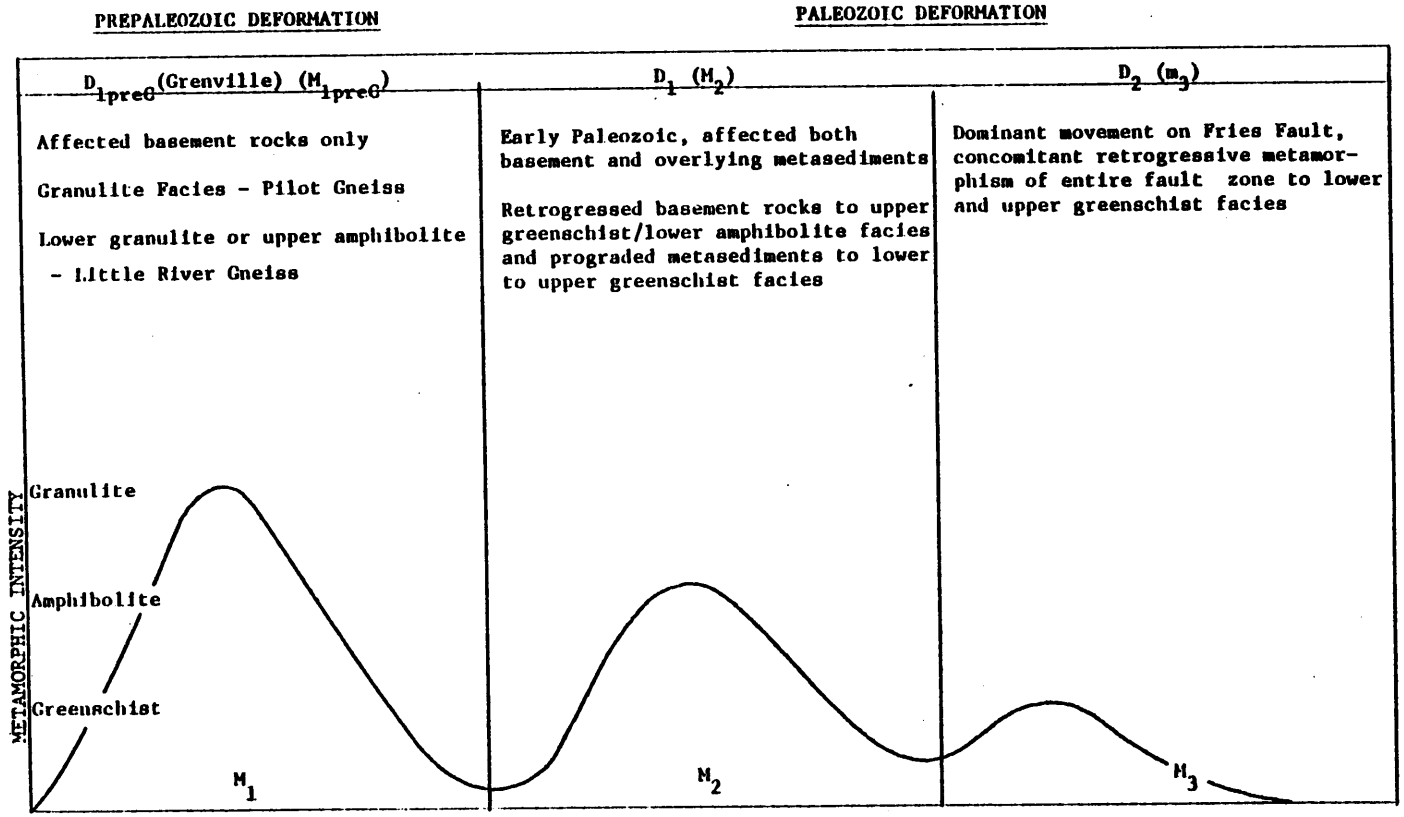

PART II: MYLONITIZATION WITHIN THE FRIES DUCTILE DEFORMATION ZONE

I. General Relationships

The Fries ductile deformation zone (DDZ), previously shown on maps as a linear feature separating basement from younger metasediments (cf. Dietrich, 1954, 1959; Lewis, 1975; Truman, 1976), although Lewis (1975) and Truman (1976) noted a mylonite zone associated with the fault, is a zone up to 2 to 2.5 kilometers in width across which there is increasing intensity of deformation towards the fault-trace and subzones of protomylonite, mylonite and ultramylonite have been delineated (Fig. 22). This zonation is present both on the hanging and footwalls and is only represented within the basement units. This is due to the fact that only the basement rocks and quartzites exhibit a mylonitic fabric in which degrees of intensity can be determined. The metasediments responded in a manner producing a fabric similar to that produced in a normal regional deformational event, although obviously much more intense. Highly polished, grooved surfaces are observed in the most intense zones. A line delineates the outer boundary of the zone of metasediments affected by faulting (Fig. 22).

The protomylonite and mylonite zones are both wide, 1.0 - 1.2 kilometers and .5 - 1.0 kilometers, respectively, while ultramylonite zones are rather narrow (cms. to meters) and interspersed as thin, discontinuous zones within the mylonites. The latter are especially prevalent just along the fault trace, probably reflecting the zone of highest strain. Although the boundaries of protomylonite and mylonites subzones are marked as linear features as well, they are more gradational in nature. As indicated in the mylonitic classification, there is a

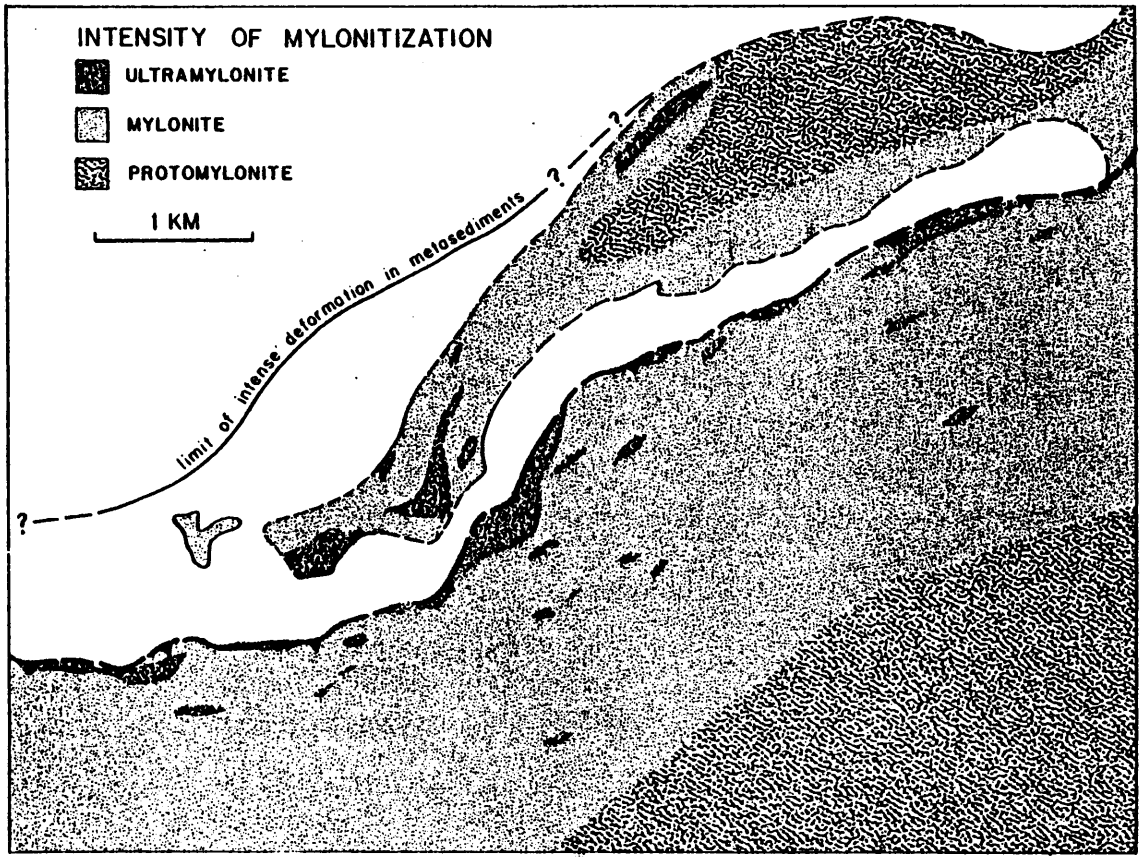

Fig. 22: Representation of zones of varying intensity of deformation across Fries Fault Zone

rather wide range of matrix proportions for the protomylonite and mylonite stages. Thus, to place a sharp, distinct boundary where the matrix proportion reaches a certain percentage is difficult. The boundaries indicated on the map are based upon outcrop and thin section observations. The ultramylonite zones, on the other hand, seem to have more distinct, sharp boundaries, but are actually gradational over centimeter distances. Thus, the nature of contacts may be similar, but appear to differ due to the scale of the zones. Clues to the nature of the ultramylonite zone boundaries and the general relationships with surrounding rocks, are evident in outcrop scale, where ultramylonite zones intermixed with mylonites are observed (Figs. 23-24). Herein, it seems that most of the intensely sheared zones are rather planar, with their boundaries parallel to subparallel to the mylonitc foliation in the surrounding rocks. These vary from centimeters to 2-3 meters in width.

It has been proposed (Ramsay and Graham, 1970) that foliation within a shear zone takes on a sigmoidal form and that smaller scale shear zones "anastomose in a way to enclose lozenge-shaped blocks of less deformed rocks" (Coward, 1976). The tectonic fabric within these blocks is at a high angle to the shear zone. Within the Fries fault zone, thin ultramylonites zones are recognized a distance away from the fault trace. This may be due to a number of factors, such as initial fine grain size of the rock, composition, level of folded fault trace with respect to the ground surface or inhomogeneity of the

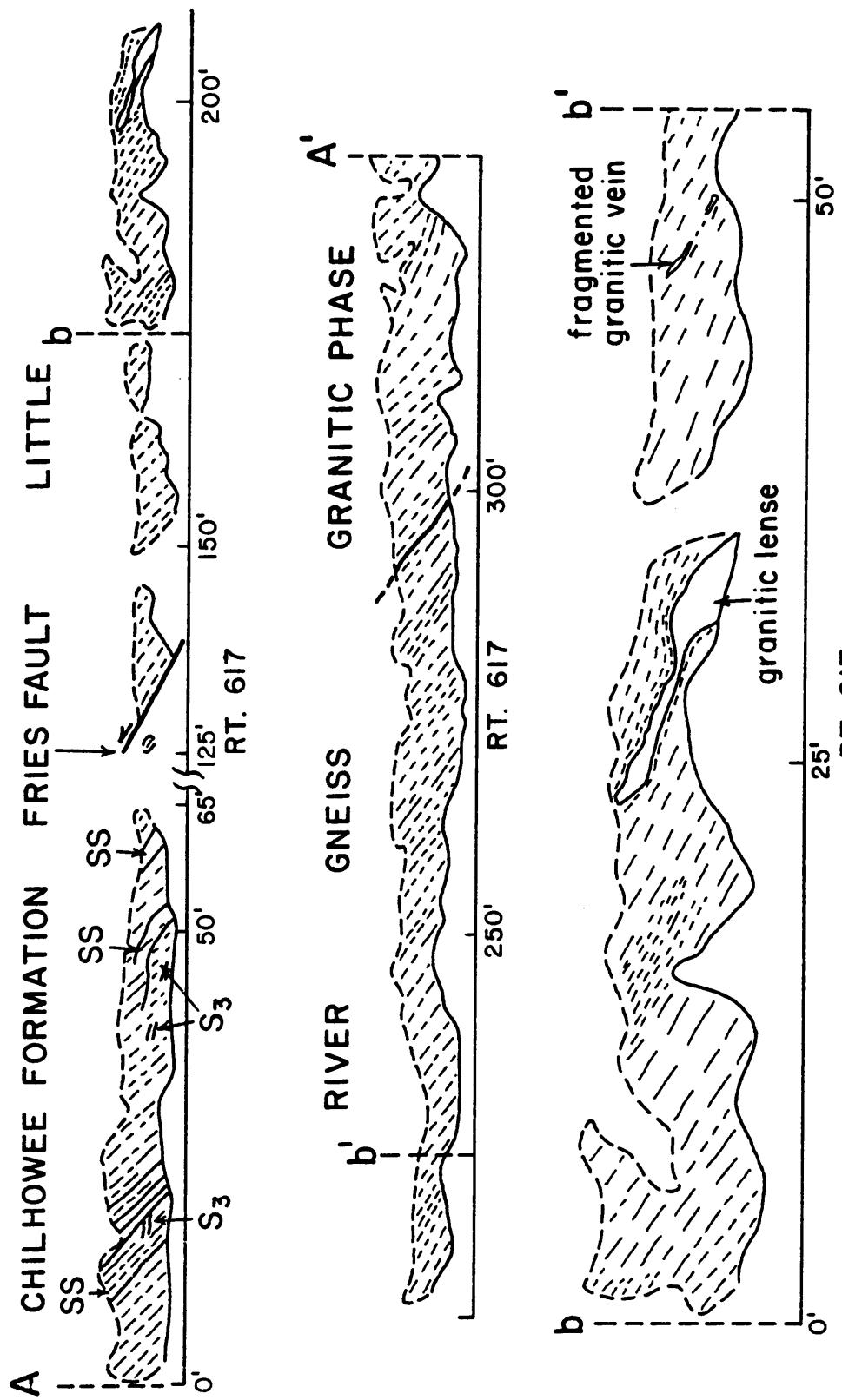

Fig. 23. Map of outcrop along Rt. 617 showing fault contact between Chilhowee Formation and Little River Gneiss, as well as variations in intensity of S_m/S_2. Note that zones of ultramylonite (short to medium dash) are parallel to surrounding mylonitic (long dash) fabric (see enlarged section b-b'). For location of A-A' see Appendix I. SS = metasandstone.

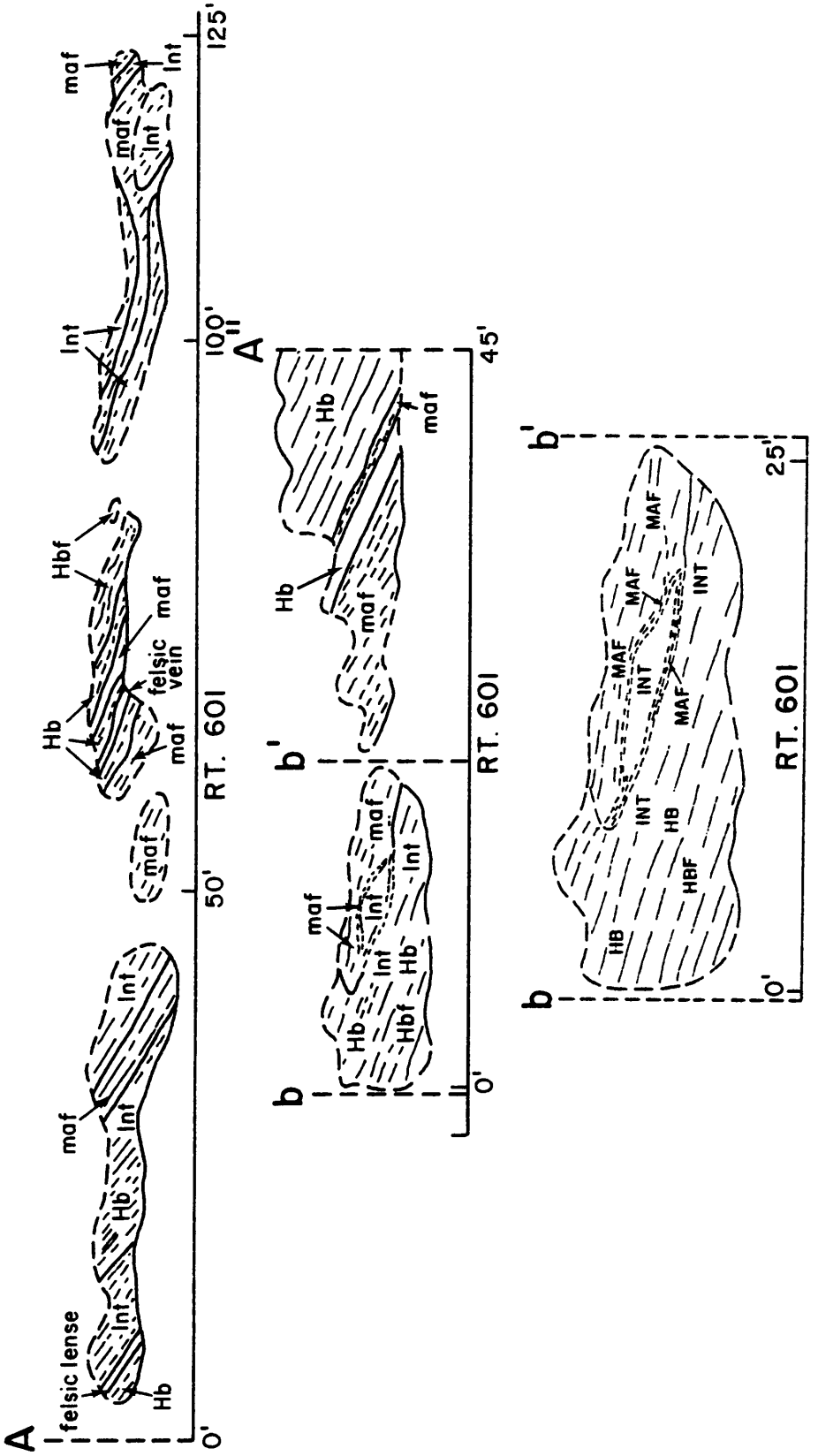

Fig. 24. Outcrop map showing variation in intensity of S_m in Pilot Gneiss and intermixed mafic dikes. Note anastomosing character of ultramylonite (short dash) in enlarged section b-b' (probably a function of composition herein). Int = intermixed Pilot and Mafics; Maf = mafic; Hb = hornblende-rich phase; Hbf = hornblende-free phase; For location of A-A" see Appendix I.

strain states reflected by the anastomosing character of the shear zone as described by Ramsay and Graham (1970). There is certainly variation in intensity across the zones, but from observations within the study area, this feature seem partly or mostly a function of initial fabric and compositional differences.

The degree and type of deformation and its development is dependent upon the initial lithology and pre-existing fabric of the deforming mass. Three different lithologies have been involved in the Fries Fault deformation. These are 1) a mica-rich, quartzo-feldspathic gneiss with an initial planar fabric (Little River Gneiss), 2) a mica-poor, quartzo-feldspathic gneiss with an initial sub-granoblastic texture (Pilot Gneiss), and 3) mica-rich metasediments with an initial well developed foliation (Chilhowee Group).

Within the Little River Gneiss, the zones of most intense deformation, as recognized in individual outcrops, seem to be parallel to subparallel to the foliation in surrounding rocks. This indicates that S_m fabric orientation is controlled by the orientation of S_1. Within the Pilot, however, due to its initial coarse grained nature, lack of micas and no pre-existing fabric, intense zones of "shearing" do anastomose locally (Fig. 24), and on the scale of a thin section, micas and epidote stringers anastomose in an irregular manner through fractured feldspars. S_m is not as well or as strongly developed in the Pilot, except near the fault trace where a well developed, banded mylonite is observed. Thus, the development, orientation and degree of anastomosing of shear zones appears dependent on the initial fabric of the rock and whether initial inhomogeneities exist.

On a megascopic scale, the protomylonite zone is represented by a little deformed, coarse to medium grained equivalent of the parent rock with a weak mylonitic foliation. In the Little River Gneiss (Figs. 25-26), S_m is parallel to subparallel to the primary gneissosity. Augen (1-3 cm) that appear to have grown during the mylonitization, are somewhat elongate parallel to the developing S_m fabric, are better defined, and are fractured at a high angle to the foliation. Biotite is still present in large amounts helping define the foliation as well as a lineation (l_1) that is at a slight angle to the quartz and feldspar elongation direction. In the mylonite zone, a very well developed mylonitic foliation and lineation is evident, the latter due to quartz and feldspar elongated down the dip of S_m. Cream colored feldspar augen in the Little River Gneiss are very well defined herein (Figs. 27-28), elliptically shaped, exhibit extensive fracturing at a high angle to S_m and are set in a finer grained quartz-mica matrix that "flows" or anastomoses around the augen. Quartz augen are less visible as they have been elongated to form ribbons that are partially to completely recrystallized. A weak biotite lineation is locally present and is either subparallel to or even perpendicular to l_m. This either represents the earlier l_1 or a post-mylonitic fabric element. Nearer the fault, large alkali porphyroblasts are recognized that are set in a very fine grained, almost ultramylonitic matrix (Fig. 28).

Mylonites, within the Pilot, although coarser grained due to the lack of micas and initial planar fabric, generally have a well developed mylonitic foliation defined by elongate pink feldspars and quartz

Fig. 25. Outcrop photo of non-mylonitized Little River Gneiss; sample #296 (see appendix).

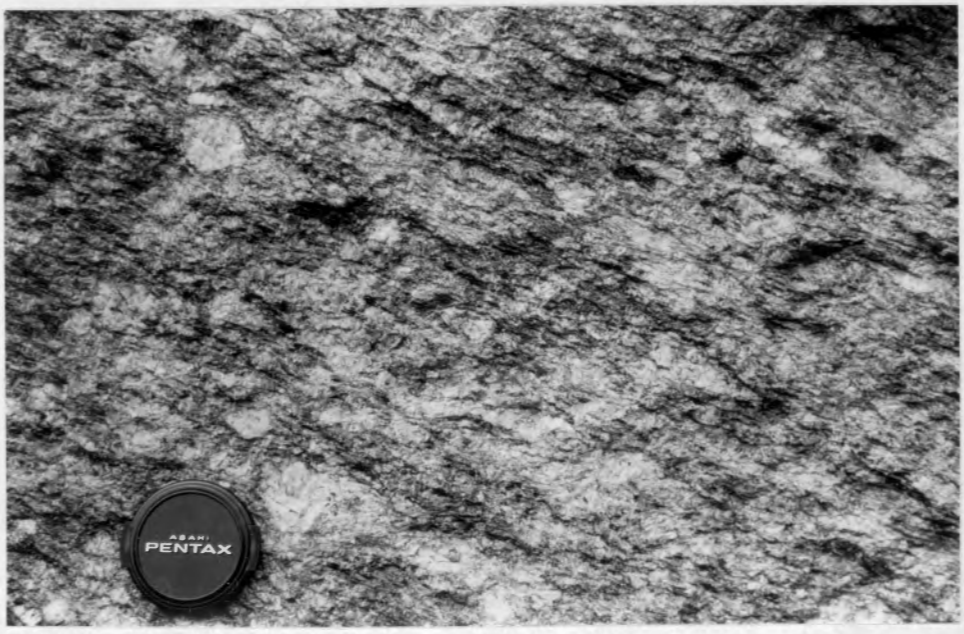

Fig. 26. Outcrop photo of protomylonite of Little River Gneiss; note augen more discrete and quartz elongated; sample #55 (see appendix).

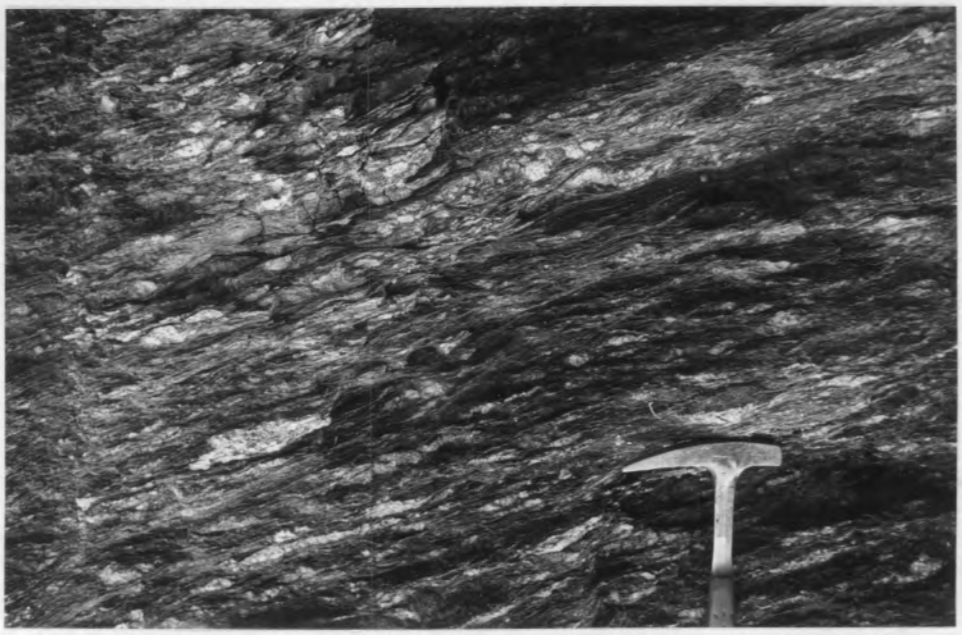

Fig. 27. Outcrop of mylonite of Little River Gneiss; note elongate augen and well developed mylonitic foliation; sample #I (see appendix).

Fig. 28. Mylonite zone of Little River Gneiss very near fault trace; note alkali feldspar porphyroblasts elongate in S_m plane; sample #B (see appendix).

alternating with light green epidote or epidote/actinolite rich bands. In the less mafic-rich phase (i.e., no hornblende), it is a cream colored rock with S_m defined only by elongate quartz and feldspar with minor sericite.

Ultramylonites in the Little River Gneiss (Fig. 29) are very fine grained, schistose rocks that are usually quite friable and micaceous. No large feldspar augen are visible except locally where the augen content may be as high as 5%. The foliation locally takes on an undulating character. The Pilot Gneiss overall is more coherent and less schistose in nature, although this is recognized locally just along the fault trace. S_m in the Pilot is either defined by alternating epidote and quartz-feldspar, or quartz-feldspar bands only, the former giving the rock a light green and pink/cream banded appearance (see Figs. 59-61).

II. Microstructure

Studies of ductile faulting and the development of mylonites has come to the forefront of research in structural geology over the past few years primarily due to experimental deformation studies and transmission electron microscopy (TEM) investigation. Both have been used to interpret those deformation mechanisms which operate in ductile deformation zones, and have shown that their deformation fabrics are dependent on temperature, stress, strain rate and amount of bulk strain. Analysis and documentation of microstructure and related strain can, therefore, yield clues to these variable within specific fault zones such as the Fries DDZ.

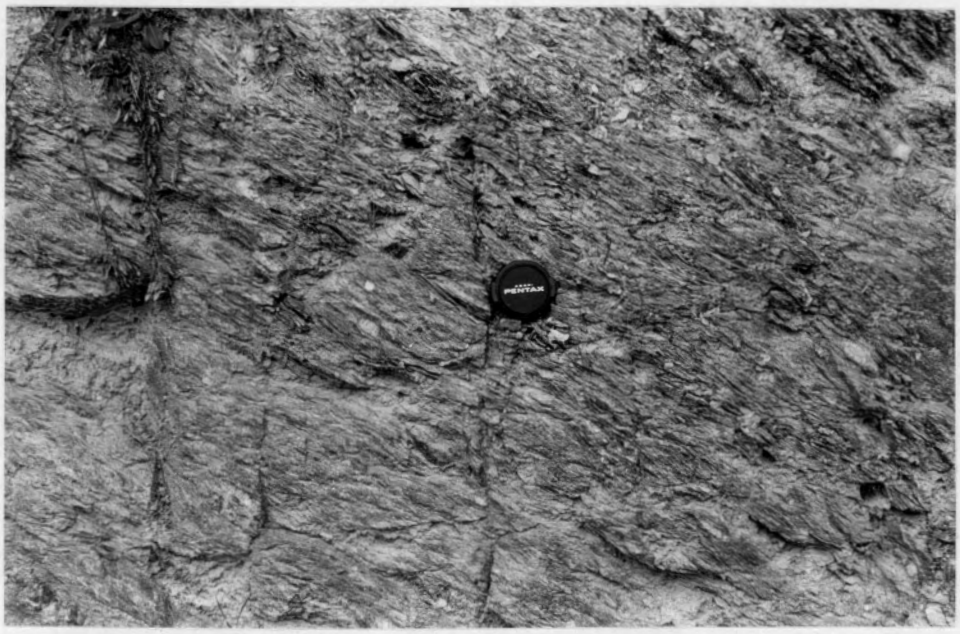

Fig. 29. Outcrop photo of ultramylonite of Little River Gneiss; now a very friable, phyllitic rock with some relict augen still noticeable locally; location is just at fault contact; sample #F-15, (see appendix).

At the grain scale, progressive or continuous deformation of quartz, plagioclase and alkali feldspar through zones of increasing deformational intensity associated with the Fries DDZ, is partly responsible for gross overall changes in fabric and consequent development of a mylonitic foliation. Although differences do exist in response to the deformation within each unit, as previously stated, grain scale deformation processes are the same (i.e., ductile in quartz vs. ductile/brittle in feldspars). The deformation of these minerals can be shown in greatest detail in the Little River Gneiss, due to good exposure and coverage across the entire fault zone. Micas and amphiboles responded to the deformation primarily by taking part in chemical reactions and this will be discussed in detail in a later section. Some fracturing of the amphibole is evident locally.

Little River Gneiss

The unmylonitized Little River Gneiss is a medium to coarse grained rock composed of alternating quartzo-feldspathic and mica-rich layers with small, indiscrete, augen of intergrown alkali feldspar, plagioclase and quartz (Figs. 30-32). The dominant size range (Fig. 33a) is .1 - 1.0 mm (70%) with 13% greater than 5.0 mm, the latter being the augen. Figs. 33 b, c, and d show this ratio as well for invidivual minerals within the matrix.

Quartz is present as relict grains, primarily .1 - .5 mm in size (Fig. 33b) and as recrystallized and normal grains, the latter a product of the early Paleozoic metamorphism (Figs. 32). The relict grains have irregular grain boundaries, exhibit undulose extinction

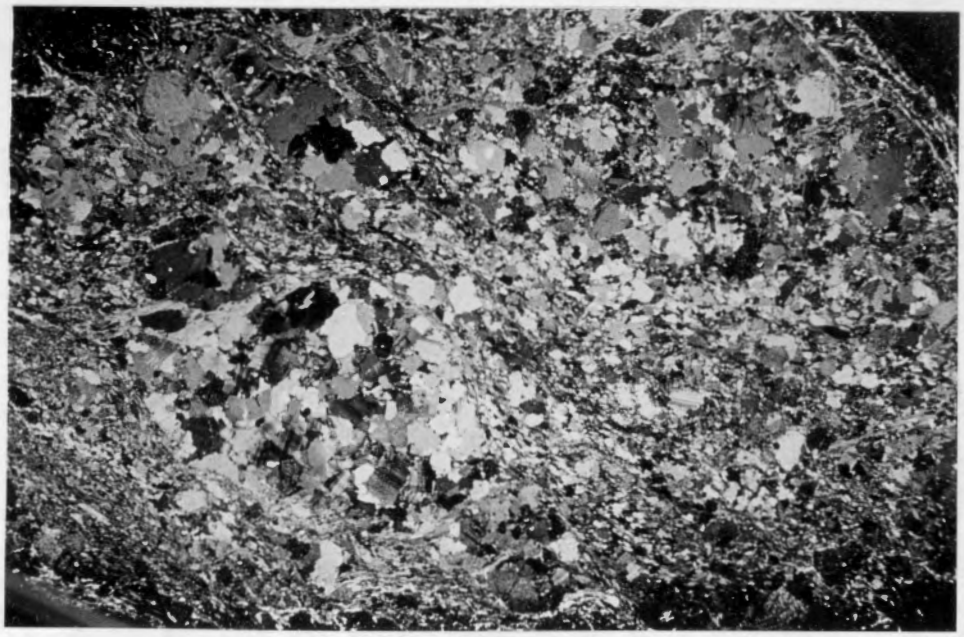

Fig. 30. Thin section of non-mylonitized Little River Gneiss; note semispherical augen consisting of a mosaic of quartz, plagioclase and alkali feldspar; 1 cm = 2.1 mm, sample #296 (see appendix).

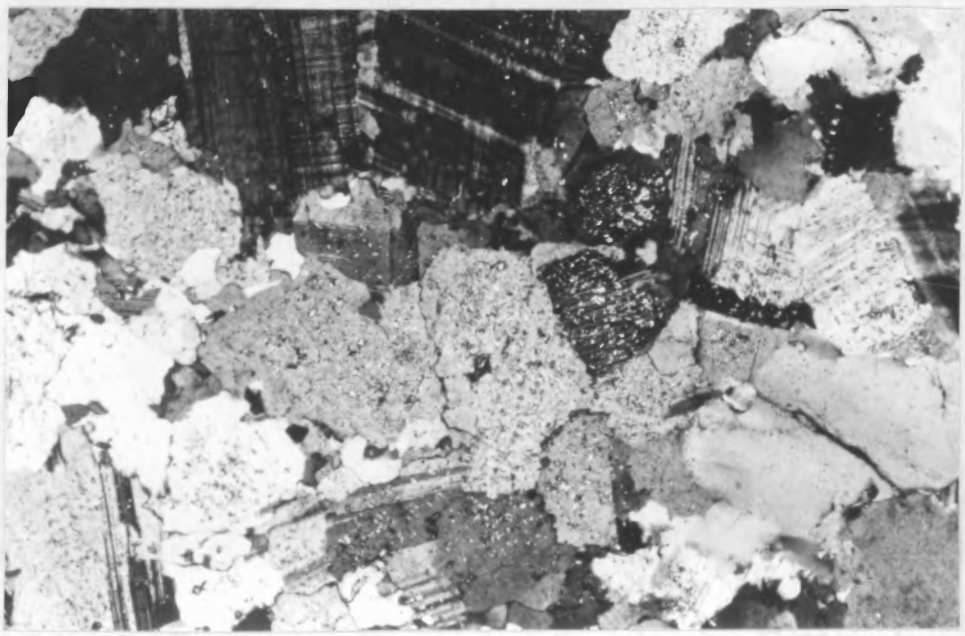

Fig. 31. Close up of augen in above photo, 1 cm = .29 mm.

Fig. 32. Thin section of non-mylonitized Little River Gneiss showing close up of matrix; S_1 foliation defined by large biotites and muscovites; 1 cm = .29 mm, sample #296 (see appendix).

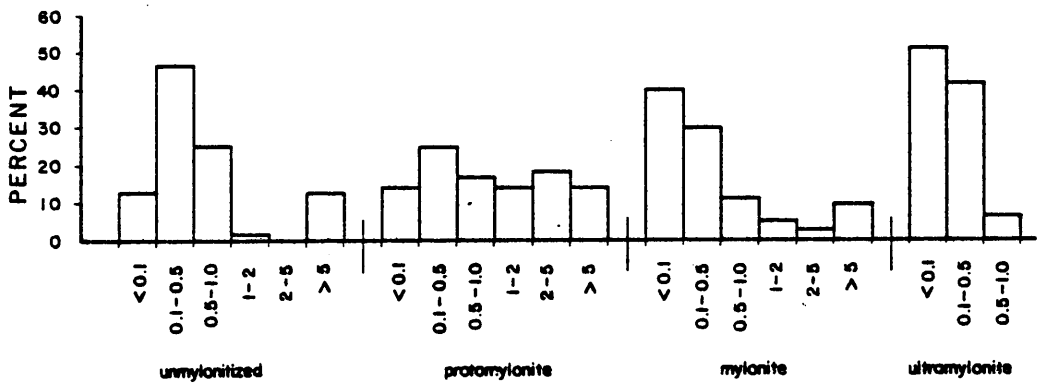

Fig. 33a: Whole rock grain size variation across fault zone (based on point counts of 10 samples, #'s 11, 14a, 14b, 42, 55, 95, 190, 236, 296, 331; see appendix).

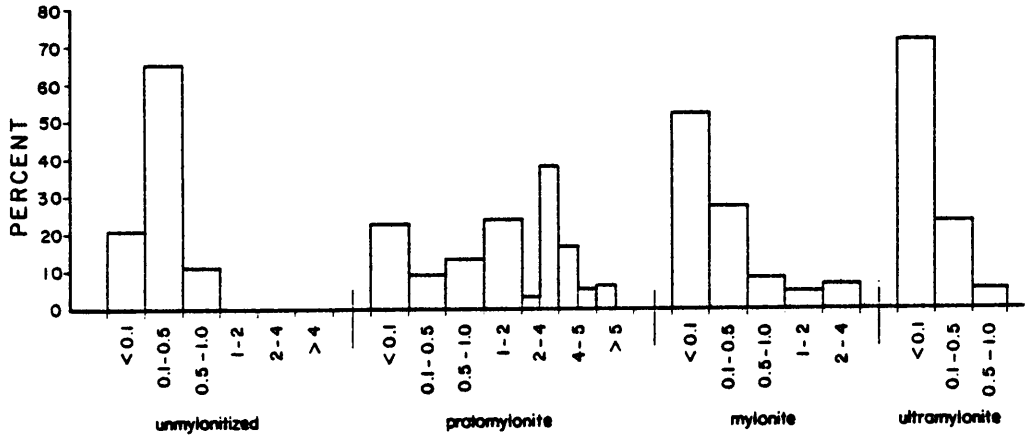

Fig. 33b: Quartz grain size variation across fault zone

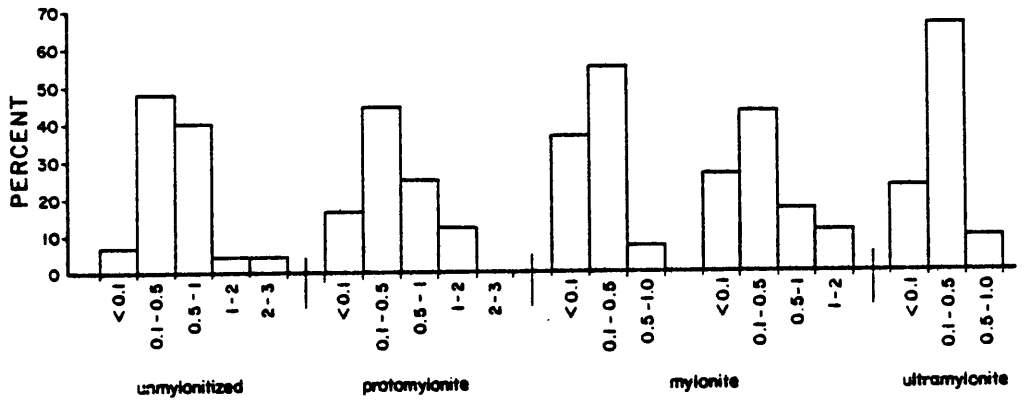

Fig. 33c: Plagioclase grain size variation across fault zone

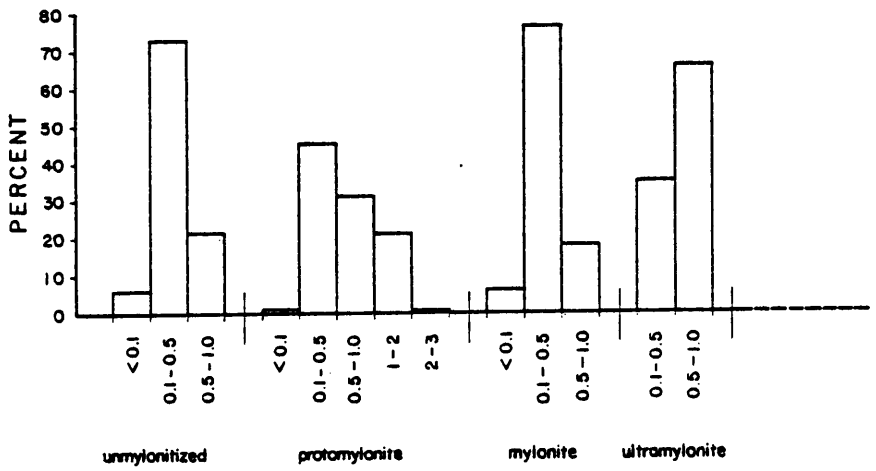

Fig. 33d: Alkali feldspar grain size variation across fault zone

and grade into recrystallized zones wherein high angle boundaries are common. About 5% of the quartz is recrystallized to an average size of 20-60 microns which are fairly equant, although grains up to .1 - .3 mm are also recognized. In one sample, recrystallization is as high as 25%. Normal grain growth is quite prevalent as well (5-15%), ranging in size from .15 up to .3 mm in an interlocking aggregate framework. These are either non-strained or very weakly strained and most show no shape preferred orientation except where present within biotite zones. In the latter, quartz may have aspect ratios up to 2:1 and the biotite is obviously a controlling factor in grain growth and shape.

Perthitic feldspar and minor microcline within the matrix are dominantly .1 - 1.0 mm in size (Fig. 33d), subhedral, strained grains, without much alteration and no apparent fracturing. It is also present as part of the larger augen wherein it is intergrown with quartz and plagioclase (Figs. 30-31).

Plagioclase crystals are .5 - 1.0 mm (Fig. 33c), subhedral grains present in an interlocking aggregate framework. Albite with clear albite twins is common as is antiperthite. Straining is not obvious and only minor recrystallization (40-70 microns) and alteration to sericite and epidote is apparent.

Protomylonite Subzone

The development of S_m is not extensive and appears subparallel to S_1. The whole rock grain size (Fig. 33a) spans a greater size range with all ranges represented fairly equally. This is primarily a function of quartz elongation and some fracturing and disaggregation

of the larger augen or grains (Figs. 34-35).

Quartz deformation is characterized by ductile yielding, recovery and recrystallization processes. Elongation of grains parallel to S_m is evident with length to width ratios primarily 2:1 - 3:1 and a few up to 4:1 - 6:1. These are highly strained, exhibiting undulose extinction, deformation lamellae and some deformation bands that are normally at a high angle to the developing foliation, i.e., between 45 and 90°. In a few, however, deformation bands change orientation from this angle to near parallelism with S_m/S_1. The sense of rotation is toward the foliation. These elongate quartz take on an undulating character due to deflection around more resistant feldspars, and some exhibit thickening and thinning as well, similar to boudinage, with recrystallization in the thinned regions. It is more elongate within more mica-rich parts where obstructions are less evident. Subgrains with serrate boundaries comprise 20-30% of the quartz content and these usually have a preferred orientation parallel to S_m/S_1. Where deformation bands parallel S_m (minor), there has been near complete subgrain development. Recrystallization is minor (8-9%) (Fig. 36) and most prevalent within pressure shadows of larger grains, where the average size is 40-50 microns; and along grain boundaries, where a smaller recrystallized grain size (20-30 microns) is observed.

Perthitic feldspar are present as subhedral to anhedral grains, both within augen and within the matrix, although in minor amounts in the latter. In the matrix, they are highly strained and have an average size of .1 - 1.0 mm (Fig. 33d). Some of these are segments of

Fig. 34. Protomylonite matrix of Little River Gneiss; elongate quartz, fractured alkali feldspar and minor recrystallization apparent; 1 cm = 2.5 mm, sample #55 (see appendix).

Fig. 35. Protomylonite matrix (Little River Gneiss) of quartz, feldspar and micas that are deflected around larger alkali feldspar augen which is fractured at a high angle to S_m; 1 cm = 2.4 mm, sample #42 (see appendix).

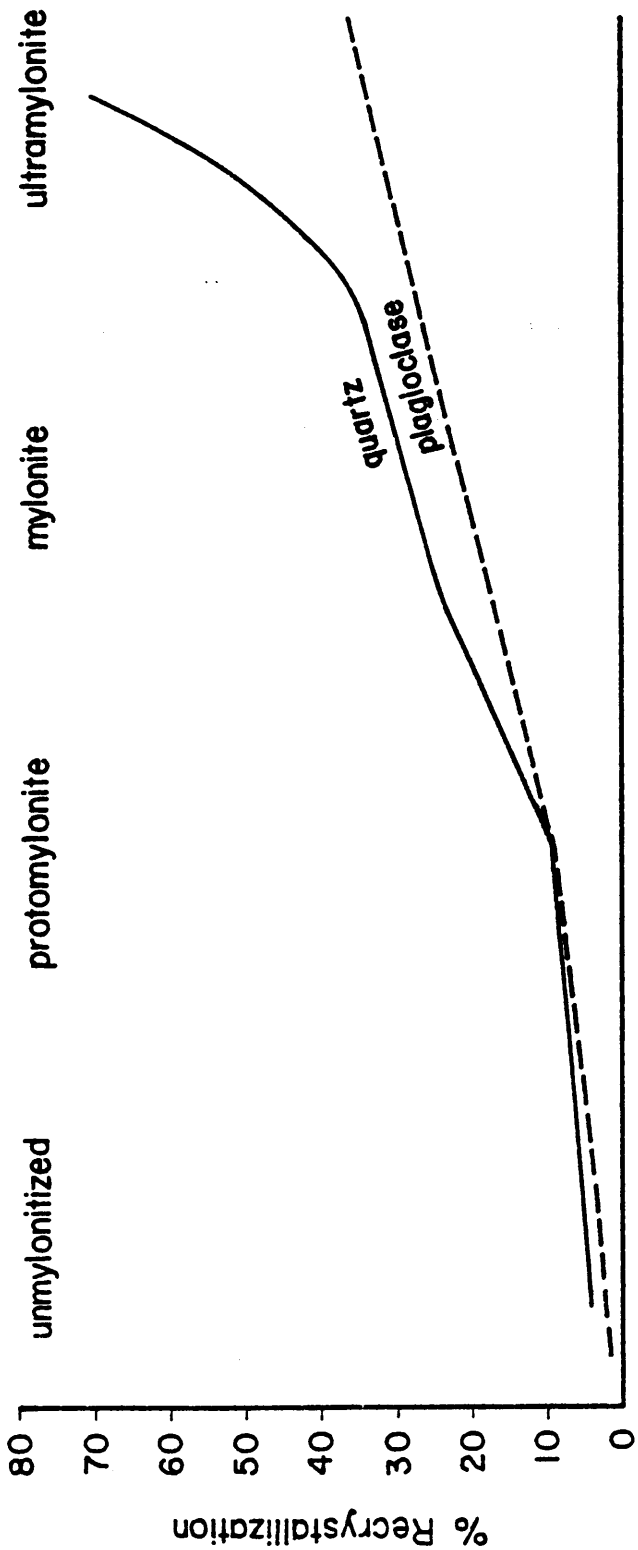

Fig. 36: Progressive recrystallization of quartz and plagioclase across fault zone.

once larger grains that were fractured and disaggregated. Fracturing is somewhat a function of size, not too apparent in the smaller grains, while in the larger grains (2.5 mm) becoming rather extensive and oriented at a high angle to the foliation. Conjugate sets are recognized in this early stage as well (Fig. 37). Recrystallization is minor.

Relict plagioclase grains are anhedral to subhedral, primarily .1 - 1.0 mm in size (but may reach 2.5 - 3 mm) (Fig. 33c), most of which have undergone extensive alteration to sericite and epidote. Twinning is not always apparent, but albite and pericline types are observed. Primary deformational features are intense straining, with kinking and minor fracturing, the latter followed by extension and rotation of grains in the S_m plane. Minor recrystallization and subgrain development has occurred along kink bands and recrystallization between fractured and extended segments. Both plagioclase and alkali feldspar are intergrown with quartz in augen pods.

Mylonite Subzone

Within this zone the rock consists of a fine grained matrix of micas, quartz, plagioclase and alkali feldspar with well defined,, dominantly alkali feldspar augen (Figs. 38-39). The whole rock grain size shifts herein to a dominant size range of less than .1 mm up to .5 mm (Fig. 33a), primarily due to extensive recrystallization and fracturing and disaggregation of grains.

Only a few relict quartz remain, present as anhedral, highly strained grains about 1.5 up to 2 mm average size, with some up to

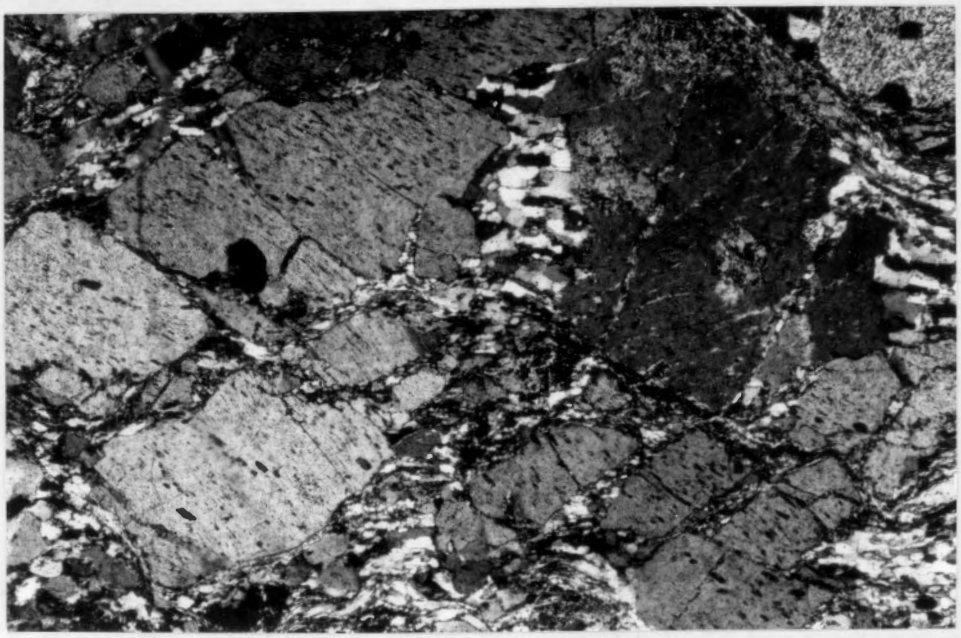

Fig. 37. Protomylonite of Little River Gneiss; Fractured and disaggregated perthitic feldspar with recrystallization of quartz with a dimensional preferred orientation between fractured segments; 1 cm = .18 mm, sample #55 (see appendix).

Fig. 38. Mylonite (Little River Gneiss) matrix of finer, largely recrystallized quartz, feldspars and micas with alkali feldspar augen fractured at a high angle to and elongate parallel to S_m; 1 cm = 2.4 mm, sample #11 (see appendix).

Fig. 39. Mylonite (Little River Gneiss) showing fine grained matrix defined by alternating mica and quartzo-feldspathic rich layers; 1 cm = 2.1 mm, sample #95 (see appendix).

3 to 4 mm in length (Fig. 33b). Only a few retain their original shape. The larger grains may have Boehm lamellae perpendicular to or at a high angle to S_m and minute inclusions parallel to the same. Most of these, however, have been quite elongated parallel to and are now helping to define S_m with length to width ratios of 3:1 to 5:1. These elongate ribbons exhibit microboudinage and, commonly, deformation bands normally oriented at a high angle (near or equal to 45°) to the foliation, although some are parallel as well. Within the latter, subgrain development with a shape preferred orientation is apparent and recrystallization common along deformation band boundaries. These ribbons thin considerably around the larger augen and within these zones recrystallization is much more extensive (Figs. 40-41 and 42). The larger relict grains grade out at their boundaries and laterally into pressure shadows composed dominantly of subgrains with a preferred orientation parallel to S_m (2:1) (Fig. 43) and then into recrystallized matrix (25-35 microns) (i.e., pressure shadows become part of the matrix.

Quartz is primarily present, however, as finely recrystallized grains (average 20-40 microns), comprising 35-50% of the quartz content and making up of the finer matrix. Many of these recrystallized grains are unstrained with no shape preferred orientation, although this is a nearly ubiquitous feature within the mica-rich zones where aspect ratios range from 2:1 to 3:1. These represent recrystallization of quartzose ribbons and a few recrystallized zones still outline the relict ribbon shape. In regions where little or no mica is present,

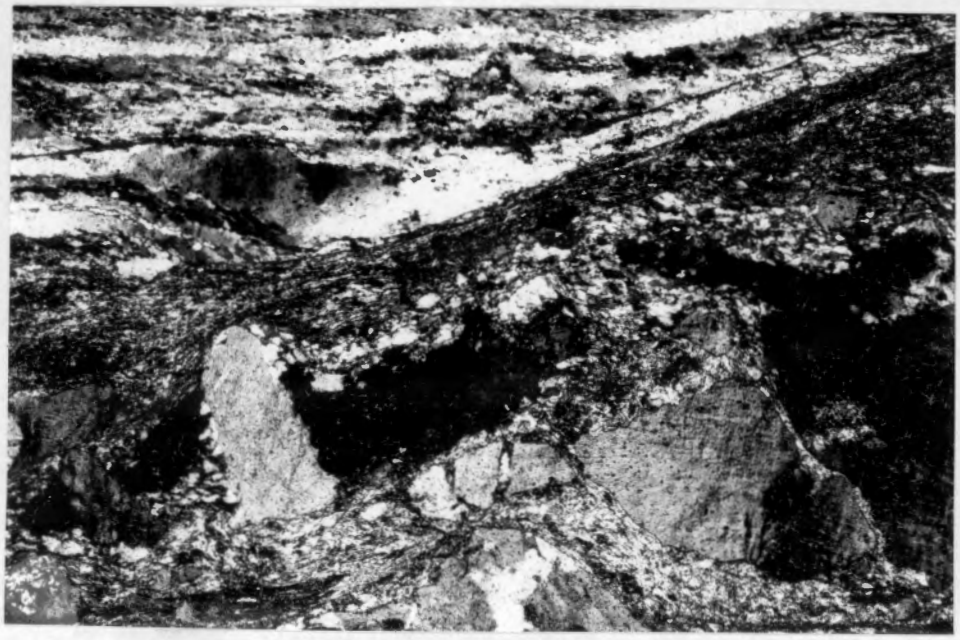

Fig. 40. Mylonite of Little River Gneiss showing elongate quartz ribbons with deformation bands parallel to S_m and recrystallization along deformation band boundaries, note thinning and deflection around augen pod; 1 cm = .18 mm, sample #B-11.

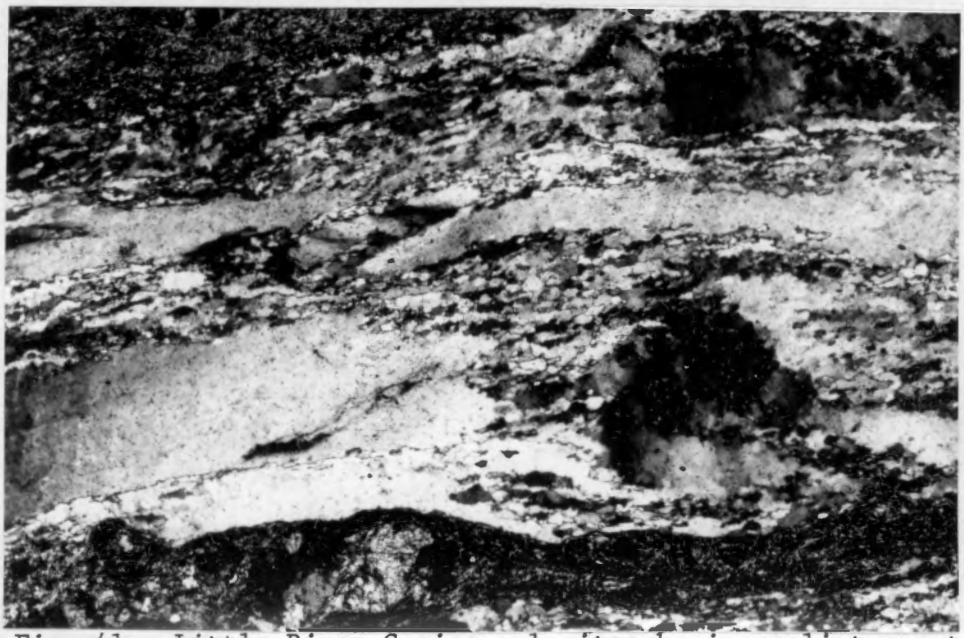

Fig. 41. Little River Gneiss mylonite showing relict quartz augen in center recrystallized quartz along deformation band boundaries; 1 cm = .18 mm, sample #B-2(2) (see appendix).

Fig. 42. Quartzose stringers thinned around augen in mylonite of Little River Gneiss with subgrains and recrystallized grains have a shape preferred orientation parallel to S_m; 1 cm = .12 mm, sample #I-5 (see appendix).

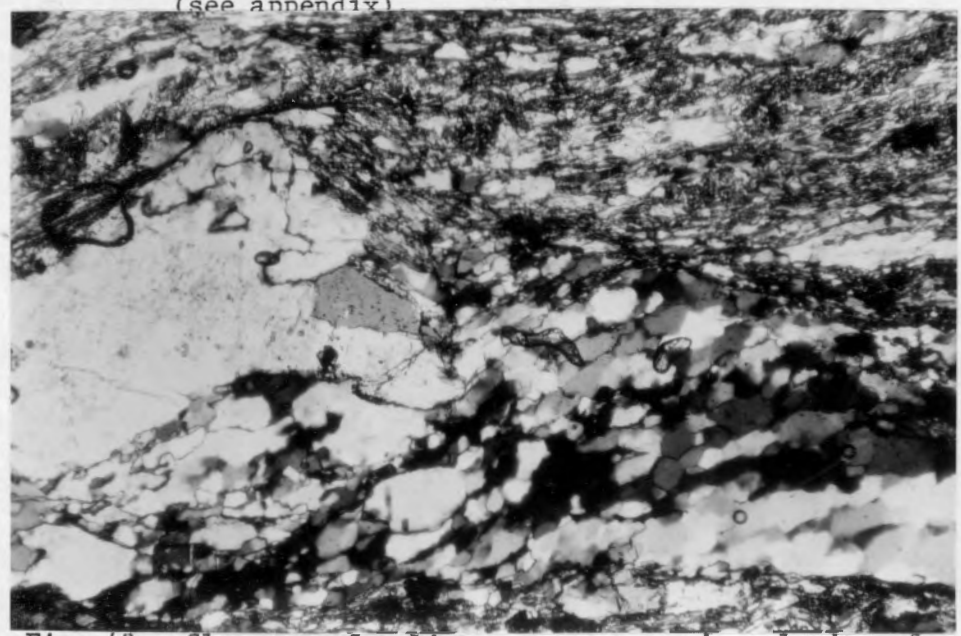

Fig. 43. Close up of relict quartz augen in mylonite of Little River Gneiss, grading into elongate quartz ribbon composed of subgrains and recrystallized grains of quartz; 1 cm = .1 mm, sample #100 (see appendix).

polygonal boundaries are common (20-40 microns). Recrystallization is quite extensive as well within pressure shadows of larger alkali feldspar augen, the recrystallized grain size being somewhat larger herein (up to 50-60 microns). These have a preferred orientation and are unstrained or only weakly strained. Normal grain growth (up to 10%) is observed primarily within mica-rich zones that average 70 - 100 microns, but may get up to .1 to .15 mm in size. The latter are usually strained and have a shape preferred orientation that is parallel to S_m.

Quartz ribbons with aspect ratios up to 12:1 and even as much as 20:1 occur in rocks closer to the fault contact (Figs. 44 and 45). These are highly strained and exhibit microboudinage. Deformation bands become more intense and increasingly parallel to S_m, although some may be oriented as high as 30° to the foliation. Most of these have undergone complete subgrain development with a preferred orientation and extensive recrystallization (20-30 microns) along grain and deformation band boundaries. Most of these newly recrystallized grains are inequant with a preferred orientation parallel to S_m, indicating syntectonic recrystallization. The ultimate product is, thus, stringers or ribbons of recrystallized quartz alternating with thin mica-rich zones (Fig. 44). Quartz is present within augen pods as well.

Perthitic feldspar and minor microcline within the matrix are about .3 - 1.0 mm in size with some as large as 2 - 3.5 mm (Fig. 33d), anhedral, strained grains set in an even finer matrix and with pressure shadows of recrystallized quartz (average size is 25-40 microns, but

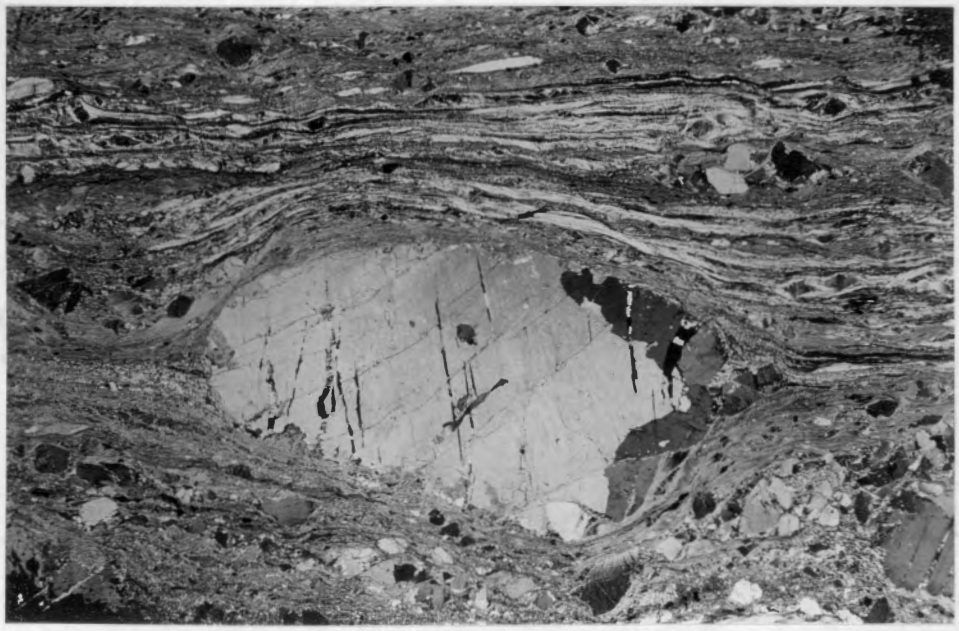

Fig. 44. Mylonitic matrix of Little River Gneiss defined by highly elongate quartzose stringers alternating with mica-rich and quartzo-feldspathic-rich zones; large potassium feldspar porphyroblast with conjugate microfractures in center; 1 cm = 3 mm, sample #B-2(4) (see appendix).

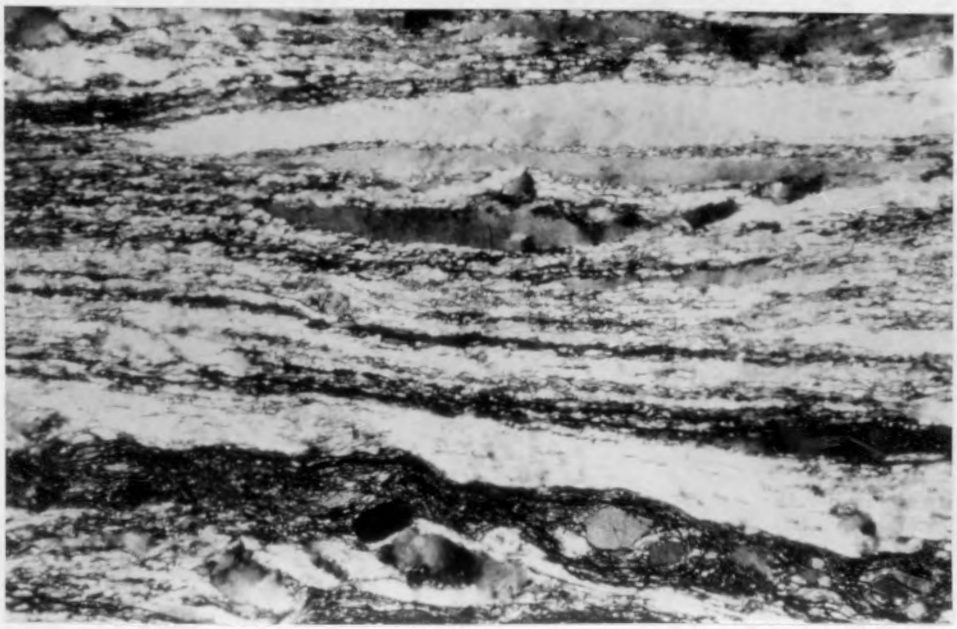

Fig. 45. Close up of mylonitic matrix of Fig. 44 showing quartzose stringers with recrystallization along deformation band boundaries; 1 cm = .27 mm, sample #B-2(4) (see appendix).

may get up to 60 microns). The majority of these small alkali feldspar grains were probably once part of a larger grain or augen that has been fractured, disaggregated and strung out parallel to S_m. In turn, some of these smaller grains have themselves undergone the same process. Alkali feldspar is primarily present, however, as large augen up to 4-5 cm in length by about 1.5-2 cm in width, forming a mylonitic lineation, l_m, down the dip of S_m (Figs. 44 and 46). Most of these are porphyroblasts obviously formed during faulting (Fig. 44). These have been fractured and have undergone offset parallel to these fractures in a stair-step fashion and/or subsequent extension combined with rotation, producing disaggregated grains (1.2-1.5 mm) strung out parallel to S_m (Figs. 47-49). These are highly strained. Recrystallized quartz is extensive within pressure shadows and between extended, fractured segments (fiber growth) (Figs. 48 and 50). With continued fracturing and disaggregation the grains eventually become part of the matrix. Fig. 51 shows a variety of natural deformation features recognized in the alkali feldspar.

Plagioclases are present as a few, relatively large (1.5-3.0 mm), relict grains, some of which are highly sericitized with faint albite twinning still visible. These are strained and grade laterally into pressure shadows of recrystallized albite (30 microns). Most are present, however, as smaller (.1-1.5 mm with an average of .5-.8 mm), anhedral, strained, untwinned to twinned grains set in a finer mica matrix. The latter have undergone extensive alteration to epidote and sericite, usually associated with extensive recrystallization

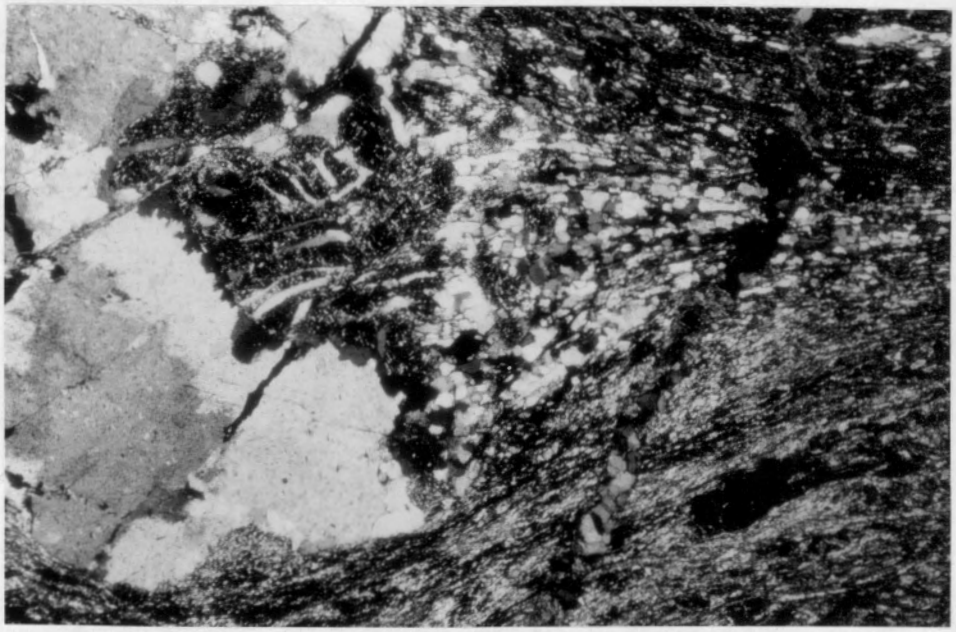

Fig. 46. Alkali feldspar augen with myrmekitic intergrowths and pressure shadow of recrystallized quartz; 1 cm = .27 mm, sample #102 (see appendix).

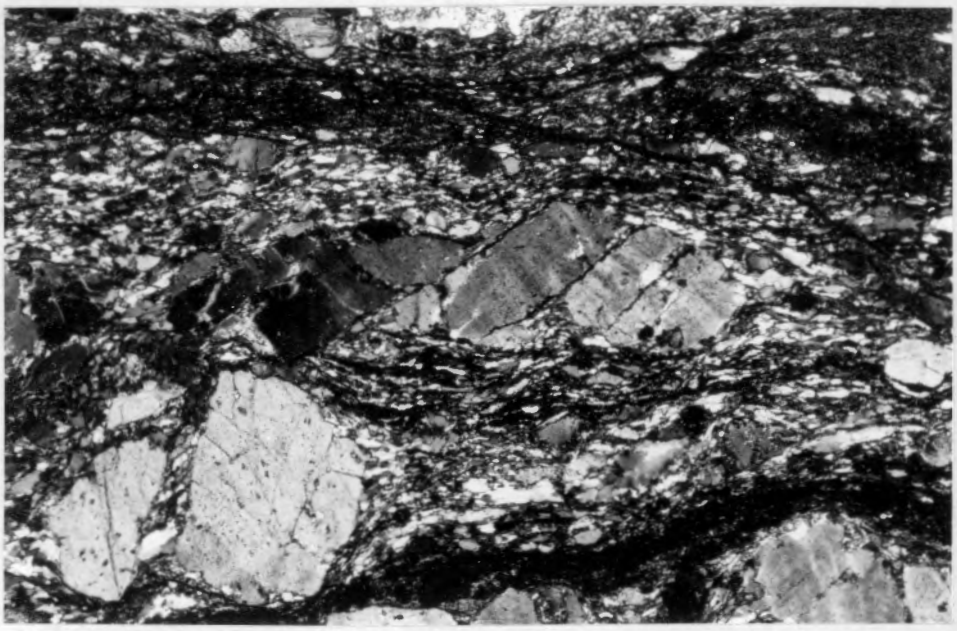

Fig. 47. Alkali feldspar fractured at a high angle to S_m and with dextral displacement parallel to micro-fractures; 1 cm = .28 mm, sample #98 (see appendix).

Fig. 48. Alkali feldspar fractured at a high angle to S_m with some disaggregation evident (granitic phase of Little River Gneiss); 1 cm = .27 mm, sample #F-18a (see appendix).

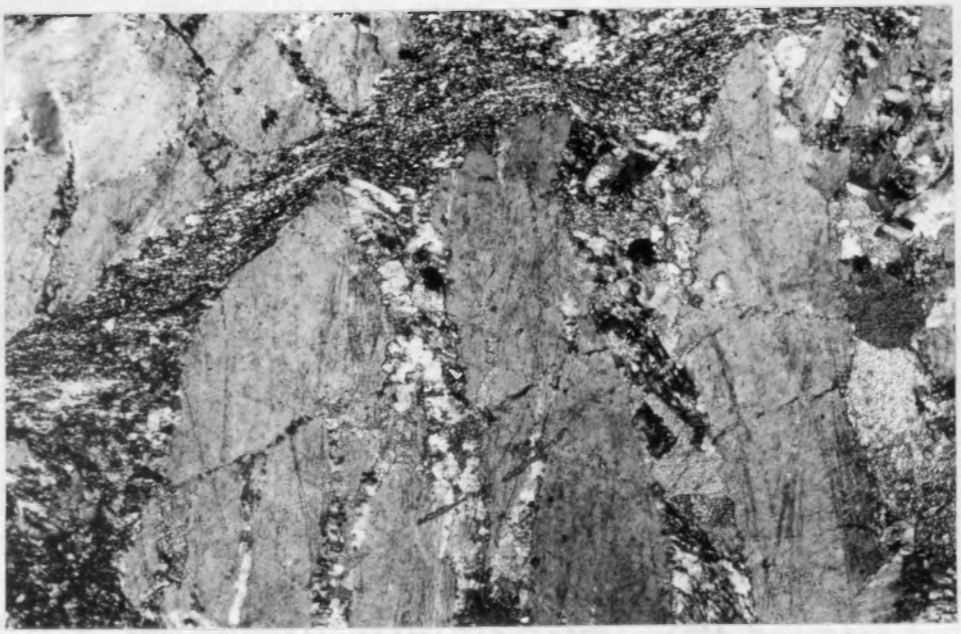

Fig. 49. Fractures in alkali feldspar at a high angle to S_m (Pilot Gneiss, mylonite); 1 cm = .32 mm, sample #E-1(5a) (see appendix).

Fig. 50. Quartz fiber growth along fracture in alkali feldspar augen, dark areas are biotite; 1 cm = .1 mm, sample #B-18 (see appendix).

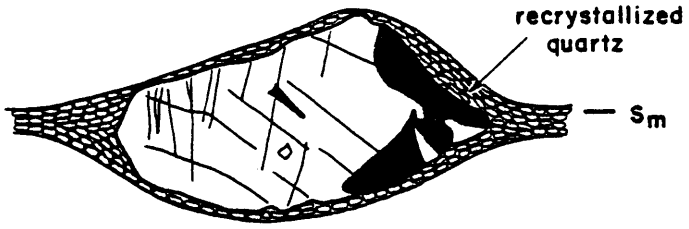

Conjugate fracture sets at high angle to S_m

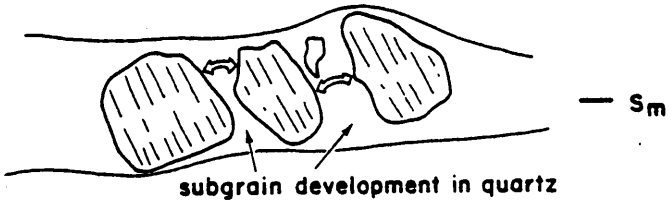

Fracturing and extension by rotation of segments

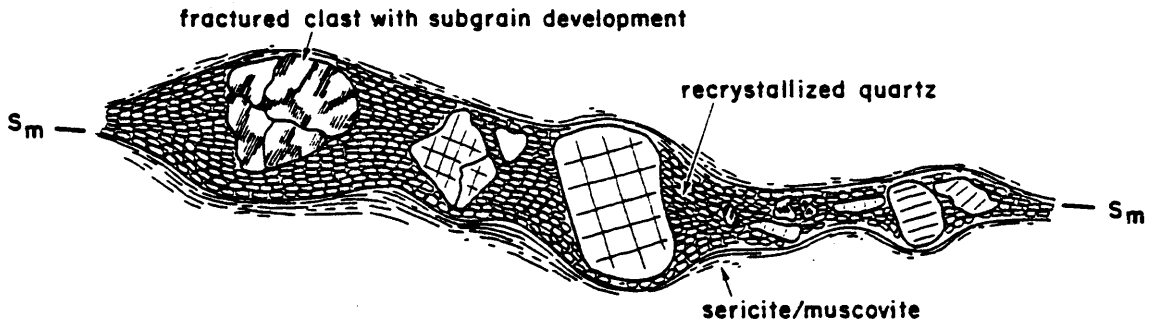

Fractured and disaggregated perthite/microcline strung out extensively, defining the l_m lineation on S_m surface

Fig. 51: Natural Deformation Features of Potash Feldspar

(20-40 microns). These recrystallized grains have a shape preferred orientation parallel to S_m that is seemingly controlled by mica distribution. Quite often, altered regions grade across rather diffuse grain boundaries into a very finely recrystallized (fairly equant) matrix, so that outlines of the relict plagioclase grains are imperceptible. Plagioclase has undergone minor fracturing (Fig. 52) accompanied by offset and/or extension and rotation of grains, but deforms primarily by straining and kinking at a high angle to S_m (Fig. 53). The latter is accompanied by recrystallization and subgrain development along kink bands (Fig. 54). Once recrystallization has progressed far enough along kink band zones, the grain has the same appearance as if it had been fractured and extended/dissociated with recrystallization between extended segments. It is thus difficult to tell what the initial process was, but kinking and recrystallization seems to dominate. Fig. 55 depicts a variety of brittle deformation features of plagioclase observed in thin section.

Ultramylonite

The ultramylonites (greater than 95% matrix) are very fine grained, well foliated, phyllitic rocks consisting of alternating mica-rich and quartzo-feldspathic-rich layers. Augen are absent except for a very few plagioclase porphyroclasts observed locally (Figs. 56-57). 90% of the grains fall in the size range of less than .1 mm up to .5 mm (Fig. 33a).

65-70% of the quartz is recrystallized and has a grain size of 20-30 microns (Figs. 56-58). These are fairly equant and relatively

Fig. 52. Offset twin planes along microfracture in plagioclase (Little River Gneiss); 1 cm = .04 mm, sample #44 (see appendix).

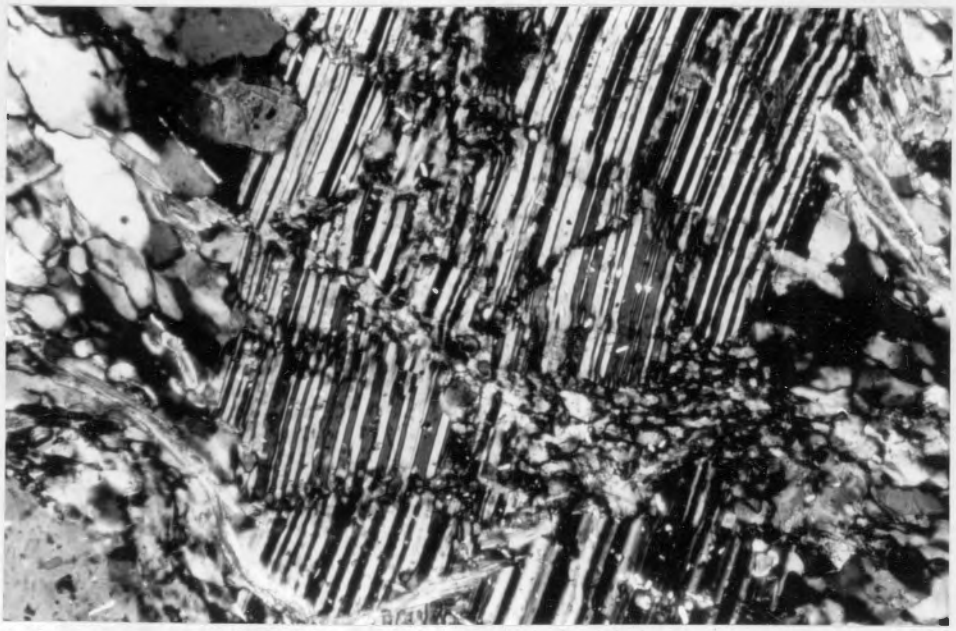

Fig. 53. Kinking of plagioclase grain with recrystallization along kink bands, mylonite zone; 1 cm = .04 mm, sample #35 (see appendix).

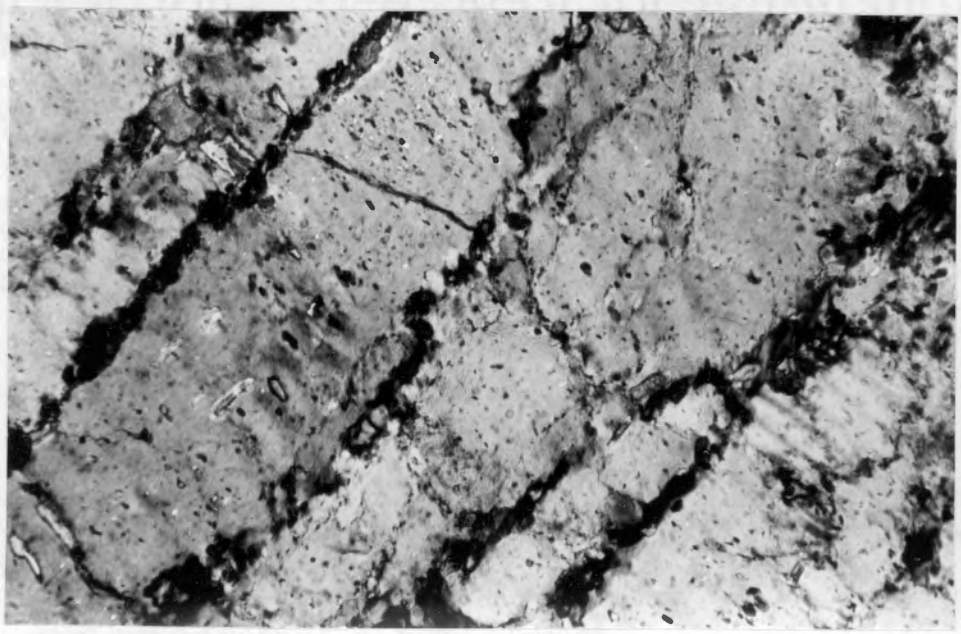

Fig. 54. Close up of kink band boundaries in plagioclase grain showing nucleation of new grains; 1 cm = .005 mm.

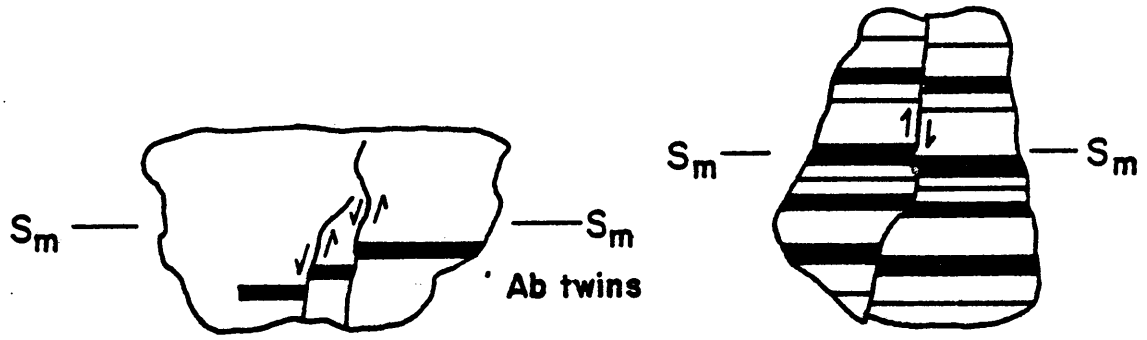

Fracturing and offset of Ab twins in a plagioclase grain

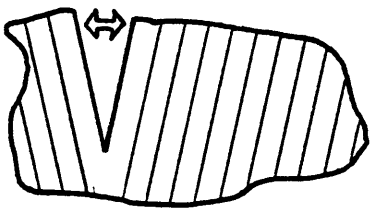

Fractured plagioclase grain with extension component due to rotation

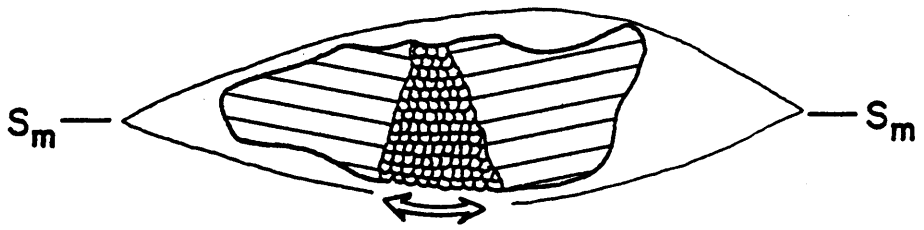

Fractured, extended and recrystallization

Fig. 55: Typical brittle deformation features observed in plagioclase in the mylonitic rocks.

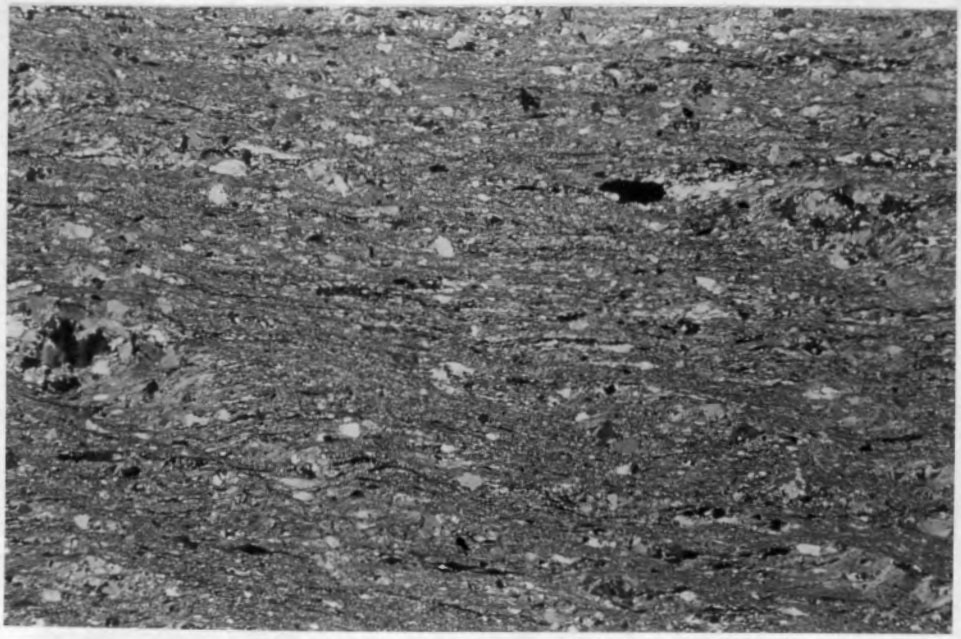

Fig. 56. Ultramylonite matrix of Little River Gneiss defined by fine grained, recrystallized quartz and plagioclase alternating with mica rich zones; a few relict, strained quartz grains still present (left - center); 1 cm = 2.2 mm, sample #100 (see appendix).

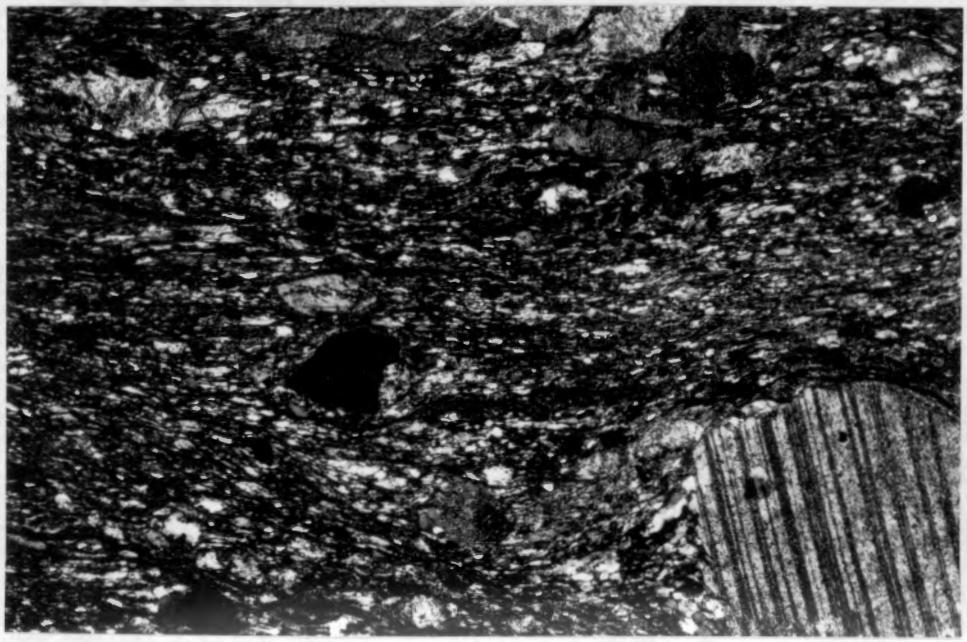

Fig. 57. Ultramylonite matrix of Little River Gneiss with plagioclase porphyroclast in lower right corner; 1 cm = .28 mm, sample #F-15 (see appendix).

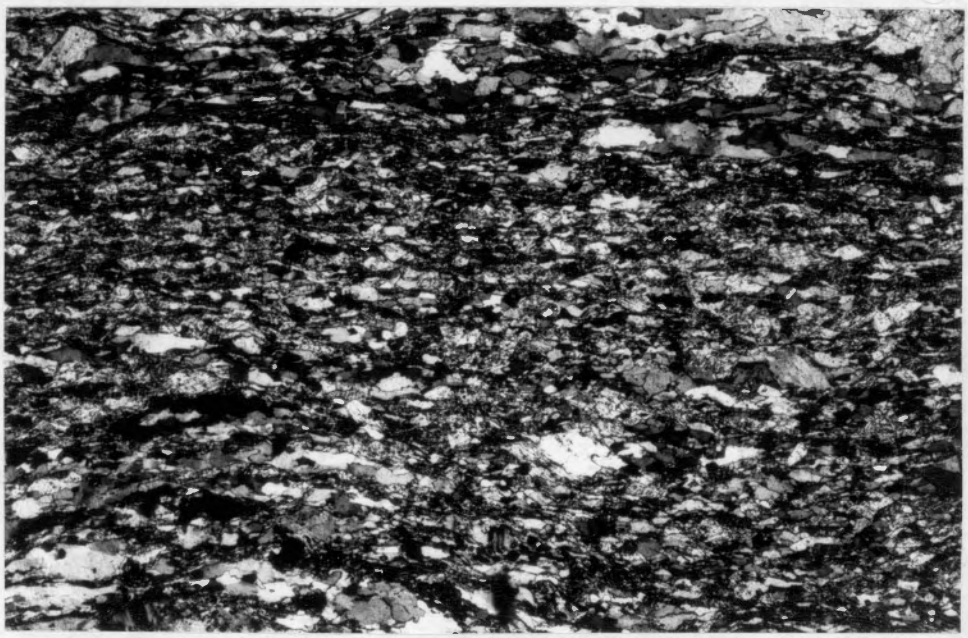

Fig. 58: Ultramylonite matrix in which quartz is largely recrystallized, and a few relict feldspar grains are evident at lower left. 1 cm = .33 mm, sample #44 (see appendix).

unstrained. Recrystallization to a smaller grain size as well as a greater degree is evident in the more mica-rich zones. Relict quartzose ribbons have undergone near complete subgrain development and minor recrystallization (30 microns), both of which have a preferred orientation parallel to S_m (aspect ratios up to 3:1). Some normal grain growth is evident as well. Minor relict quartz are .1-1 mm in size, anhedral, strained grains, grading into recrystallized zones or pressure shadows wherein the average size is about 50 microns. Most of these relict grains have inequant shapes with aspect ratios up to 3:1 and are highly strained (undulose extinction) with minute inclusions parallel to S_m.

Near the fault contact, alkali feldspar is virtually lacking (Figs. 56-57). In some of the ultramylonites at a distance from the contact, however, it is still present in minor amounts as small, anhedral grains (.2-.3 mm average size) and up to 1 mm that may have been part of a once larger grain or augen. These are extensively fractured at a high angle to S_m with series of parallel fractures. This is associated with extension and rotation as well. There are also locally recognized, relict augen pods 4-6.5 mm across wherein highly fractured alkali feldspar is observed that has undergone partial alteration to quartz and sericite.

Plagioclase has undergone extensive recrystallization and alteration to sericite and epidote. The recrystallized grains are unstrained and are 20-30 microns in size. Most are fairly equant, although some have a preferred orientation parallel to S_m. Plagioclase is also present as relatively larger (.1-.5 mm, and some up to 1 mm), anhedral

grains that are extensively altered to sericite and kinked with recrystallization to small, new strain free grains along kink band boundaries. Within pressure shadows of the relatively larger grains, recrystallization is pronounced albite matrix. It is quite difficult at times to distinguish between recrystallized albite and quartz unless this gradational tional texture can be observed. There are a few unstrained albite porphyroclasts with albite twinning present locally (Fig. 57).

Pilot Gneiss

In the most intensely deformed mylonite zones of the Pilot Gneiss, the mylonitic foliation is defined by alternating elongate quartzose layers and quartzo-feldspathic rich layers, with minor amounts of white mica or alternating epidote-quartzo feldspathic rich layers (Figs. 59-61). Actinolite helps to define S_m in the hornblende bearing phase. A near completely recrystallized schistose rock consisting of alternating sericite and quartzo-feldspathic layers as seen in the Little River Gneiss is only locally recognized just at the fault contact. However, according to the classification chart, and by comparing to the parent rock, these should be classified as ultramylonites. Mineral deformation is the same as that described in the Little River Gneiss.

Chilhowee

Quartzites in the Chilhowee near the fault trace exhibit the mylonitization as well by extreme ductile flattening of the quartz to shape ratios of up to 20:1 (Fig. 62). In adjacent, more phyllitic units, however, the strain is taken up by the micas primarily and not

Fig. 59: Pilot Gneiss mylonite in which S_m is defined by elongate quartzose ribbons alternating with quartzo-feldspathic rich zones. 1 cm = .27 mm, sample #E-1(4a) (see appendix).

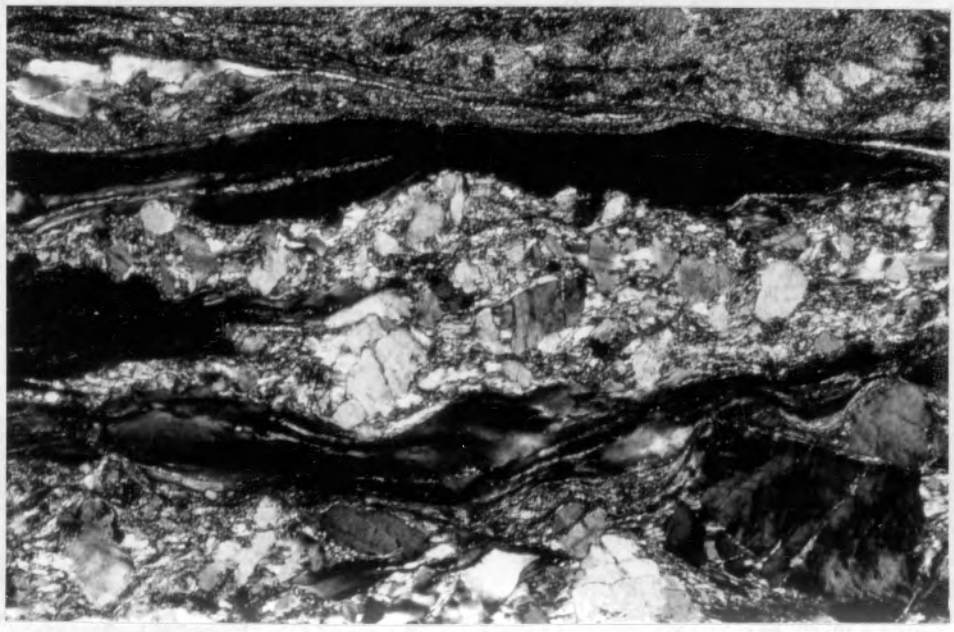

Fig. 60: Pilot Gneiss mylonite in which S_m is defined by alternating quartzose ribbons and quartzo-feldspathic rich layers. 1 cm = .27 mm, sample #E-1(10) (see appendix).

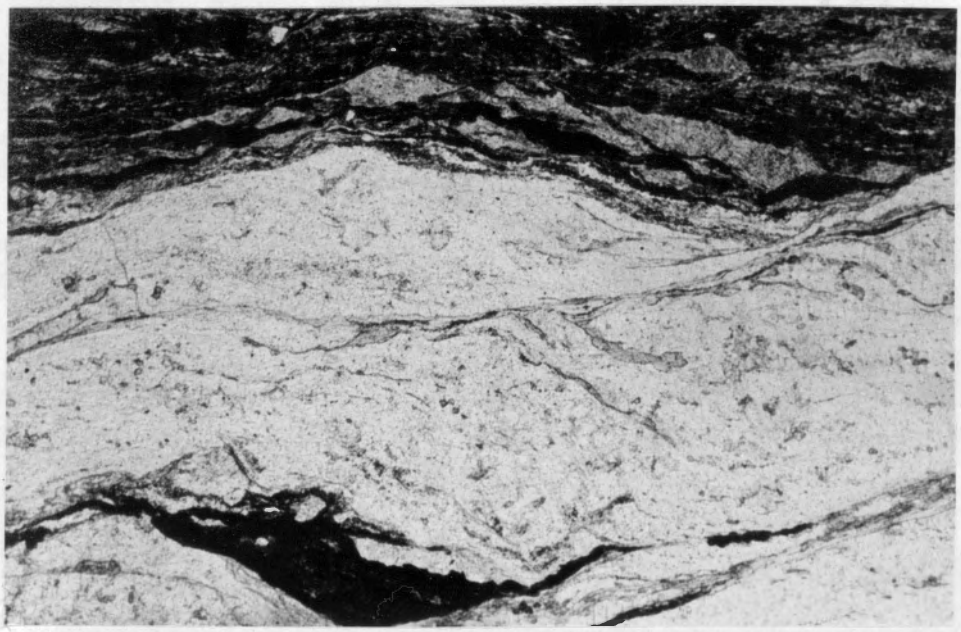

Fig. 61. Pilot Gneiss mylonite with alternating quartzo-feldspathic and epidote (dark)-rich layers; 1 cm = .31 mm, sample #E-1(5a) (see appendix).

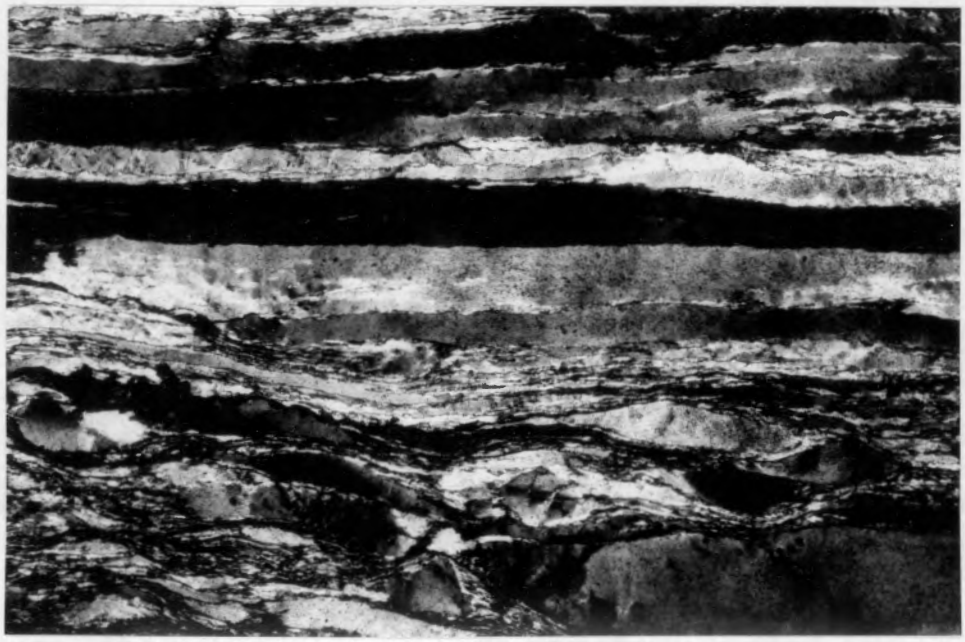

Fig. 62. Chilhowee quartzite very near fault trace showing elongated quartz ribbons with deformation band boundaries parallel to S_m; 1 cm = .28 mm, sample #26 (see appendix).

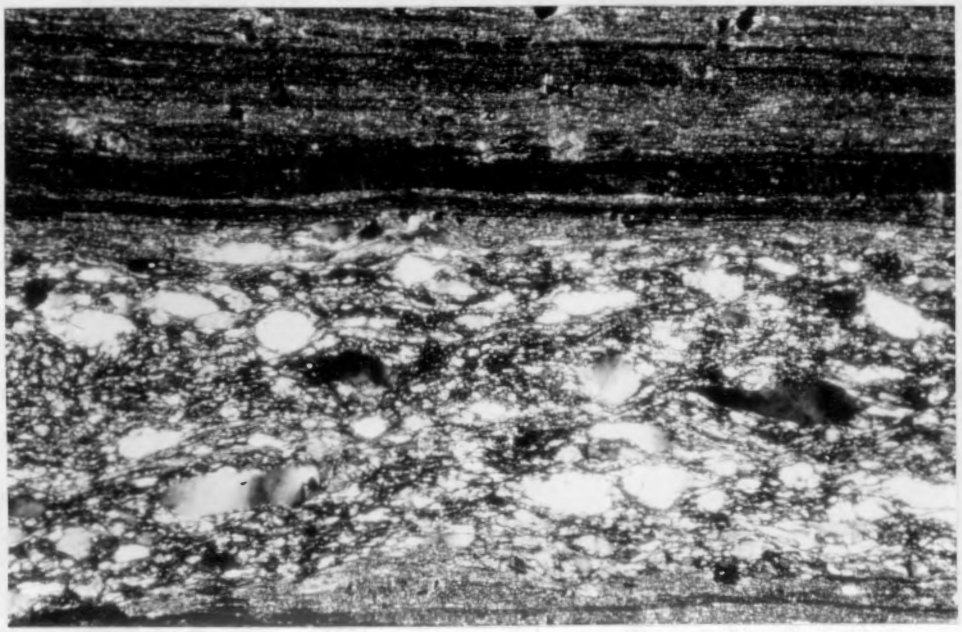

Fig 63. Phyllitic metasediment of Chilhowee Formation in contact with quartzite of Fig. 62; note that quartz is only moderately deformed due to most of the strain being absorbed by mica matrix; 1 cm = .28 mm.

much quartz deformation is recognized (Fig. 63). However, the intensity of the development of the S_2 crenulation cleavage within these rocks is much greater than that of metasediments outside of the fault zone.

In summary (Table 5), as deformational intensity increases across the fault zone, the overall grain size reduces (Fig. 33a) by recrystallization (Fig. 36) processes as well as by brittle fracturing. Chemical alteration is also partly responsible for grain size reduction and is discussed in detail in a later section. Quartz deformed by ductile flattening, producing elongate ribbons, and by recovery (subgrain development) and recrystallization processes. Deformation bands within quartzose ribbons are initially at a high angle to the mylonitic foliation, S_m, but become increasingly more parallel to it into the most intense zones. At this point, recrystallization and subgrain development is the most extensive. Plagioclase deformed primarily by kinking and recrystallization, but also by brittle fracturing, while alkali feldspar deformed solely by brittle fracturing normally at high angles to the foliation (near 45°). The percent of plagioclase recrystallization (Fig. 36) is gradual across protomylonite, mylonite and ultramylonite zones while the percent of quartz recrystallization increases moderately across the protomylonite and mylonite zones and very sharply in the ultramylonite zones. This indicates that recrystallization is increasingly dominant as a deformation mechanism in quartz, while plagioclase continued to undergo chemical alteration and brittle failure.

TABLE 5: MICROSTRUCTURE ASSOCIATED WITH ZONES REFLECTING DIFFERING INTENSITIES OF DEFORMATION

DEFORMATION INTENSITY	QUARTZ	PLAGIOCLASE	ALKALI FELDSPAR
PROTOMYLONITE (10% < .1 mm)	Undulose extinction; minor fracturing; 8-10% recrystallization; incipient ductile flattening (length to width ratios of 2:1 to 3:1	Straining with deformation twinning; minor fracturing; 10% recrystallization; minor alteration to epidote, sericite and albite	Fracturing at a high angle to the foliation; some disaggregation and rotation
MYLONITE (50-90% < .1mm)	Ductile flattening (length to width ratios up to 12:1); recovery (subgrains) and recrystallization (40-50%) processes evident; deformation bands common and increasingly parallel to S_m although some still as high as 30^o; recrystallization along deformation band boundaries and especially those that are parallel to the foliation.	Kinking dominant with recrystallization along kink bands; some microfracturing at high angles to the foliation with concomitant rotation and extension of fractured segments; continued breakdown to epidote and sericite along with recrystallization to (20%) to fine grained albite	Continued fracturing at high angles to S_m associated with rotation and extension of fractured segments; this is responsible for the feldspar being strung out parallel to the foliation and forming a lineation down the dip of the S_m plane; pressure solution along grain boundaries is evident as well producing elliptically shaped augen
ULTRAMYLONITE (95% < .1 mm)	Flattening extreme (aspect ratios up to 20:1); deformation bands parallel to S_m with recrystallization along their boundaries; 80-90% recrystallization	Near complete recrystallization and breakdown to epidote, sericite and fine grained albite	Near complete breakdown to quartz and muscovite with less than 5% relict grains

III. Operative Deformation Mechanisms

Although the overall bulk deformation in mylonite zones is of a ductile nature (see Bell and Etheridge, 1973), there are three competing deformation mechanisms operative in these zones. These are: 1) brittle, 2) ductile and 3) diffusive processes.

Brittle deformation is recognized quite early in the deformation and dominates in alkali feldspar while being only partially responsible for plagioclase deformation. This is due to the low number of slip systems within the feldspars and, thus, strain must be accompanied by brittle failure rather than by ductile processes.

Ductile deformation, on a grain scale, is actually a reflection of intragranular processes that can be explained by the existence of lattice defects called dislocations (Hobbs et al., 1976; Nicolas and Poirier, 1976 and Wilson, 1972). Microstructural changes occur in order to decrease the stored plastic strain energy by decreasing dislocation density and thereby achieve equilibrium with new physical conditions incurred during deformation. This is accomplished by their displacement/slip through the lattice along specific crystallographic planes and in certain slip directions. The given slip system operating in a particular mineral is a function of temperature and strain rate. The greater the dislocation density, the greater the internal energy, which provides the driving force for recovery and recrystallization processes (Nicolas and Poirier, 1976) at higher temperatures (i.e., thermally activated). Thus, the most highly strained grains tend to undergo subgrain development and/or recrystallization the most readily,

a process involving dislocation climb. Dislocation glide (stress activated) is responsible for such optical strain features as undulose extinction, deformation bands, deformation lamellae and kink banding, and is accompanied by recovery and recrystallization (cf. White, 1976). Progressive development of these features in quartz with increasing strain is shown in Fig. 64. These intragranular processes result in permanent grain shape changes, most readily apparent in quartz, due to external rotation of the crystal structure (Tullis et al., 1973), and are, in part, responsible for fabric development, i.e., S_m in mylonites.

Diffusive processes are generally operative at lower stresses and lower strain rates and involve Coble creep (grain boundary diffusion) at lower temperatures and Nabarro-Herring Creep (lattice diffusion) at higher temperatures. Pressure solution is generally considered to lie within the field of Coble creep and is probably one of the most important diffusive deformation mechanisms in the low temperature deformation regime (cf. Durney, 1972). In mylonites, it is usually initiated as well by a reduction in grain size.

Concept of Deformation Mechanism Maps

Temperature-stress-strain rate realms over which ductile and diffusive processes are operative have been determined experimentally for some minerals and are represented on deformation mechanism maps (Ashby, 1972). The most important of these minerals with regard to the present study is quartz, due to its ubiquitous presence in Fries DDZ mylonites, its importance in the development of the mylonitic foliation and as an indicator of operative deformation parameters. Experimental

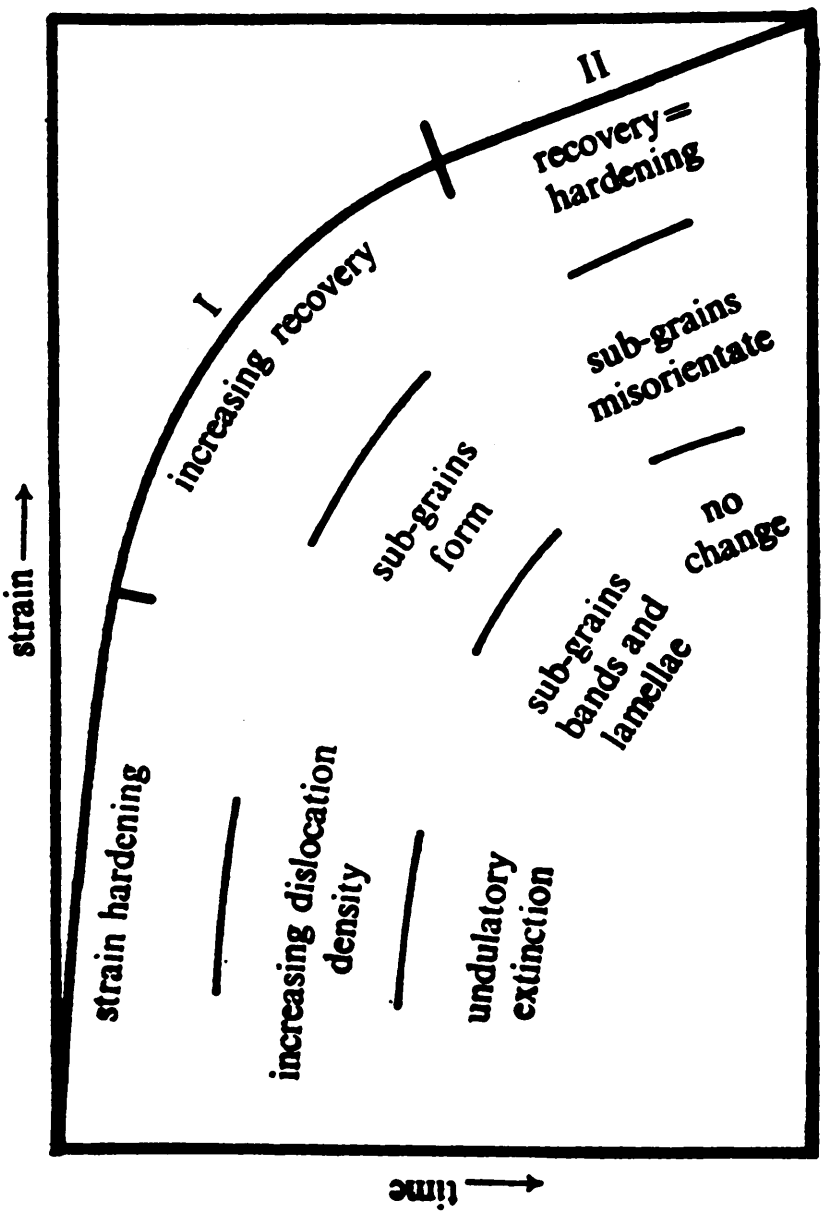

Fig. 64: Progressive development of optical strain features in deformed quartz with an increase in intracrystalline strain, as shown by grain elongation. (Taken from White 1975)

deformation studies have been caried out extensively on quartz due to its relatively simple structure and optical properties (variety of microstructures) in comparison to other minerals.

Fig. 65 is a deformation mechanism map for quartz that was determined for a 100μm grain size and stress values at 900°C. These show plastic flow dominates at higher temperatures, stresses and strain rates, while diffusive processes dominate at low stresses and strain rates. For a constant stress value, dislocation processes become increasingly dominant with higher strain rates. The effect of reducing grain size is to increase strain rates in the Nabarro-Herring and Coble creep fields (Fig. 66), so that the size of these increases at the expense of dislocation flow fields (Rutter, 1976). The dominant deformation mechanism may then switch from dislocation glide to pressure solution (Kerrich et al., 1977). Fig. 67 shows the map represented in Fig. 65, but with the addition of a pressure solution field. This tends to increase strain rates in and increase the size of the Coble creep field.

The dislocation glide field included in Figs. 65 and 67 lies outside of likely crustal conditions and, thus, is omitted in Fig. 66 (White, 1976). White suggests that glide, due to strain hardening, will ultimately produce cataclasis rather than mylonitization. This theory is not borne out by the Fries DDZ mylonites, however. According to the deformation mechanism maps, stresses and temperatures must have been quite high (≥ 1 kb) in order for plastic yielding by dislocation glide to take place. Estimates from recrystallized grain size, how-

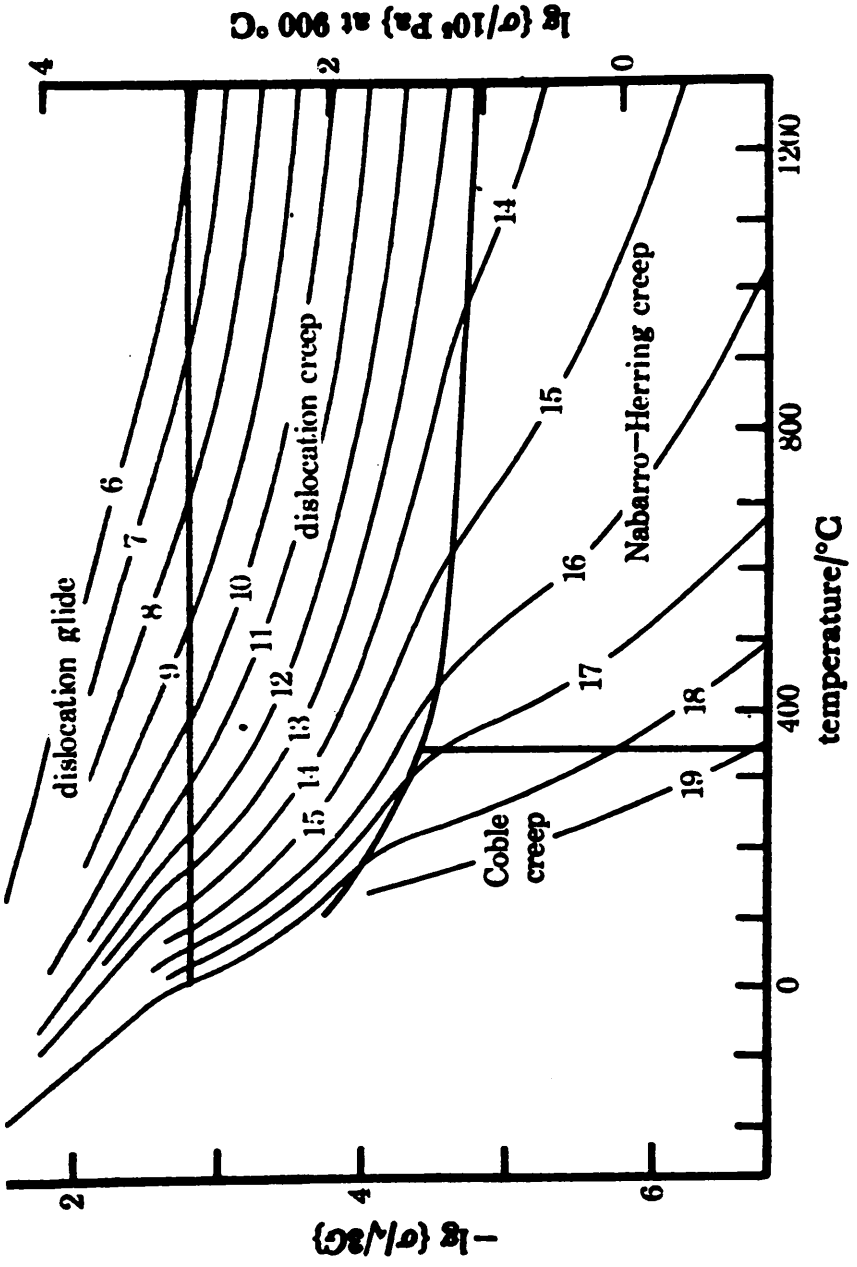

Fig. 65: Deformation mechanism map for quartz without pressure solution. Contours of -lg strain rate are shown. σ is differential stress ($\sigma_{11} - \sigma_{33}$). d = 100 µm; V = 22 cm^3. (From Rutter, 1976)

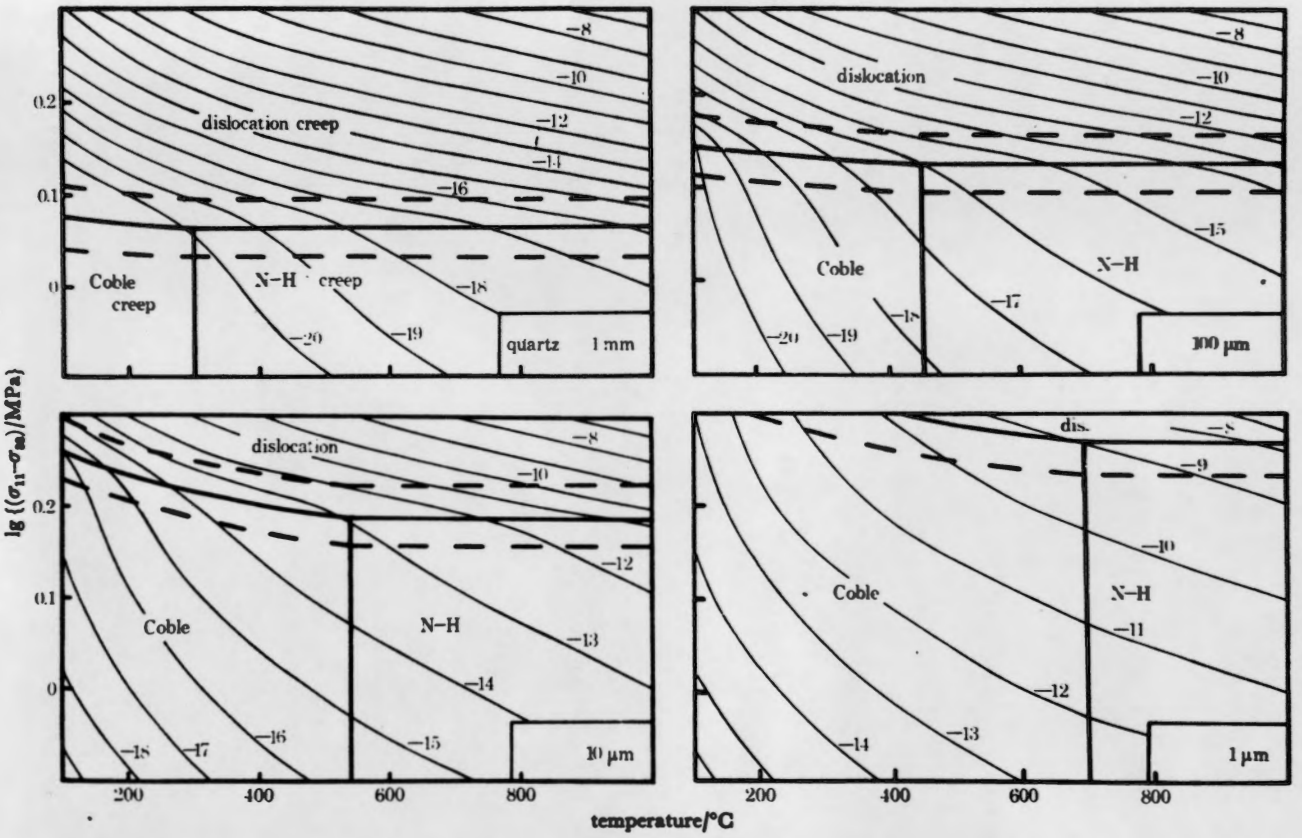

Fig. 66: Deformation mechanism maps for quartz of differing grain size. Strain rate contours, $\lg_{10} s^{-1}$, are shown. The values of $\sigma_{11}-\sigma_{33}$ are based on values of the shear modulus at 900°C (see Rutter, 1976). (From White, 1976).

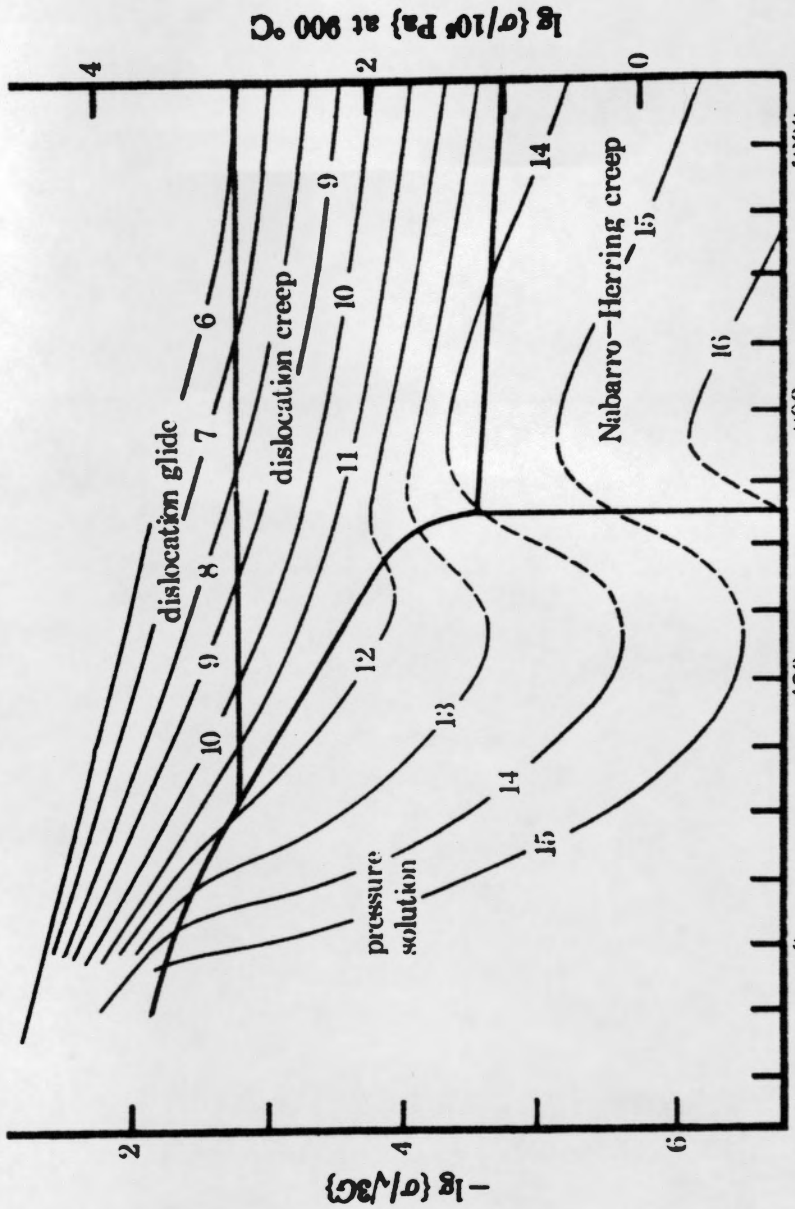

Fig. 67: Deformation mechanism map for quartz modified by the addition of a pressure solution field. The region of dashed strain rate contours represents the inhibition of pressure solution thrgugh decrease in pore water concentration. d = 100 μm; V = 22 cm³. (From Rutter, 1976)

ever, yield a differential stress from 500-600 bars and mylonitization occured at greenschist grade (350-450°C) as determined by mineral assemblages. The magnitude of the paleostress was determined using a formula derived by Goetze (1975) and a new proportionality constant by D. Anderson (in France, 1978). The differential stress is given by:

$$\sigma_1 - \sigma_3 = (.027 \text{ kb cm}^{\frac{1}{2}})(\text{recrystallized grain size})^{-\frac{1}{2}}$$

This formula was based upon the correlation of stress and dislocation density in both experimentally and naturally deformed quartz and olivine. The determination of stress, then allowed for its correlation with secondary grain size. The average recrystallized grain size of quartz in the Little River Gneiss mylonites is 20-30 microns which gives a differential stress of 500-600 bars within the fault zone. The discrepancy with the deformation mechanism maps may be explained by the influence of water in the crystal structure. It has been shown experimentally that trace quantities of hydroxyl ions in quartz greatly reduces its mechanical strength (Griggs, 1967, 1974). Above a certain critical stress, temperatures at which dislocation glide is maintained depends on strain rate. As the rate is increased, the critical temperature increases. The latter decreases with increasing H_2O content, however, and depending on the concentration of hydroxyl impurities, plastic flow is possible at temperatures of 200-300°C (Jones, 1975). Thus, ductile yielding of quartz can occur at much lower temperatures, strain rates and stresses than that shown on the deformation mechanism maps. Unless the effect of the OH^- in quartz is taken into consideration, these maps can only be used in a general

way, i.e., indicating that dislocation processes are operative at higher temperatures, stresses and strain rates giving way to diffusive processes (particularly pressure solution) at lower temperature or strain rates and at lower stresses.

Deformation Behavior of Minerals in Fries DDZ

Experimental work can be used in conjunction with optical observations previously described to provide a better understanding of the development of microstructures in the primary minerals (quartz and feldspar) during progressive deformation within the Fries DDZ rocks. These can, in turn, be used for determination of external deformation parameters such as orientation of principal stresses, strain rates, temperatures, etc.

Quartz

Experimental deformation studies of quartz have accelerated over the past 15 years (Tullis et al., 1973; Green et al., 1970; Carter et al., 1964 and Christie et al., 1964, 1966) and have provided valuable knowledge for the understanding of its deformation in natural environments. It should be noted, however, that most experimental deformation involves axial compression and very large strains. Deformation is obviously much more complicated and strains lower in naturally deformed rocks. Quartz undergoing axial compression at a temperature of 700°C and a strain rate of 10^{-7}/sec produced a fabric, with a sequential development of microstructure accompanying increasing strain, very similar to the sequence observed across the Fries Fault Zone (from protomylonite into ultramylonite zones) (Tullis et al.,

1973). At lowest strains, incipient recovery and recrystallization at grain boundaries is apparent, with some flattening and the development of both deformation bands and undulose extinction. The recrystallized grains had inequant shapes with their short dimension parallel to σ_1. As the strain was increased a greater degree of flattening was evident with a smaller recrystallized grain size. At very high strains, very few relatively undeformed quartz remain as most had been flattened normal to σ_1. Recrystallization along deformation band boundaries at this point was quite extensive. At higher temperatures and slower strain rates recrystallization was near complete.

In addition to a dimensional preferred orientation defined by grain shape, quartz also develops a lattice preferred orientation. This is a function of temperature and strain rate only, and does not change with increasing strain, although its intensity may. The experiments have shown that undulose extinction zones and deformation bands parallel the c axes, and form 45° to σ_1, i.e., along the favored glide plane (Tullis, 1973; Carter et al., 1964). During deformation, c axes rotate toward σ_1, and the sense of internal rotation is opposite that of external rotation of the crystal (Fig. 68). This suggests that the lattice preferred orientation can be used as an interpretive tool for determining the orientation of paleostress. Investigation of mylonites in the Fries DDZ suggests that although there is probably a relationship between quartz c-axes and σ_1, knowledge of the stress field is virtually impossible to determine and cannot necessarily be implied to be normal to the foliation. The grain shape foliation can be used

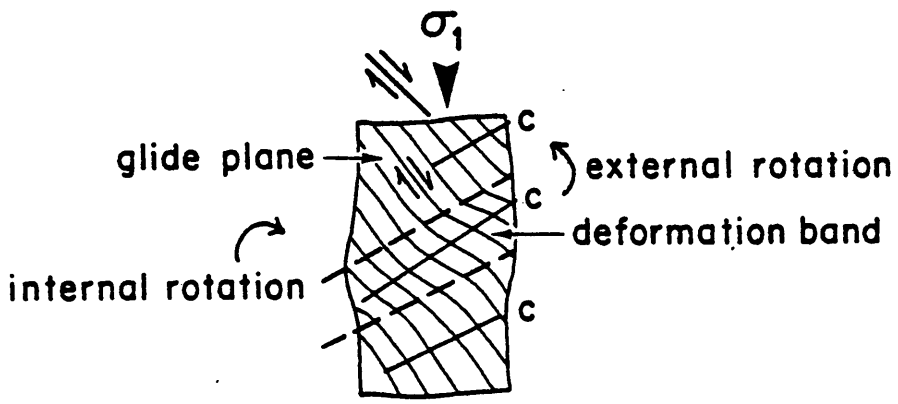

Fig. 68: Experimentally deformed quartz showing deformation bands parallel to c axes and forming 45° to σ_1; c axes rotate toward σ_1 during deformation (sense of internal rotation opposite external rotation). (From Nicolas and Poirier, 1976; after Turner and Weiss, 1963).

quite reliably, however, as a marker for the XY plane of the finite strain ellipsoid (Lister and Price, 1978; Ramsay and Graham, 1970; Wilson, 1972). Although the dimensional preferred orientation may parallel the orientation of the finite strain axes, the crystallographic preferred orientation may be independent of such, and, instead develop in relation to the kinematic framework (Lister and Price, 1978).

The presence of relict quartz augen or relatively undeformed, yet strained grains in the more intensely deformed zones (mylonites and ultramylonites), may be explained as those that are initially unfavourably oriented for glide (i.e., those in which the c axis is parallel to or perpendicular to σ_1) (Tullis et al., 1973). This implies that the Schmid factor of the active slip system (critical resolved shear stress) will be different in different grains (Nicolas and Poirier, 1976) and only favourably oriented grains will begin to yield first.

Flattening of quartz is more apparent above and below the more resistant feldspar grains, giving an undulating character to the foliation (cf. "anvil effect" of Lister and Price, 1978, Fig. 14). These local undulations around the clasts probably reflect local curvature in trajectories of the axes of finite strain (Lister and Price, 1978, p. 51). In the protomylonite zone, the feldspars seem to prohibit ductile yielding of quartz, but with increasing strain the latter eventually yields and deflects around them (Fig. 69).

Plagioclase

Plagioclase within the fault zone deforms primarily by kinking at a high angle to the foliation with small misorientations (less than

10^{o}) and associated recrystallization along these zones. Recrystallization along kink boundaries may, at times, give the appearance of fracturing and offset of segmented parts extended parallel to S_m (Fig. 70). Very little is known about deformation and recovery mechanisms in feldspars, and in particular, the alkali feldspars. Some experimental studies have been carried out on plagioclase, however, and slip systems have generally been inferred from the study of kink bands (Borg and Heard, 1969, 1970). Kinking is an important contributor to the ductility of minerals with only 1 or 2 slip planes, as in feldspar (Vernon, 1975; Debat et al., 1978). Experimental deformation of low temperature, albitic-rich composition plagioclase, showed slip occurring on (010) parallel to the direction that probably is the glide direction of albite twinning (Borg and Heard, 1969). However, grains oriented favourably for slip do not twin and vice versa. The slip is accompanied by kinking and local rotations up to 7^{o}. Slip on other planes has not been observed. It is suggested that (010) must be properly oriented with respect to σ_1 for slip to occur (Borg and Heard, 1969). Optical studies of naturally deformed plagioclase (Vernon, 1975; Debat et al., 1978) show deformation bands or kinks as common features as well, some having a maximum misorientation of 7^{o} similar to that observed in experimental deformation. Recrystallization is common along deformation band boundaries and in local patches of relatively high strain and recrystallized grains have a crystallographic orientation close to the host grain. As with quartz, plagioclase must have a favourable orientation for slip and consequential

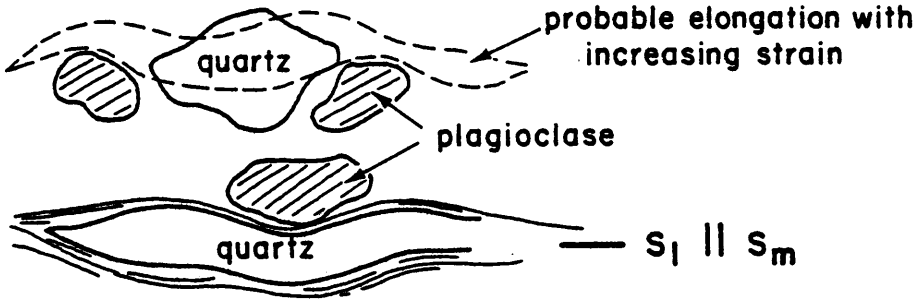

Fig. 69: Quartz deformation in mylonites affected by its location with respect to more resistant feldspar grains. Ductile flattening is hindered initially but with increasing strain, they eventually deform and deflect around feldspar.

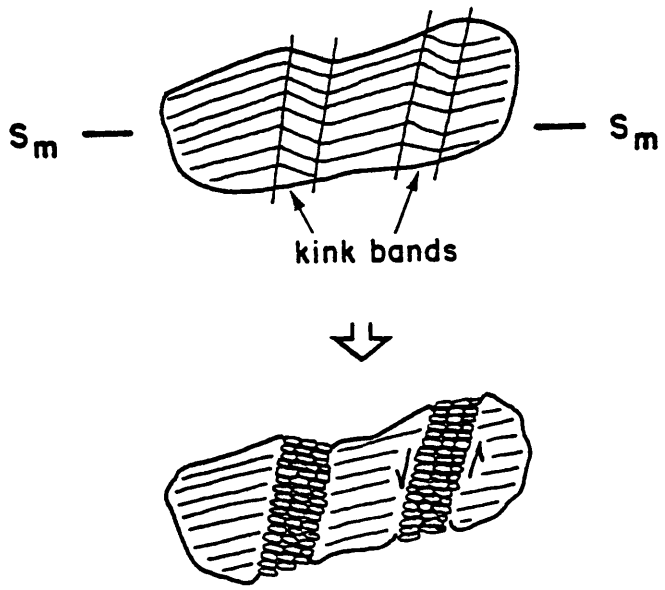

Fig. 70: Plagioclase undergoes kinking at a high angle to S_m; complete recrystallization along kink bands gives the sense of brittle failure and annealing.

development of kink bands. This could be responsible for the observed consistently high angle kink bands.

Kinking is normally attributed to compression normal to the kink plane. However, kinks observed in individual plagioclase grains in these mylonites form at a high angle to the foliation (i.e., subparallel to the compression direction), and the axial plane is perpendicular to the albite twins. This implies a different mechanism for kinking, that of slip along crystallographic planes and Fig. 71 diagrammatically shows their development.

Experimental work in deforming slates was conducted by Donath (Gay and Weiss, 1974) in order to determine the relationship between the direction of maximum compressive stress and single kinks. It was shown that principal stress directions control the orientation of kink boundaries and the angle appeared to be independent of confining pressure and total strain. Although the mechanism of development is different, this could possibly be extrapolated to grain-scale kinking of plagioclase.

Microfracturing at a high angle to S_m is apparent, as well, with offset along twin planes and is often accompanied by extension and rotation of segmented grains. This may occur in grains unfavourably oriented for kinking, and thus, strain must be accomodated by brittle fracturing. Rigid body rotation is also evident, and in a sense so as to bring the long face of the grain parallel to the foliation plane, S_m.

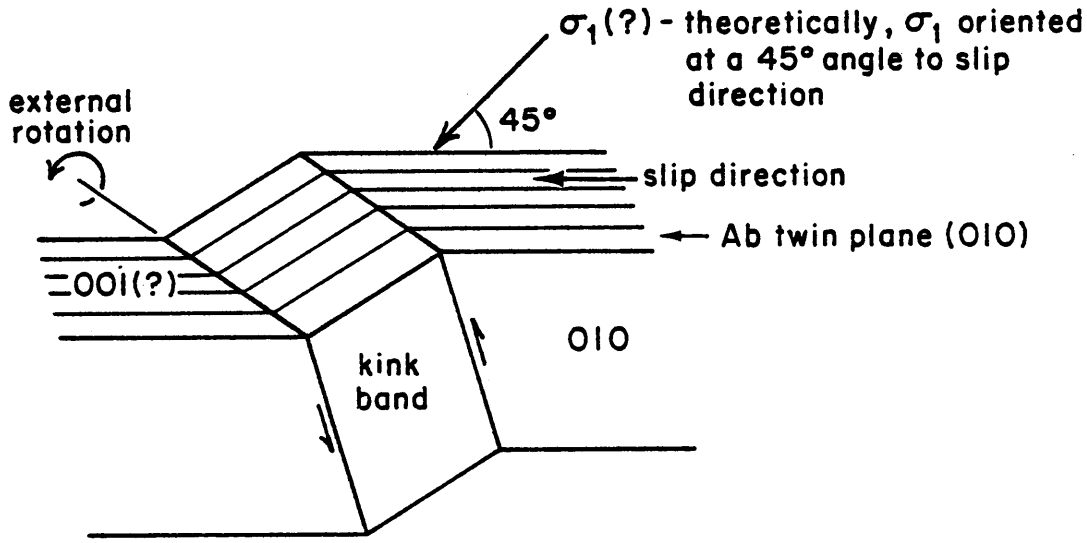

Fig. 71: Possible development of kink in plagioclase. (modified for plagioclase from Vernon, 1976)

Alkali Feldspar

Alkali feldspar, present primarily as augen, has deformed by brittle fracturing along conjugate or unidirectional shear planes inclined at a high angle to the foliation (usually between 20 and 45°). Virtually no experimental data on alkali feldspar deformation exists, but studies of naturally deformed grains indicate similar deformational features to those observed in Fries DDZ mylonites (Debat et al., 1978). Initially, fracturing is accompanied by offset along parallel shear planes and may be accompanied by rigid-body rotation. The latter is such as to bring the long face parallel to S_m. Pressure shadows around clasts contain recrystallized quartz and are elongate parallel to S_m. They define a lineation down the dip of the foliation surface. Late stage pressure solution is important in the development of augen shape. A schematic representation of the development of these augen structures is shown in Fig. 72. Their development is due to shear along planes inclined to the principal flattening direction, accompanied by a rotational component of simple shear. Commonly, these are strung out even further than that shown in the ideal model, with numerous disaggregated grains strung out parallel to S_m. Eventually, many of these become part of the finer grained matrix, either by chemical alteration or brittle communition.

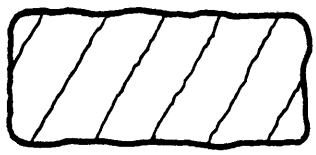

a) initial high angle microshears

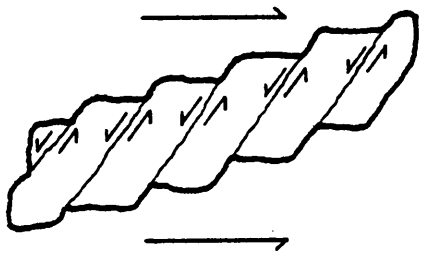

b) offset along microshears in a stair-step fashion which may be accompanied by some rotation of segments

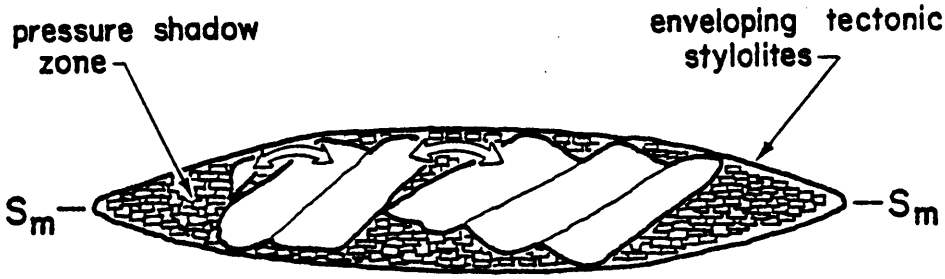

c) rotation of segments accompanied by late stage presure solution, modifying the shape

Fig. 72: Development of Alkali Feldspar Augen in Fault Zone

IV. Interaction of Chemical Processes with Mylonitization

The role of chemical processes in the formation of mylonitic foliations has long been neglected in studies of fault zones and fabric development therein. Many studies attribute development of mylonitic layering solely to mechanical processes (Schmidt, 1932; Prinz and Poldevaart, 1964; Sclar, 1965; Vernon, 1974; Boullier and Guegen, 1975; and Bell and Etheridge, 1976). More recently, however, the importance of chemical differentiation (Ramberg, 1952) and the interaction of chemical processes with deformation (Subimal, 1977; White and Knipe, 1978; Allison et al., 1979; Wintsch, 1975) has been realized.

This study indicates, in a qualitative sense, that chemical processes are as significant as mechanical ones in the formation of S_m. The entire zone affected by Fries faulting underwent a retrogressive metamorphism during which a complex interplay of chemical activity and mechanical processes were responsible for producing the mylonitic foliation. Mineral assemblages of the fault zone basement rocks (Table 6) indicate retrogression from lower amphibolite or ab-epidote amphibolite to greenschist facies conditions (biotite zone), while metasediments remained at greenschist conditions (chlorite zone). Associated mineral reactions have been inferred from textural relationships and microprobe analyses (appendix) of specific minerals.

Little River Gneiss

The mineralogy, as well as the fabric and related strain, of the Little River Gneiss appear deformation dependent. Mineral proportions vary through stages of increasing deformational intensity (Fig. 73) suggesting a continuous transition in mineralogy between non-mylonite

TABLE 6. PRE TO SYN FAULTING MINERAL ASSEMBLAGES

	PRE-FAULTING ASSEMBLAGE	RETROGRESSIVE ASSEMBLAGE
Little River Gneiss	Quartz - 35% Plagioclase (An_{1-5}), some antiperthite - 30-35% Alkali Feldspar (perthite and minor microcline - 5-20% Brown Biotite - 16% Muscovite (Fe rich) - 7-20% Epidote/clinozoisite - 5-6% accessory sphene, apatite, zircon, chlorite, calcite	Quartz - 22-25% Plagioclase(An_{0-2}) - 22-25% Alkali feldspar (perthite) - 10-18% (and 0% in some) Biotite (green to pale brown)- 4-10% Muscovite/sericite (phengitic) - 22-28% epidote/clinozoisite - 4-6% accessory apatite, zircon, opaques, chlorite, calcite, stilpnomelene
Pilot Gneiss (hornblende phase)	Quartz - 20% Plagioclase - 13-15% (up to 35) Alkali feldspar (perthite) - 23% sericite/saussarite - 15-30% ± brown hornblende (up to 10%) ± epidote, chlorite, biotite, sphene, zircon, opaques	Quartz - 5-22% Plagioclase - 18-25% Alkali feldspar (perthite) - 17-25% sericite - 6-30% muscovite - 2% epidote/clinozoisite - 16-21% actinolite - 2-10% ± chlorite, calcite, stilpnomelene, sphene
Mafic dikes and sills (coarse grained)	Hornblende - 20-85% Calcic plagioclase - 35-65% ± minor biotite (5-6%) accessory sphene, epidote, calcite	Actinolite - 10-12% (up to 35%) Plagioclase (Ab) - up to 50-55% Epidote/clinozoisite - 15-30% Chlorite - up to 5% accessory sericite, sphene, opaques, stilpnomelene, calcite, quartz

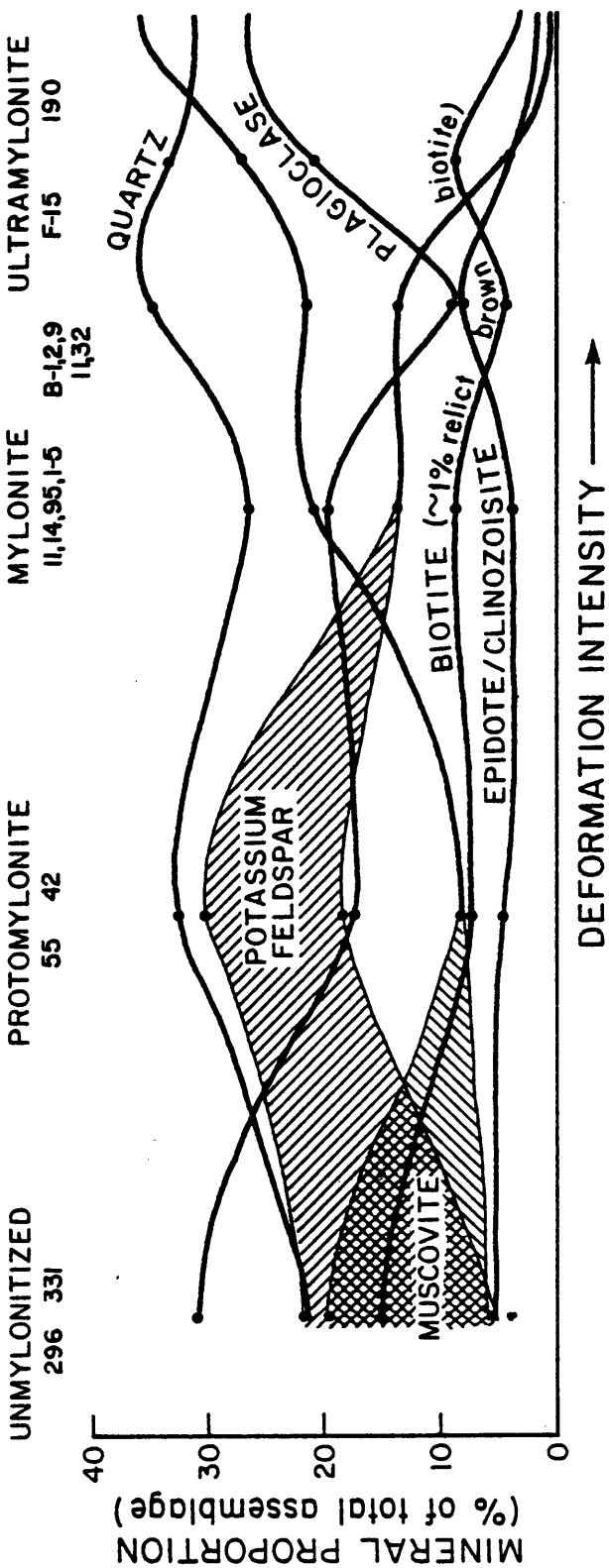

Fig. 73: Mineralogical % changes through stages of increasing deformational intensity. Based on point counts of 15 samples across fault zone (samples listed above, see appendix for location).

and ultramylonite end members. The mineral proportion curves only define general trends showing overall increases or decreases of specific minerals. Small undulations in the curves do not necessarily reflect actual chemical changes, but most likely are a function of original compositional variability. In the non-mylonitic rocks (M_2 assemblage) the alkali feldspar content varies considerably and is proportional to the muscovite content (5-20% alkali feldspar vs. 7-20% muscovite). This may suggest that the feldspar has reacted to form muscovite or reflect initial compositional variability. Plagioclase is albite and the presence of relatively large epidote and clinozoisite crystals scattered along muscovite-biotite zones suggests the Ca from the plagioclase was used in their formation.

Probably the most conspicuous reaction in the mylonitic rocks is the breakdown of plagioclase to sericite, epidote/clinozoisite and fine grained albite. The An content of plagioclase in the pre-faulting assemblage was rather low (An_{1-2}), such that most of the plagioclase has broken down to produce sericite and albite, with only a slight increase in epidote content. The Ca content of the plagioclase, however, may have varied from locality to locality prior to faulting, as suggested by the large drop in plagioclase % at the mylonite-ultramylonite transition, corresponding to the largest increase in the epidote content. Often, relict outlines of completely sericitized and epidotized plagioclase are still evident with very faint albite twinning. In some cases, biotite seems to be involved in this reaction as well, as suggested by the presence of fine grained epidote strung out in muscovite/sericite - biotite rich zones, and fine, green biotite as inclu-

sions in plagioclase. Some of this fine-grained epidote, however, may be due to the recrystallization of the larger crystals present in the unmylonitized rocks. In the latter, they are present primarily within the biotite-muscovite layers. Chlorite is often associated with epidotized areas as well and calcite, recognized locally in trace amounts, may also be a product of this reaction.

Other obvious changes that need to be accounted for are the decrease in alkali feldspar and brown biotite content, while green biotite is produced in amounts up to 5%. Augen within the unmylonitized and into the mylonite zones consist of intergrowths of plagioclase, postassium feldspar and quartz, with potassium feldspar becoming more dominant with increasing intensity of deformation. In the mylonite-ultramylonite transition zone, alkali feldspar porphyroblasts are recognized. It appears that early during the deformation and especially in areas of higher strain, biotite reacts to yield these porphyroblasts that replace the augen mosaics of the original gneiss. Chlorite and stilpnomelene are by-products of this reaction. This transformation may be primarily deformation dependent (Wintsch, 1975).

With increasing intensity of deformation, i.e., within the ultramylonite zones, alkali feldspar almost disappears completely by breaking down to form muscovite and quartz. Some of the K^+ is probably mobile so that reactions are not purely isochemical. Studies of chemical/mineralogical variation in other fault zones suggest that mylonitization at greenschist facies conditions is neither isochemical nor isovolumeric (Kerrich et al., 1977; Subimal, 1977; Beach and Fyfe, 1972). In an adamellite shear zone (Kerrich et al., 1977) brittle fracturing is

associated with concomitant diffusional transfer of more mobile chemical species (Na, SiO_2) into extension veins. These extension veins have been recognized extensively within the Pilot Gneiss, in which both quartz and plagioclase have crystallized. This probably is a function of the initially isotropic nature of these rocks. Kerrich et al. (1977) suggests that large-scale chemical redistribution is most likely to occur in structures where "sinks" such as extension veins can form. Subimal's (1977) study also suggests mobility of some species, although mylonites from different regions did not record similar trends. In shear zones at Scourie, Sutherland (Scotland) chemical analyses showed that K^+ is mobile, as sheared rocks are enriched in K^+ relative to undeformed rocks (Beach and Fyfe, 1972). Wintsch (1975) has suggested that K^+ could be mobile in this reaction as well and has developed a model that is primarily deformation dependent.

Relict brown biotite has been absorbed almost completely in the above mentioned reactions and only a few relict grains are still evident, wrapped by S_m. Smaller and finer, new green (and sometimes pale brown) biotite is present oriented parallel to and helping to define the mylonitic foliation. Biotite also reacted to form chlorite, stilpnomelene, minor sphene and ilmenite, and underwent recrystallization to the finer grained crystals. The green color may indicate a different oxidation state, although no studies have shown this definitively. Beach and Fyfe (1972) have shown in their studies of the Laxfordian shear zone (Scourie, Sutherland) that there is an increase in oxidation.

Pilot Gneiss

During faulting, the hornblende bearing Pilot Gneiss was transformed into a light pink and green banded rock that is almost charnokitic in appearance. It consists of alternating quartzo-feldspathic rich layers and epidote or epidote-actinolite rich layers with locally interspersed, very light green, elongate pods or veinlets of epidote. Micas, with the exception of sericite, which locally may reach as high as 30%, and minor stilpnomelene, are virtually lacking.

The retrogressive assemblage produced during metamorphism associated with faulting is given in Table 6. A major reaction responsible for producing the retrogressive assemblage in both phases of the Pilot Gneiss is the breakdown of plagioclase to sericite, albite and epidote/clinozoisite. Sericite can be seen almost psuedomorphically replacing plagioclase, with relict outlines still visible in some. Where completely altered, minor amounts of sericite form anastomosing stringers defining S_m. Some of the sericite has recrystallized to platy phengitic muscovite. Albite produced by the reaction is very fine grained as is epidote/clinozoisite which are usually strung out parallel to S_m.

The alteration of hornblende to actinolite, chlorite and epidote in the hornblende-rich phase is suggested by a number of textural relations. Blue-green hornblende cores pale-green actinolite crystals, the latter present as larger porphyroblasts wrapped by S_m. Whether this transformation occurred during a time of decreasing temperatures towards the termination of the early Paleozoic event (M_2), or early during faulting, but prior to development of S_m is unclear. The hornblende are strained, however, and have gone from brown to a blue-green

color. These larger actinolite crystals have, in turn, altered to colorless, fibrous actinolite and, locally, biotite that is synchronous with and helps to define S_m (Fig. 74). In some samples, small hornblende crystals that are wrapped by S_m, are relatively unaltered(Fig 75).

Epidote produced by this reaction occurs as larger crystals, as opposed to the fine aggregates produced by plagioclase breakdown, and are usually observed in aggregates as stringers of veinlets that contain hornblende. It is often seen forming a core within actinolite, obviously a complete replacement of hornblende. Chlorite (clinochlore) is very abundant in some parts of the unit and where observed, appears to primarily be an alteration product of hornblende. Calcite is a minor product of the above mentioned reactions as well.

Mafic Dikes and Sills

The numerous mafic bodies within the fault zone have undergone retrogression to fine grained greenschists (Fig. 76). The coarser grained amphibolites (described in stratigraphy section) now consist of alternating mica/epidote-rich and plagioclase-rich layers with larger porphyroblasts of actinolite. The retrogressive assemblage is given Table 5. Plagioclase comprises up to 50-55% as part of a finely recrystallized groundmass, but is also present as a few (5-8%) relatively larger (up to 2 mm) relict grains. Actinolite makes up 10-12% (but may get as high as 25-35%) and is present as wide, columnar crystals and as fibrous sheaths. Epidote comprises 15-30%. Originally these bodies seem to be of two types; medium to coarse grained amphibolites and very fine grained rocks of basaltic composition. Fig. 77 is an

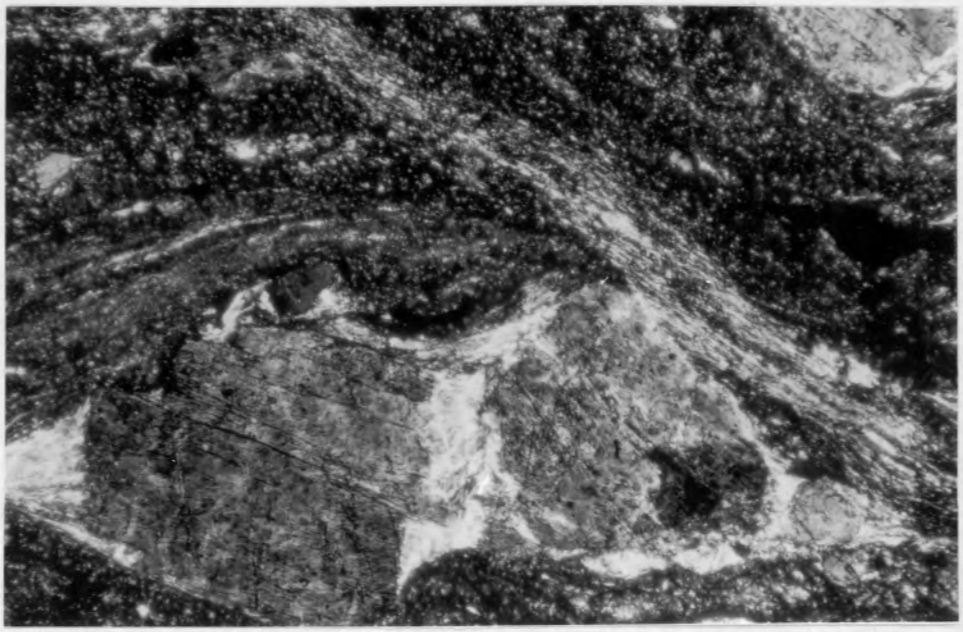

Fig. 74. Pre S_m hornblende (Pilot Gneiss mylonite) altering to fibrous actinolite that is syn S_m; cross-cutting S_3 evident in upper right corner; 1 cm = .11 mm, sample #E-6 (see appendix).

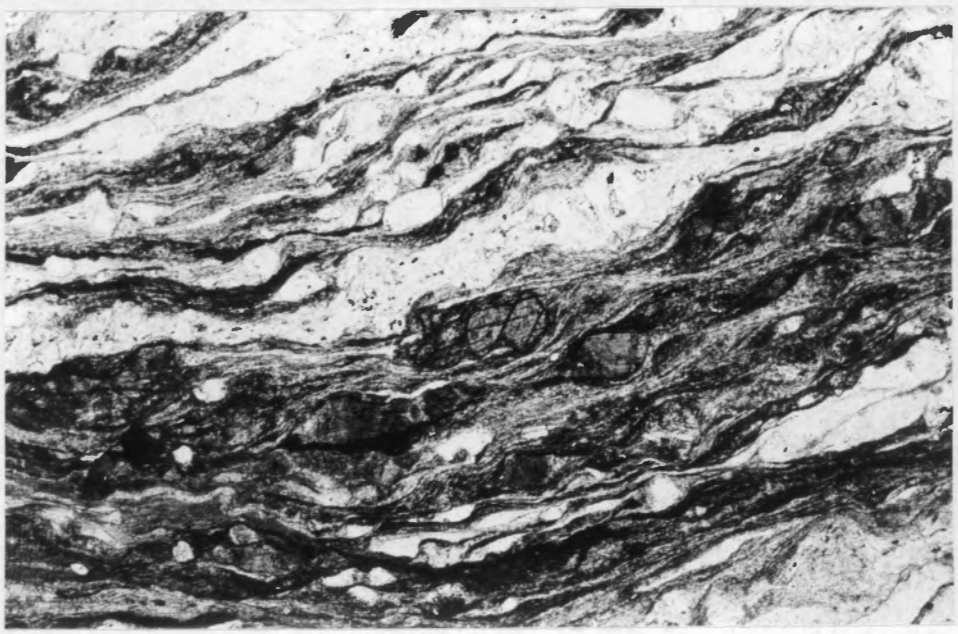

Fig. 75. Pilot Gneiss mylonite showing small hornblende crystals wrapped by S_m; 1 cm = .23 mm, sample #21 (see appendix).

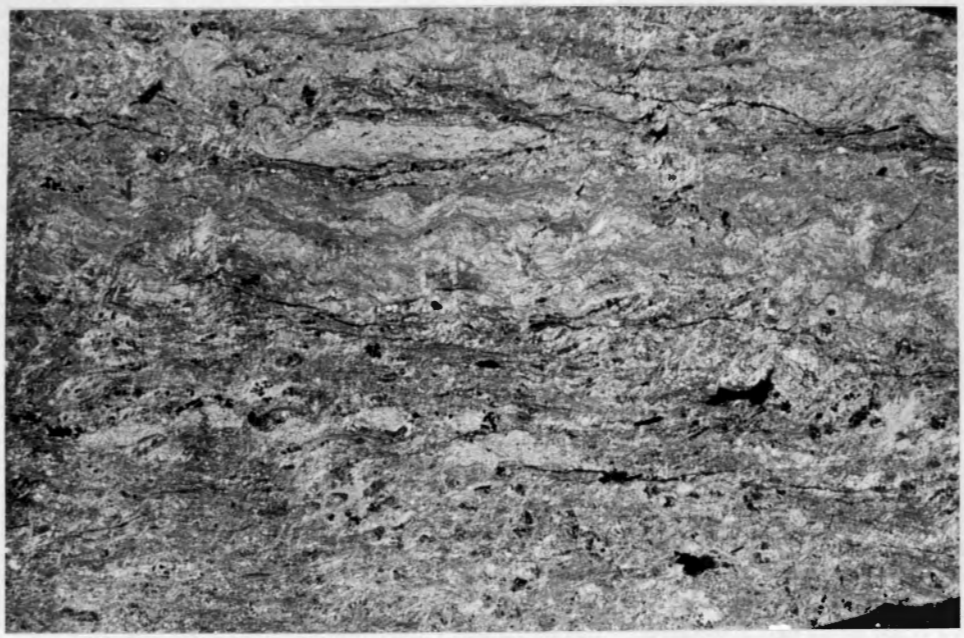

Fig. 76. Mafic dike or sill within fault zone, retrogressed to a fine grained greenschist; 1 cm = 2.2 mm, sample #D-12 (see appendix).

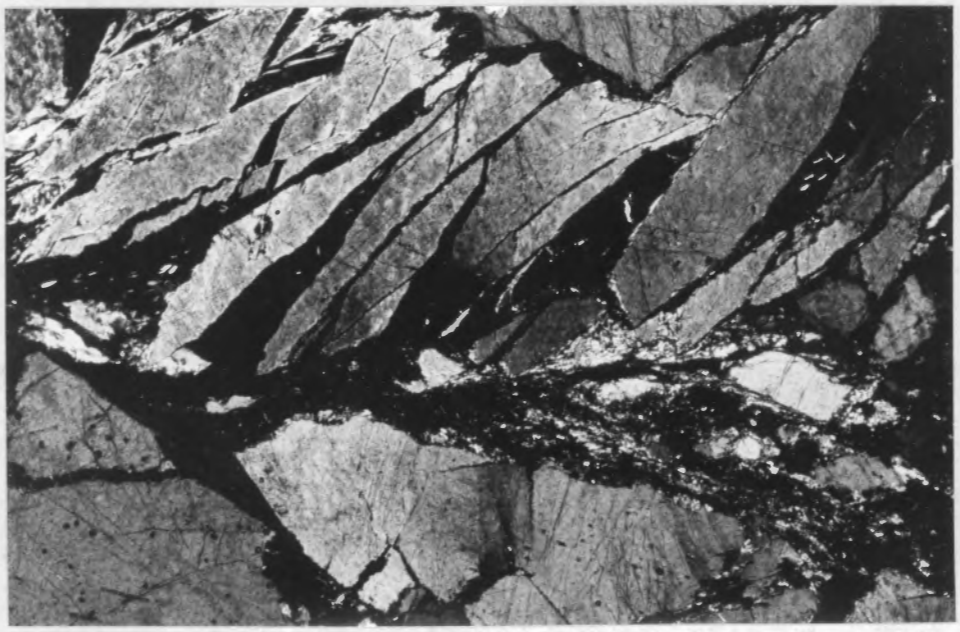

Fig. 77. Relatively undeformed and unaltered coarse grained amphibolite showing large hornblende crystals with minor alteration to chlorite (dark areas between grains); 1 cm = .28 mm, sample #247 (see appendix).

example of the coarse grained amphibolite.

The primary reaction is the breakdown of hornblende to actinolite, chlorite and epidote. Relict blue-green hornblende is observed in minor amounts in most samples coring actinolite, or in some cases altering to fibrous actinolite or to chlorite (Fig. 78). Pale green to colorless actinolite replaces hornblende almost psuedomorphically locally and is present as randomly oriented, porphyroblasts that are wrapped by the foliation. These have also altered to fibrous actinolite that is synchrounous with and helps define S_m. Some of the larger relict hornblende crystals have undergone random fracturing. Textural evidence thus indicates that mafics have undergone at least one metamorphic event prior to faulting, suggesting that intrusion was at least pre-faulting.

As in the basement rocks, plagioclase broke down to form epidote, minor sericite and fine grained albite, although the epidote content herein is much greater due to the originally high calcium content of the plagioclase. Epidotes associated with hornblende alteration are generally larger, single crystals, whereas those of plagioclase alteration are very fine grained aggregates.

The Chilhowee metasediments remained at lower greenschist facies during faulting. The primary mineralogical changes are the nearly complete recrystallization of muscovite to phengitic sericite parallel to and defining S_2, along with minor amounts of chlorite. Near the fault, larger muscovite crystals are present and metamorphic grain growth is much more pronounced. Opaques become abundant near the fault contact, concentrated along S_2 surfaces, and stilpnomelene is present

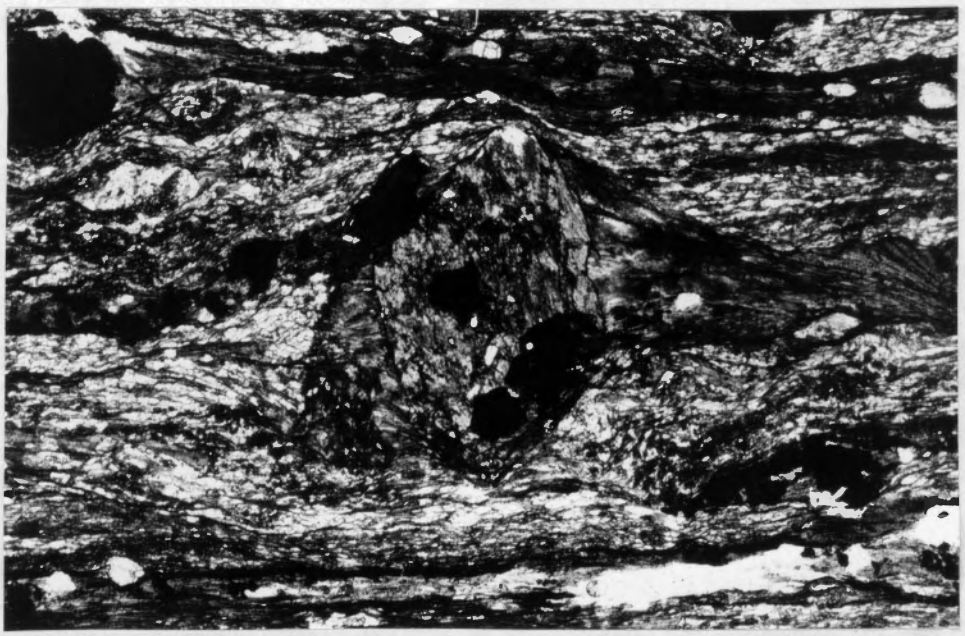

Fig. 78. Actinolite crystal in mafic dike wrapped by fibrous actinolite that is parallel to and helping to define S_m; 1 cm = .29 mm, sample #17 (see appendix).

in trace amounts.

From the above discussion of retrogressive mineral assemblages formed during faulting, all indicate recrystallization in the Greenschist facies. The transformation from actinolite to hornblende occurs at about 500°C and the lowest stability limit of actinolite is 375°C (Winkler, 1976, p.171, 238). The appearance of stilpnomelene indicates temperatures less than 450°C (Winkler, 1976, p. 238). Thus, temperatures were in the range of 375°C and 450°C during recrystallization and mineralogical transformations. A geothermal gradient of 30°C/km would indicate a depth of about 12-15 km. This is consistent with Sibsons (197) fault model wherein the transition from brittle failure to ductile faulting occurs between 10 and 15 km depth and at 250°C to 350°C. This suggests that temperatures were probably lower than those mentioned above.

V. The Role of Pressure Solution in the Formation of the Mylonitic Fabric

Concomitant with chemical reactions that produced phyllosilicates, quartz and recrystallized albite with a shape preferred orientation parallel to S_m and fine grained epidote, are mechanical processes discussed in a previous section. In addition, pressure solution becomes important and increasingly dominant as grain size decreases, which may be associated with decreasing temperatures and lower strain rates.

Tectonic styolites and phyllosilicate/epidote-rich bands imply solution transport of the more soluble components, such as SiO_2 and Na, into low pressure regions of pressure shadows and quartzo-feldspathic zones leaving concentrations of oxides, phyllosilicates and epidote (Figs. 79-80). In the Pilot, the latter is an alteration product of both plagioclase and hornblende/actinolite rich concentrations that define the foliation. Migration and consequent concentration and depletion of primary minerals (mineralogical differentiation) thereby developed an S_m fabric defined by alternating quartzo-feldspathic rich and mica/epidote (Little River Gneiss) or epidote and/or actinolite/mica/epidote rich bands (Pilot Gneiss). This mechanism is further confirmed by the chemistry of quartzo-feldspathic-rich and phyllosilicate-rich bands studies by Subimal (1977) that show a consistent relationship with material transfer between these zones.

Extension veins are quite abundant in the Pilot in which quartz and plagioclase have crystallized. As suggested by Kerrich et al. (1977), this is an indication of mass loss of quartz and albite due

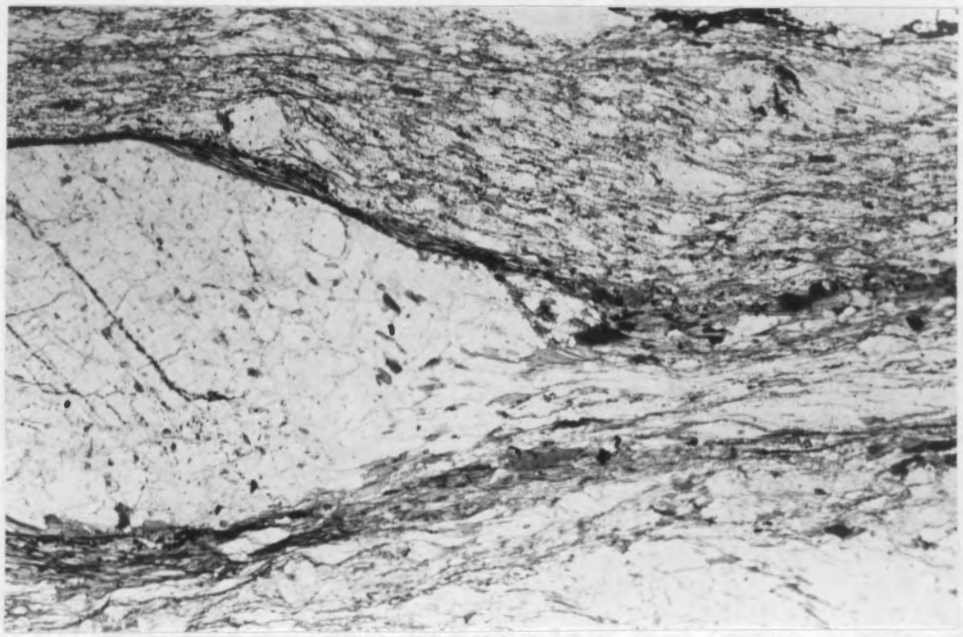

Fig. 79. Pressure solution mechanism evident by residual mica concentrations around large feldspar augen in Little River Gneiss mylonite; quartz reprecipitated in pressure shadows; 1 cm = .27 mm, sample #35 (see appendix).

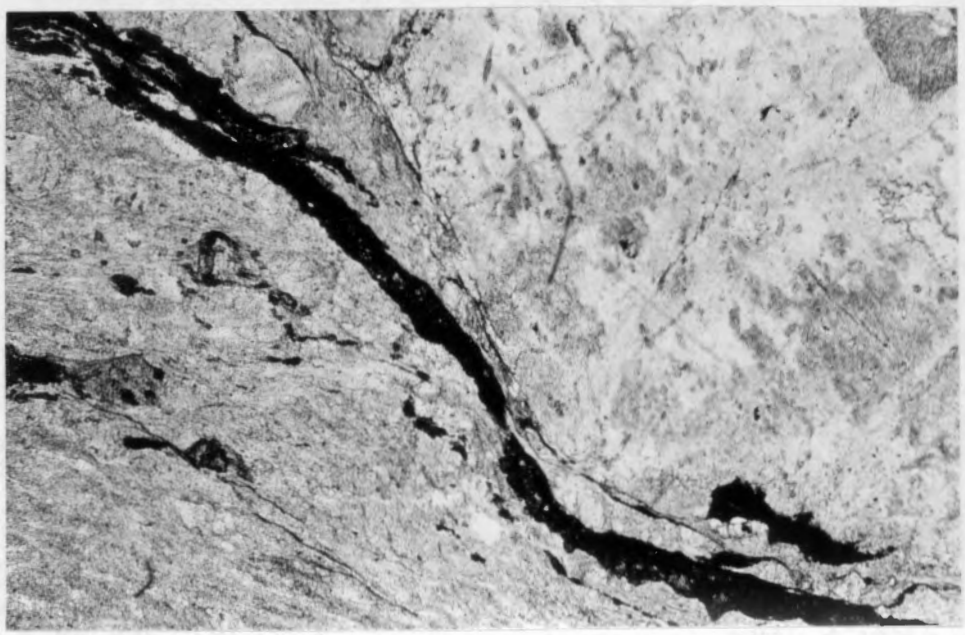

Fig. 80. Pressure solution responsible for residual epidote concentrations around large augen in Pilot Gneiss; 1 cm = .28 mm, sample #E-1(4a) (see appendix).

to pressure solution with concomitant diffusional transfer of more mobile chemical species into extension veins. Solution thinning of pre S_m veins is an additional indicator that solution processes are significant in these rocks.

In summary, development of the mylonitic fabric is a similar process within both the Little River Gneiss and Pilot Gneiss, involving both mechanical and chemical processes although the primary anisotropic nature of the Little River Gneiss seems to have some control over orientation. Initially, dislocation processes in quartz causing elongation are associated with mechanical fracturing, segregation and rotation of feldspar augen and are responsible for incipient development of a shape fabric (S_m) and rodding lineation (l_m). Mechanical processes dominate initially, giving way to chemical processes, primarily pressure solution, during the later stages of the deformation.

VI. Strain State and Deformation History

Despite intensive study of mylonites since their recognition in the late nineteenth century (Lapworth, 1885), there is still no clear understanding of their associated strain histories (cf. Johnson, 1967; Ross, 1973; Wilkinson et al., 1975; Bell, 1978). A major controversy concerns the role of progressive simple shear versus progressive pure shear for mylonite zones. Confusion still exists because:

1) there is a general lack of suitable markers to determine strain in shear zones,
2) where markers are present only the finite (i.e., total) strain can be determined,
3) finite strains from some markers are only minimum estimates of whole rock strain as there is commonly a rigidity/ductility contrast between marker and matrix, and
4) rotational strains cannot be determined from most finite strain techniques available.

Due to 2) and 4) inferences can therefore only be made about the strain history within mylonite zones.

Symmetry patterns of crystallographic elements (e.g., 'c' axes of quartz) have also been used to infer type of operative strain in mylonite zones (cf. Johnson, 1967; Hara et al., 1973; Nicolas et al., 1973; Marjoribanks, 1976; Lister et al., 1979). Again, there are problems because the degree and symmetry of crystallographic preferred orientation of fabric elements in mylonites must reflect the cumulative strain (i.e., the total strain). However, orthorhombic versus mono-

clinic symmetry of quartz 'c' axes is used to specify pure shear versus simple shear respectively in both theoretical and natural situations (cf. Lister et al.; 1978; Bell, 1978; Nicolas et al., 1973). These two are often interspersed indicating inhomogeneous deformation (Bell, 1978).

Unless incremental strain techniques (e.g. Durney and Ramsay, 1973) can be devised and applied to mylonites, then only an integrated approach utilizing finite strain data and symmetry patterns of fabric elements remains.

Determination of Finite Strain State

Despite the problems discussed above, determination of (1) the type of operative strain (i.e., 'k' value of Flinn, 1965) and (2) the magnitude of the strain within mylonite zones must provide data which will give a more complete understanding of the origin of fabrics and mesoscopic structure within these zones.

Three approaches have been used to analyze finite strain within mylonite zones. These are:

1) Marker Shape Changes:

This method involves determination of the orientation and axial ratios of the finite strain ellipse (Flinn, 1965 and Ramsay, 1967, p. 202-211). A variety of strain markers have been used for this method which includes pebbles (Hutton, 1979); garnets (Ross, 1973) and buckled aplite dikes (Themistocleous, S. G. and Schwertdner, W. M., 1977).

2) Marker Orientation Changes (particles or linear markers)

This method involves measurement of changes in orientation of

markers with respect to tectonic fabric elements during the deformation. Markers used include skolithos tubes (McLeish, 1971; Wilkinson et al., 1975) and feldspar phenocrysts (Borradaile, 1976).

3) Marker Orientation Changes (planar elements):

This involves measuring the variation in foliation orientation across the shear zone (after Ramsay and Graham, 1970), and is useful for continuous shear zones where no other markers are present. This method has been used by Burg and Laurent (1977) (French massif Central); Bak, Korstgaard and Sprensen (1975) (West Greenland) and Wakefield (1977) (Eastern Botswana).

It is important to realize that the analysis and interpretation of finite strain data from these zones requires some caution, since accurate determination for all three approaches is hindered by some of the following:

1) Homogeneous strain is generally assumed, and yet, even on the scale of a thin section, strain is obviously heterogeneously distributed (Lister and Price, 1978).

2) Volume change is assumed to be negligible, which may not always be true.

3) Pre and post deformational events complicate accurate determination of strain associated with faulting alone.

In methods 1 and 2,

4) "Flow" may tend to destroy such strain markers as may have originally been present (Wilkinson et al., 1975).

5) Ductility contrast between markers and matrix is assumed to be

negligible, yet the markers may actually have different mechanical properties from the rest of the rock and, thus, the recorded strain may differ from the total bulk strain.

6) Strain markers are assumed to be initially spherical or ellipsoidal in shape; or circular (skolithos tubes). However, this cannot always be accurately determined.

7) The mutual interference of rotating strain markers (which depends upon matrix content) may preclude accurate strain determination.

Method 2

8) It is assumed deformation was rotational, however, this is extremely difficult to determine from finite strain analyses alone. Also, an initial preferred orientation may cause further complications.

9) Very large strains may lead to small angular discordances that are difficult to interpret and measure (Wilkinson et al., 1975).

10) Strain is assumed planar and, in the case of skolithos tubes, that they lie in the plane of deformation containing maximum and minimum principal strains (McLeish, 1971).

Method 3

11) Assumes an undeformed state outside of the shear zone (Ramsay, 1970), and

12) That deformation was continuous (Ramsay, 1970).

Finally,

13) there are usually few independent strain parameters to be measured and, thus, a complete finite strain solution is near impossible (Wilkinson et al., 1975).

Strain Determinations from Other Mylonite Zones

Although a number of finite strain analyses have been carried out (Fig. 81), the data indicate extreme variability in both 'k' values and magnitudes of finite strain. Strain values do not consistently plot in the same fields on the modified (after Wood, 1976, Fig. 1) Flinn diagram (Fig. 81), suggesting different types of deformation and contrasting values of finite strain. Most plot in the flattening field or close to the K=1 line (oblate ellipsoid), indicating similar strain states and type of strain operative in the major shear zones studied. Different strain markers may, in part, be responsible for some of the variation. A constrictional strain (prolate ellipsoid) associated with the Moine mylonites (Fig. 81, #5 and 9) appears anomalous and may reflect irregularities in the surface.

Strain Determination From the Fries Fault Zone

Determination of the strain in the Fries DDZ mylonites was attempted using feldspar augen (Fig. 81). These are elongate in the plane of S_m, although some may be oriented as much as 30^o to such, and generally define a lineation (l_m) (Fig. 82). The latter is generally parallel to the dip. Although strain was obviously inhomogeneous, calculation of the mean strain ellipsoid may "smooth out" inhomogeneities and the deformation may thus be considered to approximate homogeneity (Hobbs et al., 1976). Due to the ductility contrast between the more resistant feldspar and finer grained mica-rich matrix, the augen will only give a minimum estimate of the finite strain. An important limitation as well in these rocks is the pre and post

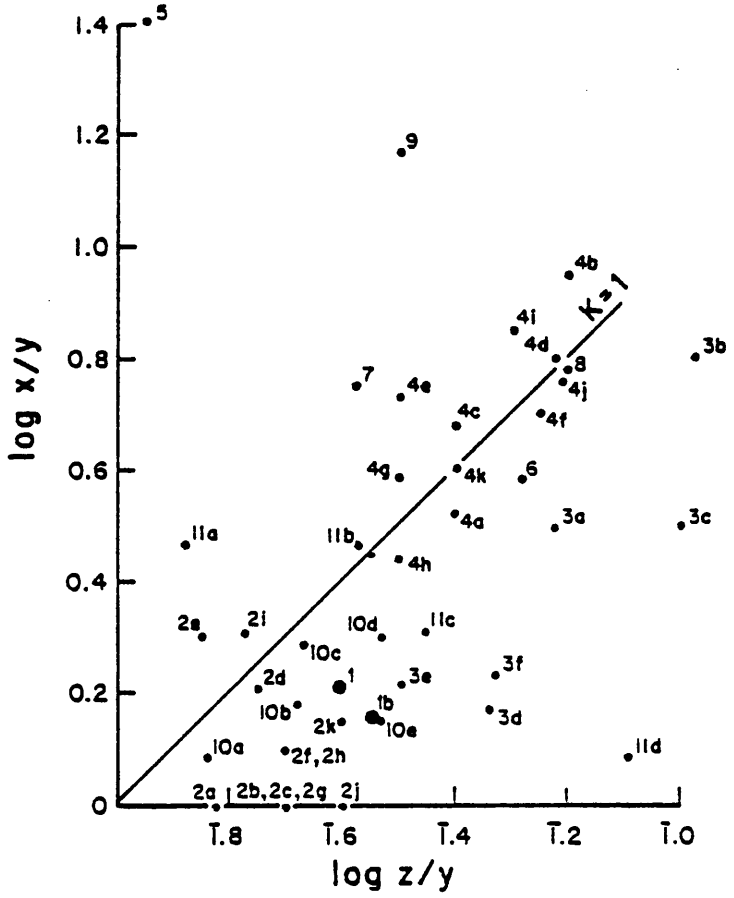

Fig. 81: Logarithmic plots of axial ratios of mean strain ellipsoids calculated from alkali feldspar augen (1). Data from finite strain studies within other major shear zones plotted for comparison and these were taken from the following sources:

1) Present study; a. 1 km from fault; b. just at fault trace (#B and 433)
2) Marjoribanks, 1976 (Australia-Orimston Nappe Complex)
3) Themistocleous and Schwertdner, 1977 (Kettle Lake Fault, Grenville Front)
4) Hutton, 1979 (Dalradian Slide)
5) Wood, 1973 (Moine Thrust)
6) Hossack, 1968 (Betic Orogenic Zone, SE Spain)
7) Burg and Laurent, 1978 (French massif)
8) Bak et al., 1975 (West Greenland)
9) McLeish, 1971 (Moine Thrust)
10) Coward, 1975; Coward and James, 1974
    a) Shabani Belt, Africa
    b) Bulawaya Belt, Africa
    c) Lower Gwanda Belt, Africa
    d) Tafi Belt, Africa
    e) Fort Victoria Belt, Africa
11) Borradaile, 1976 (Bygdin area, Southern Norway)

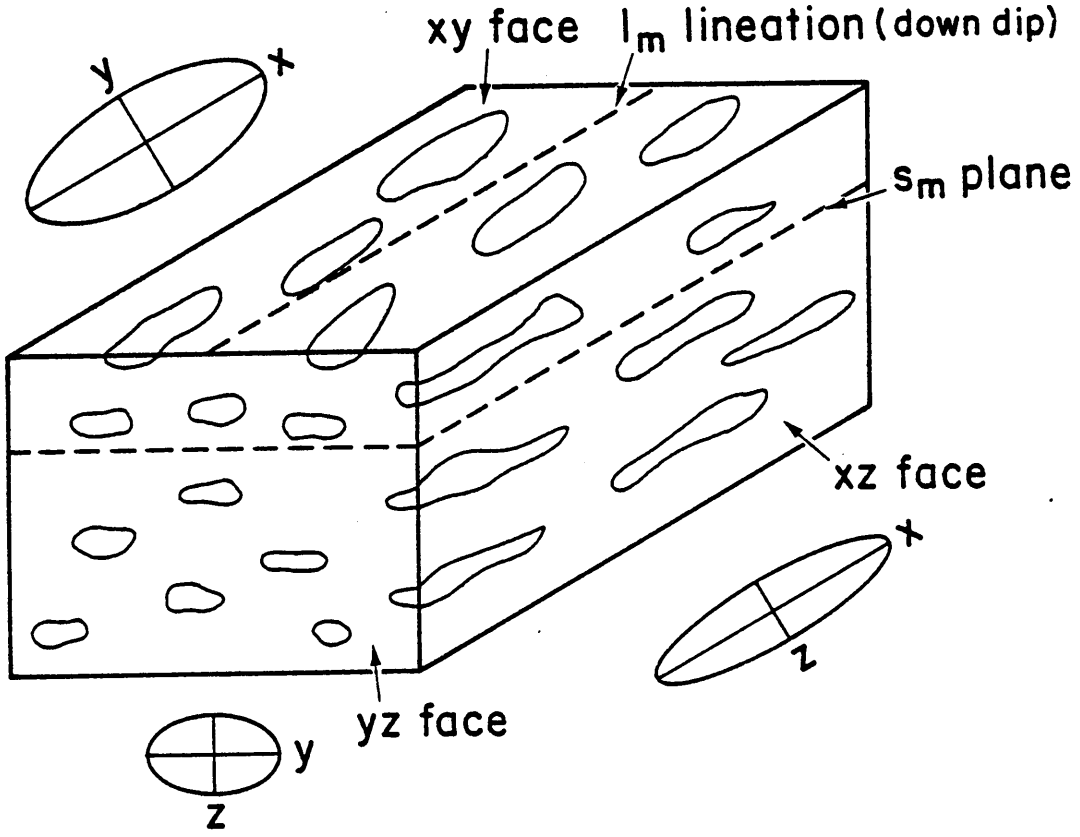

Fig. 82: Block diagram showing "L-S tectonite" (cf. Wood, 1976) nature of Fries DDZ mylonites and relative amount of deformation in three principal directions. (Cuts made parallel to these three faces for finite strain analyses.)

deformational events.

Sections were cut, as nearly as possible, to correspond to the principal planes of the finite strain ellipsoid (Fig. 82) and measurements of the X/Z, Y/Z and X/Y (where possible) axial ratios taken. Fig. 84 shows stages in the mylonitization of a granitoid gneiss as related to the finite strain ellipsoid. The augen approximate these strain ellipsoids with the smallest principal axis normal to the foliation (S_m) and the longest axis parallel to the lineation. These are representative of Flinns (1958, 1965) L-S tectonites (i.e., schistose-lineated rock: tectonites that lie between the two end points of L and S tectonites where schistosity is as well developed or a little better developed than the lineation). Augen in the unmylonitized are poorly developed and ill defined as growth was dominantly synchronous with the deformation. Thus, only elongate augen in the mylonitized zones could be measured, giving an indication of finite strains. As seen in Fig. 81, these plot in the flattening field, consistent with other major mylonite zones. The absence of measureable augen in the unmylonitized rocks precluded accurate determination of the deformation path and amount of bulk strain. In the most intensely deformed zones, the augen may be elongated in two mutually perpendicular directions, and this may partially account for the overlap between X/Z and Y/Z (see Fig 83, a and b).

Measurements of elongation ($\varepsilon = \frac{l_1 - l_o}{l_o}$) and shear strain ($\gamma$) were taken on potash feldspar augen, which had not yet undergone disaggregation in an attempt to determine 1) magnitudes of shear strain and

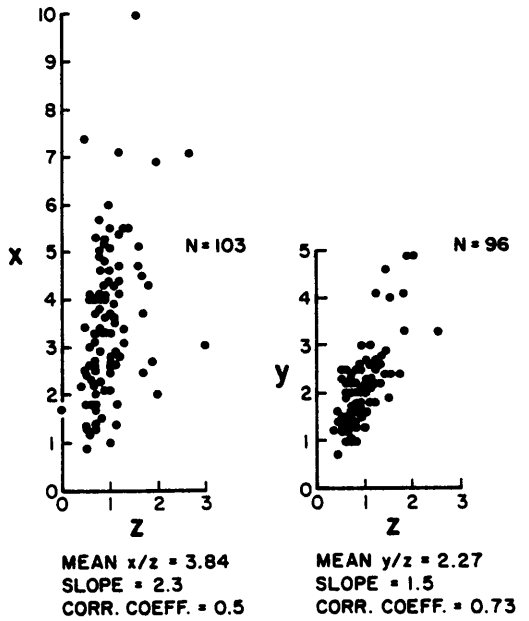

(a) 1 km from fault, mylonite zone

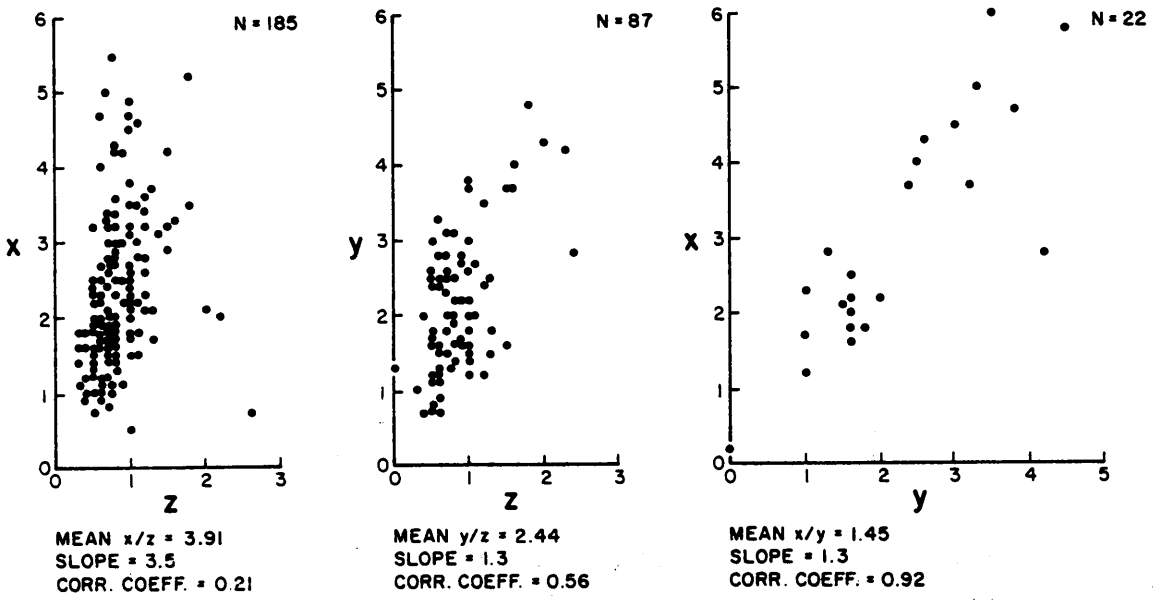

(b) just at fault trace, mylonite

Fig. 83: Plots of X/Z, Y/Z and X/Y as measured from alkali feldspar augen from fault zone; (Sample location B and 433, see Appendix I).

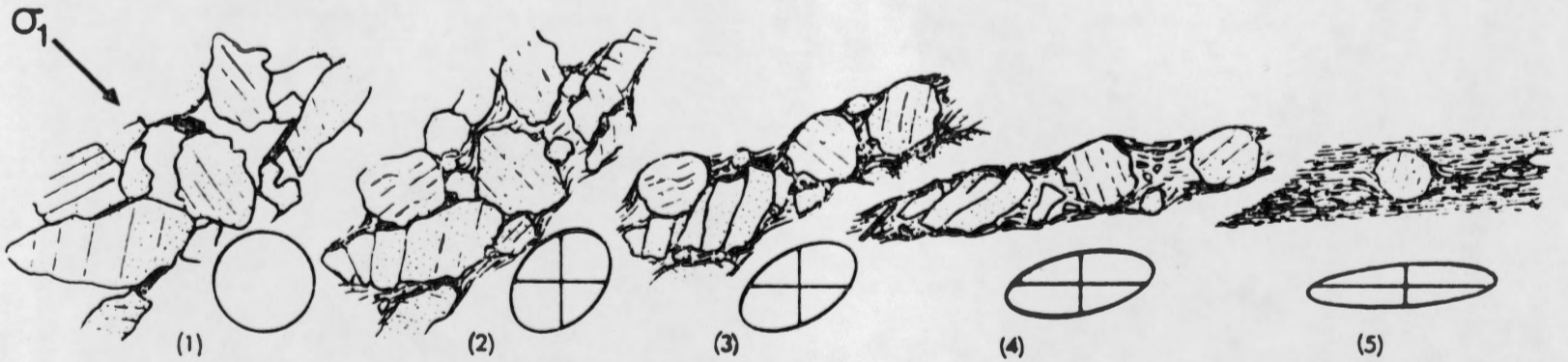

Fig. 85: Stages in the mylonitization of granitoid gneiss, related to the finite strain ellipsoid. (From Wakefield, 1977)

2) possible relationships between ε and γ. The method is schematically illustrated in Fig. 85. These do not show a linear relationship (Fig. 86), but elongation appears to reach a maximum at about .6, regardless of the amount of shear strain, which is, expectedly, greatest in the ultramylonite zones. This indicates that elongation can proceed to only a certain point (critical limit) before rotation and disaggregation become important.

The magnitude of shear strain lies between .2 and .4 in the protomylonite zone, .2-.7 in the mylonite zone and primarily greater than .6 in the ultramylonites. Thus, an increase in shear strain magnitude is evident with increasing intensity of deformation. In the Pilot, shear strain seems to reach higher magnitudes which suggests that more of the strain within the Little River Gneiss was accomodated by the matrix. This is supported by the microstructure.

Deformational History

As stated previously, there is at present no agreement on generalized strain paths within mylonite zones. Three hypotheses, each categorizing a different deformation history, have been postulated. These are:

1) In shear zones of infinite length with no deformation outside of the zone, deformation is relateable to heterogeneous simple shear or volume change or a combination of the two (Ramsay and Gramham, 1970). The developing schistosity (S_m) is not parallel to the walls of the shear zone, but formed perpendicular to principal axes of finite shortening. The strain shows a sigmoidal pattern of the XY trajectory

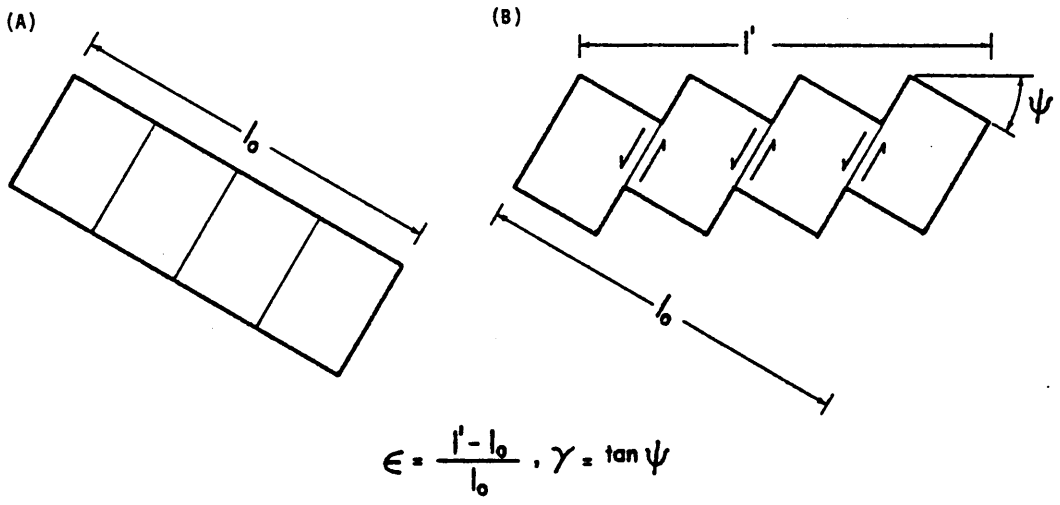

Fig. 85: Method of measuring elongation (ε) and shear strain (γ) for alkali feldspar augen. (a) undeformed state, (b) deformed state; l_o = undeformed length, l = deformed length, ψ = angular shear. (Formula from Ramsay, 1967)

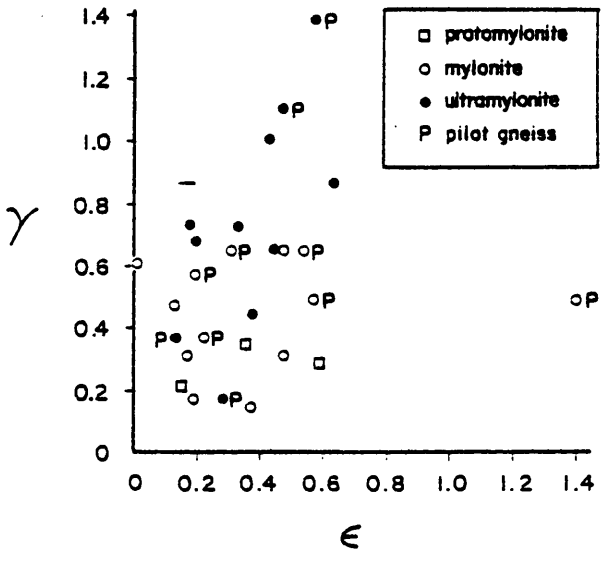

Fig. 86: Plot of shear strain (γ) vs. elongation (ε) from measurements of deformed feldspar augen (see above); samples from Little River Gneiss and Pilot Gneiss (labeled P).

surfaces giving an associated sigmoidal S_m variation (Fig. 87 and 88). This simple shear mechanism has been proposed for a number of shear zones (Eisbacher, 1970; Escher et al., 1975; Stowe, 1974; Bak et al., 1975; Wilkinson et al., 1975; Jain, 1975; Wakefield, 1977; Burg and Laurent, 1978; Roermund et al., 1978; Escher and Watterson, 1974).

2) Deformation is due to bulk flattening (pure shear) with no large translative movements (irrotational) and the mylonitic foliation is parallel to the margins of the shear zone (Johnson, 1967; Hossack, 1968; McLeish, 1971; Ross, 1973; Marjoribanks, 1976).

3) A combination of simple and pure shear (Coward, 1976, Subimal, 1977; Bell, 1978, Mitra, 1979).

Although both simple and pure shear are recognized in the latter (3), the actual relationship between them during mylonitization is interpreted quite differently. Determination of strain trajectories from shape changes of mafic and felsic minerals in shear zones from Botswana and Scotland (Coward, 1974) indicates simple shear dominant initially, while ductile mylonitic microstructures developed during a later flattening stage. A model proposed by Subimal (1977) is one in which initially developed planes of maximum shear strain rotate toward each other and into parallelism with the plane of flattening at later stages. This model is adhered to by Mitra (1979) as well. Studies of the Woodroffe Thrust led Bell (1978) to conclude that progressive pure shear dominated initially, gradually giving way to progressive simple shear until brittle rupture occurred. The transition from ductile to brittle deformation, he suggests, may have been due to an

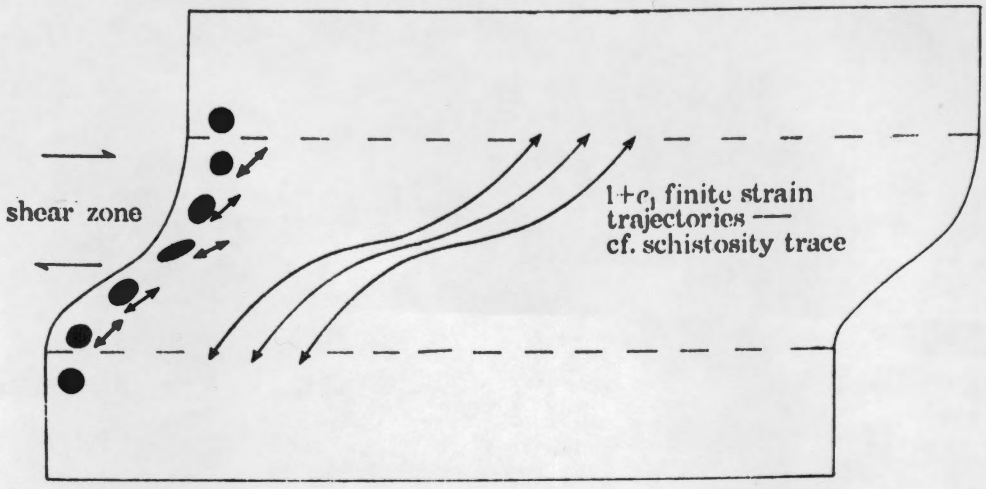

Fig. 87: Characteristic strain pattern in a shear zone. (From Ramsay, 1976)

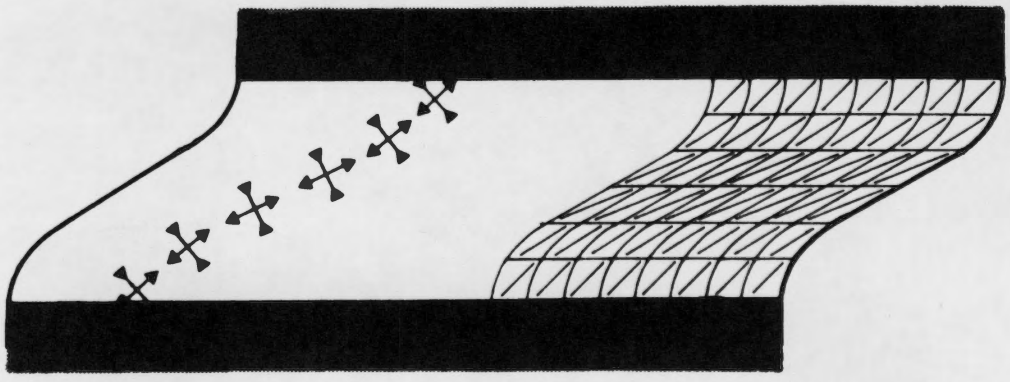

Fig. 88: Model of an ideal heterogeneous simple shear zone. The deformation at every point is progressive simple shear. The trajectories of the axes of finite strain are shown. The orientation of the instantaneous stretching axes remains constant at 45^{o} to the shear plane. (From Roermund et al., 1978)

increase in rate of work hardening.

The nature of changes in S_m orientation across the Fries DDZ and its angle to the shear zone boundary are virtually impossible to determine due to the large scale nature of the zone, the lack of outcrops in critical locations and polydeformation. Despite this, the importance of both simple and pure shear is obvious in the development of the microstructures and mylonitic fabric. Experimental work, as described previously, shows that simple shear is not necessary to explain the microstructures developed in both quartz and plagioclase (i.e., flattening operative on grain scale) and the strain measurements of augen indicate that the finite strain values plot in the flattening field. High angle fracturing associated with rotation and extension in alkali feldspar and plagioclase indicates simple shear on a grain scale is operative as well.

The original anisotropic character of the Little River Gneiss was a controlling factor in the orientation of the newly developing fabric, S_m, as recognized by parallel to subparallel allignment of the S_1 and S_m across the zone. The initial high angle conjugate shear zones described by Subimal (1977) and Mitra (1979) are not evident, even in the transition between the protomylonite and the mylonite zones. This precludes the rotation of such into the flattening plane. However, in the much coarser grained Pilot Gneiss where a primary fabric was not present, these conjugate shear zones are recognized locally. This indicates that composition and fabric are responsible for variations in the orientation and development of the mylonitic foliation.

Thus, for the Fries DDZ, although the bulk deformation path is progressive simple shear, flattening within the zone is important and becomes increasingly dominant during the latter stages of the deformation (evidenced by pressure solution features). The developing planar fabric (S_m) is defined by both preferred shape and crystallographic orientation of grains, although studies of the latter were not carried out on these rocks. At the grain scale, however, the strain is heterogeneously distributed due to differing mechanical responses of individual minerals to the deformation. In particular, feldspar grains play an important role in determining the local strain environment (cf. Lister and Price, 1978). This is reflected by differences in microstructure and crystallographic orientation between regions in the same thin section, suggesting that different fabric domains may have undergone different deformational histories.

VII. Conclusions

1. The Fries Fault, a major tectonic discontinuity in the Appalachian Orogen, constitutes a ductile deformation zone characterized by mylonitic fault rocks covering a 2.5 kilometer wide zone. It may be one of the most extensive features of the central and southern Appalachians.

2. The fault zone has undergone polydeformation. In the study area (near Riner, Montgomery County, Virginia), at least four phases of Paleozoic deformation have been recognized:

a. D_1 is characterized by large-scale, northeast trending, isoclinal F_1 folding. A penetrative S_1 gneissosity occurs in the Little River Gneiss, and slaty cleavage and schistosity in the Chilhowee and Ashe Formation metasediments respectively. The Pilot and leucocratic phases of the Little River Gneiss retained a granoblastic or subgranoblastic texture.

b. D_2 is characterized by a mylonitic foliation (S_m) in the basement and a crenulation cleavage (S_2) in the overlying metasediments. These foliations dominate across the entire fault zone. S_m is associated with a stretching lineation (l_m) which is defined by elongated quartz and feldspar. Small-scale, northeast trending, tight F_2 folds are present locally.

c. D_3 is characterized by a locally developed crenulation cleavage (S_3). It is most evident in the finer grained

metasediments of the most intensely deformed, finer grained zones of the basement units. This local nature is probably a function of competence. Small-scale, mesoscopic, northeast trending and microscopic tight to open F_3 folds are recognized locally. These occur primarily within the Little River Gneiss. Large-scale F_3 folds are present as well, one of which refolds the large F_1 anticline in the Pilot Gneiss.

d. D_4 includes all post D_3 deformation and is characterized by broad, northwest trending, open warps and by brittle fracturing.

3. At least three periods of metamorphism have affected rocks within the study area:

a. M_1 - PreCambrian Grenville metamorphic event that prograded the Pilot Gneiss to granulite and the Little River Gneiss to upper amphibolite or lower granulite facies.

b. M_2 - Early Paleozoic event synchronous with D_1 that retrogressed basement rocks to albite-epidote amphibolite or lower amphibolite facies and prograded overlying metasediments to lower and upper greenschist facies.

c. m_3 - Local retrogressive metamorphism synchronous with, but peaking early during faulting deformational event (D_2). Basement rocks within the fault zone were retrogressed to greenschist facies (chlorite, biotite and actinolite zones), while metasediments remained at lower greenschist facies

(chlorite zone). A biotite zone boundary is coincident with the trace of the Fries Fault, indicating that latest movement along the fault occurred after the peak of metamorphism.

4. The Fries Fault is actually a zone up to 2.5 kilometers in width, across which an increasing intensity of deformation is represented by subzones of protomylonite (1-1.2 km), mylonite (.5-1.0 km) and ultramylonite (cms to meters), the latter present within the mylonite subzone as thin, discontinuous zones, but especially prevalent along the fault trace. Boundaries across these zone are gradational in nature.

5. Mylonitization is characterized by:

   a. Inhomogeneity of strain states; initial inhomogeneities such as an initially developed fabric seem to control fabric orientation.

   b. A progressive decrease in grain size with increasing intensity of deformation.

   c. Brittle yielding in alkali feldspar, brittle combined with ductile yielding in plagioclase, and ductile yielding in quartz.

6. Both mechanical and chemical processes were operative during development of the mylonitic foliation, the former dominant initially giving way to chemical processes, primarily pressure solution, during later stages.

7. Although the bulk deformation path is progressive simple shear, flattening is important and increasingly dominant during the latter

stages of deformation. Finite strain studies indicate that the deformation path lies in the flattening field, consistent with most other major shear zones.

REFERENCES CITED

Ashby, M. P., 1972, A first report on deformation mechanism maps: Acta Metallurgica, v. 20, p. 887-897.

Allison, I., Barnett, R. L., and Kerrich, R., 1979, Superplastic flow and changes in crystal chemistry of feldspars: Tectonophysics, v. 538, p. T41-T46.

Bak, J., Korstgard, J., and Sorensen, K., 1975, A major shear zone within the Nassugtogidian of West Greenland: Tectonophysics, v. 27, p. 191-209.

Bartholomew, M. J., in press, Geology of the Stewartsville Quadrangle, Virginia: Virginia Division of Mineral Resources Publication.

Bartholomew, M. J., Gathright, T. M., II, and Henika, W. F., in press, A tectonic model for the Blue Ridge in Central Virginia: American Journal of Science.

Bartholomew, M. J., and Lewis, S., 1977, Relationships of the Fries Thrust to the basement complex and Paleozoic deformation in the Blue Ridge of northwestern North Carolina and southwestern Virginia: Geological Society of America Abstracts with Programs, v. 9, no. 2, p. 116-117.

Bartholomew, M. J., and Lowry, W. D., 1979, Geology of the Blacksburg Quadrangle, Virginia: Virginia Division of Mineral Resources, Publication 14, G.M.-81B; Abstract in Geological Society of America Abstracts with Programs, 1979, v. 11, no. 4, p. 170.

Beach, A. and Fyfe, W. S., 1972, Fluid transport and shear zones at Scourie, Sutherland: evidence for overthrusting?: Contributions to Mineralogy and Petrology, v. 36, p. 175-180.

Bell, T. H., 1978, Progressive deformation and reorientation of fold axes in a ductile mylonite zone: The Woodroffe Thrust: Tectonophysics, v. 44, p. 285-320.

Bell, T. H., and Etheridge, M. A., 1973, Microstructure of mylonites and their descriptive terminology: Lithos, v. 6, p. 337-348.

Bell, T. H., and Etheridge, M. A., 1976, The deformation and recrystallization of quartz in a mylonite zone, Central Australia: Tectonophysics, v. 32, p. 235-267.

Borg, I. Y. and Heard, H. C., 1969, Mechanical twinning and slip in experimentally deformed plagioclase: Contributions to Mineralogy and Petrology, v. 23, p. 128-135.

Borg, I. Y., and Heard, H. C., 1970, Experimental deformation of plagioclase, in Paulitsch, P., ed., Experimental and Natural Rock Deformation, Berlin-Heidelberg, Springer-Verlag, p. 375-404.

Borradaile, G. J., 1976, A strain study of a granite - granite gneiss transition and accompanying schistosity formation in the Betic Orogenic zone, southeast Spain: Journal of the Geological Society of London, v. 132, p. 417-428.

Boullier, A. M., and Gueguen, Y., 1975, SP mylonites: Origin of some mylonites by superplastic flow: Contributions to Mineralogy and Petrology, v. 50, p. 93-104.

Bryant, B., and Reed, J. C., Jr., 1970, Structural and metamorphic history of the Southern Blue Ridge, in Fisher, G. W., and others, eds., Studies of Appalachian Geology, Central and Southern: New York, Interscience Publishers, p. 213-225.

Burg, J. P. and Laurent, P. H., Strain analysis of a shear zone in a granodiorite: Tectonophysics, v. 47, p. 15-42.

Butler, J. R., 1972, Age of Paleozoic regional metamorphism in the Carolinas, Georgia and Tennessee, Southern Appalachians: American Journal of Science., v. 272, p. 319-333.

Cahn, R. W., 1965, Recovery and recrystallization, in Cahn, R. W., ed., Physical Metallurgy: New York, John Wiley & Sons, Inc., p. 925-987.

Carter, N. L., Christie, J. M., and Griggs, D. T., 1964, Experimental deformation and recrystallization of quartz: Journal of Geology, v. 72, no. 6, p. 687-733.

Christie, J. M., 1960, Mylonitic rocks of the Moine Thrust Zone in the Assynt Region, northwest Scotland: Transactions of the Edinburgh Geological Society, v. 18, p. 79-93.

Christie, J. M., Griggs, D. T. and Carte-, N. L., 1964, Experimental evidence of basal slip in quartz: Journal of Geology, v. 72, p. 734-756.

Christie, J. M., Griggs, D. T. and Carter, N. L., 1966, Experimental deformation and recrystallization of quartz and experimental evidence of basal slip in quartz: A reply: Journal of Geology, v. 74, p. 368-371.

Coble, R. L., 1963, A model for boundary diffusion controlled creep in polycrystalline materials: Journal of Applied Physics, v. 34, p. 1979-1982.

Cook, F. A., Albaugh, D. S., Brown, L. D., Kaufman, S., and Oliver, J. E., 1979, Preliminary interpretation of COCORP seismic reflection data across the Brevard Zone in northeast Georgia: Geological Society of America Abstracts with Programs, v. 11, no. 4, p. 175.

Cook, F. A., Albaugh, D. S., Brown, L. D., Kaufman, S. and Oliver, J. E., 1979, Thin-skinned tectonics in the crystalline southern Appalachians; COCORP seismic-reflection profiling of the Blue Ridge and Piedmont: Geology, v. 7, p. 563-567.

Coward, M. P., Graham, R. H., James, P. R. and Wakefield, J., 1973, A structural interpretation of the northern margin of the Limpopo Orogenic Belt, Southern Africa: Philosophical Transactions of the Royal Society of London, v. A273, p. 487-491.

Coward, M. P., and James, P. R., 1974, The deformation patterns of two Archean greenstone belts in Rhodesia and Botswana: PreCambrian Research, v. 1, p. 235-258.

Coward, M. P., 1976, Archaean deformation patterns in southern Africa: Philosophical Transactions of the Royal Society of London, v. A283, p. 313-331.

Coward, M. P., 1976, Strain within ductile shear zones: Tectonophysics, v. 34, p. 181-197.

Debat, P., Soula, O., Kubin, L., and Vidal, J., 1978, Optical studies of natural deformation microstructures in feldspar (gneiss and pegmatites from Occitania, Southern France): Lithos, v. 11, p. 133-145.

Dietrich, R. V., 1954, Geology of the Pilot Mountain Area, Virginia: Virginia Polytechnic Institute Bulletin, Engineering Experimental Station Series, no. 91, 32 p.

Dietrich, R. V., 1959, Geology and mineral resources of Floyd County of the Blue Ridge Upland, southwestern Virginia: Virginia Polytechnic Institute Bulletin, Engineering Experimental Station Series, no. 134, 160 p.

Dietrich, R. V., Fullager, P. D., and Bottino, M. L., 1969, K/Ar and Rb/Sr dating of tectonic events in the Appalachians of southwestern Virginia: Geological Society of America Bulletin, v. 80, p. 307-314.

Durney, D. W., 1972, Solution transfer, an important geological deformation mechanism: Nature, v. 235, p. 315-317.

Durney, D. W., 1976, Pressure solution and crystallization deformation: Philosophical Transactions of the Royal Society of London, v. A283, p. 229-240.

Durney, D. W., and Ramsay, J. G., 1973, Incremental strain measured by syntectonic crystal growths, in Kees, A., and Scholten, R., eds., Gravity and Tectonics: New York, Wiley & Sons, Inc., p. 67-96.

Eisbacher, G. H., 1970, Deformation mechanics of mylonitic rocks and fractured granites in Cobequid Mountains, Nova Scotia, Canada: Geological Society of America Bulletin, v. 81, p. 2009-2020.

Elliott, D., 1973, Diffusion flow laws in metamorphic rock: Geological Society of America Bulletin, v. 84, p. 2645-2664.

Engelder, J. T., 1974, Cataclasis and the generation of fault gouge: Geological Society of America Bulletin, v. 85, p. 1515-1522.

Escher, A., and Watterson, J., 1974, Stretching fabrics, folds and crustal shortening: Tectonophysics, v. 22, p. 223-231.

Escher, A., Escher, J., and Watterson, J., 1975, The orientation of the Kangamiut Dike Swarm, West Greenland: Canadian Journal of Earth Sciences, v. 128, p. 158-173.

Flinn, D., 1958, On the nappe structure of northeast Shetland: Quarterly Journal of Geological Society of London, v. 114, p. 107-136.

Flinn, D., 1965, On the symmetry principle and the deformation ellipsoid: Geology Magazine, v. 102, p. 36-45.

France, B. J., 1978, Deformation microstructures in mylonites from the Norumbega Fault, Maine: Thesis, Department of Geological Sciences, Brown University,

Gay, N. G. and Weiss, L. E., 1974, The relationship between principal stress directions and the geometry of kinks in foliated rocks: Tectonophysics, v. 21, p. 287-300.

Goetze, C., 1975, Textural and microstructural systematics in olivine and quartz (abs.): EOS (American Geophysical Union Transactions), v. 56, p. 455.

Green, H. W., Griggs, D. T. and Christie, J. M., 1970, Syntectonic and annealing recrystallization of fine-grained quartz aggregates, in Paulitsch, P., ed., Experimental and natural rock deformation: Berlin-Heidelberg, Springer-Verlag, p. 272-335.

Griggs, D. T., 1967, Hydrolytic weakening of quartz and other silicates: Geophysical Journal of the Royal Astronomical Society, v. 14, p. 19-31.

Griggs, D. T., 1974, A model of hydrolytic weakening in quartz: Journal of Geophysical Research, v. 79, p. 1655-1661.

Hara, I., Takeda, K. and Kimura, T., 1973, Preferred lattice orientation of quartz in shear deformation: Hiroshima University Journal of Science, v. 7, p. 1-10.

Hatcher, R. D., 1978, Tectonics of the western Piedmont and Blue Ridge, Southern Appalachians: Review and Speculation: Journal of Science, v. 278, p. 276-304.

Hobbs, B. E., Means, W. D., and Williams, P. F., 1976, An Outline of Structural Geology: Wiley, New York, 571 p.

Hossack, J. R., 1968, Pebble deformation and thrusting in the Bygdin Area (Southern Norway): Tectonophysics, v. 5, p. 315-339.

Hutton, D. H. W., 1979, The strain history of a Dalradian Slide; using pebbles with low fluctuations in axis orientation: Tectonophysics, v. 55, no. 3-4, p. 261-273.

Jain, A. K., 1975, Structure and petrology of mylonites and related rocks from the lesser Himalaya, Garhwal India: Geologische Rundschau, v. 64, no. 1, p. 230-248.

Johnson, M. R. W., 1967, Mylonite zones and mylonitic banding: Nature, v. 213, p. 246-247.

Jones, M. E., 1975, Water weakening of quartz and its application to natural rock deformation: Journal of the Geological Society of London, v. 131, p. 429-432.

Kerrich, R., Fyfe, W. S., Gorman, B. E., and Allison, I., 1977, Local modification of rock chemistry by deformation: Contributions to Mineralogy and Petrology, v. 65, p. 183-190.

Lapworth, , C., 1885, The Highland controversy in British geology: its causes, course and consequences: Nature, v. 32, p. 558-559.

Lewis, S., 1975, Geology of the southern part of the Riner Quadrangle, Montgomery and Floyd Counties, Virginia (Masters Thesis): North Carolina State University, 106 p.

Lister, G. S., and Price, G. P., 1978, Fabric development in a quartz feldspar mylonite: Tectonophysics, v. 49, p. 37-78.

Lister, G. S., Paterson, M. S., and Hobbs, B. E., 1978, The simulation of fabric development in plastic deformation and its application to quartzites: the model: Tectonophysics, v. 45, p. 107-158.

Marjoribanks, R. W., 1976, The relation between microfabrics and strain in a progressively deformed quartzite sequence from central Australia: Tectonophysics, v. 32, p. 269-293.

Mitra, Gautram, 1978, Ductile deformation zones and mylonites: the mechanical proce-ses involved in the deformation of crystalline basement rocks: American Journal of Science, v. 278, p. 1057-1084.

Mitra, Gautram, 1979, Ductile deformation zones in Blue Ridge basement rocks and estimation of finite strains: Geological Society of America Bulletin, v. 90, no. 10, p. I935-I951.

McLeish, A. J., 1971, Strain analysis of deformed pipe rock in the Moine Thrust Zone, northwest Scotland: Tectonophysics, v. 12, p. 469-503.

Nicolas, A., Boudier, F. and Boullier, A. M., 1973, Mechanisms of flow in naturally and experimentally deformed peridotites: American Journal of Science, v. 273, p. 853-876.

Nicolas, A., and Poirier, , 1976, Crystalline plasticity and solid state flow in metamorphic rocks: New York, John Wiley & Sons, Inc., 444 p.

Prinz, M., and Poldevaart, A., 1964, Layered mylonite from Beartooth Mountains, Montana: Bulletin of the Geological Society of America, v. 75, p. 741-744.

Ramberg, H., 1953, The origin of metamorphic and metasomatic rocks: University of Chicago Press, Chicago, 317 p.

Ramsay, J. G., 1967, Folding and Fracturing of Rocks: McGraw-Hill, New York,

Ramsay, J. G., 1976, Displacement and strain: Philosophical Transactions of the Royal Society of London, Ser. A., v. 283, no. 1312, p. 3-25.

Ramsay, J. G., and Graham, R. H., 1970, Strain variation in shear belts: Canadian Journal of Earth Sciences, v. 7, p. 786-813.

Rankin, D. W., 1970, Stratigraphy and structure of PreCambrian rocks in northwestern North Carolina, in Fisher, G. W., and others, eds., Studies of Appalachian Geology, Central and Southern: New York, Interscience Publishers, p. 227-245.

Rankin, D. W., Espenshade, G. H., and Shaw, K. W., 1973, Stratigraphy and structure of the metamorphic belt in northwestern North Carolina and southwestern Virginia: A study from the Blue Ridge across the Brevard Fault Zone to the Sauratown Mountains anticlinorium: American Journal of Science, v. 273-A (Cooper volume), p. 1-40.

Rankin, D. W., 1975, The continental margin of the eastern North America in the Southern Appalachians; the opening and closing of the proto-

Atlantic Ocean: American Journal of Science, v. 275-A, p. 298-336.

Roermund, H. van, Lister, G. S., and Williams, P. F., 1978, Progressive development of quartz fabrics in a shear zone from Monte Mucrome, Sesia-Lanzo Zone, Italian Alps: Journal of Structural Geology, v. 1, no. 1, p. 43-52.

Ross, J. V., 1973, Mylonitic rocks and flattened garnets in the southern Okanagan of British Columbia: Canadian Journal of Earth Sciences, v. 10, no. 1, p. 1-17.

Rutter, E. H., 1976, The kinetics of rock deformation by pressure solution: Philosophical Transactions of the Royal Society of London, v. 283, p. 209-219.

Schmidt, W., 1932, Tektonik und Verformungslehre: Borntraeger, Berlin, 208 p.

Sclar, Charles B., 1965, Layered mylonites and the processes of metamorphic differentiation: Geological Society of America Bulletin, v. 76, p. 611-612.

Sibson, R. H., 1977, Fault rocks and fault mechanisms: Journal of the Geological Society of London, v. 133, p. 191-213.

Stirewalt, G. L., and Dunn, D. E., 1973, Mesoscopic fabric and structural history of Brevard Zone and adjacent rocks, North Carolina: Geological Society of America Bulletin, v. 84, p. 1629-1650.

Stose, A. J., and Stose, G. W., 1957, Geology and mineral resources of the Gossan Lead District and adjacent areas in Virginia: Virginia Division of Mineral Resources Bulletin, no. 72, 233 p.

Stowe, C. W., 1974, Alpine-type structures in the Rhodesian basement complex at Selukwe: Journal of the Geological Society of London, v. 130, p. 411-426.

Submial, Sinha Roy, 1977, Deformation and chemical processes in mylonite genesis: Geologiska Foereningens i Stockholm Foerhandlingar, v. 99, p. 3-9.

Themistocleous, S. G., and Schwerdtner, W. M., 1977, Estimates of distortional strain in mylonites from the Grenville Front tectonic zone, Tomiko area, Ontario: Canadian Journal of Earth Sciences, v. 14. no. 8, p. 1708-1720.

Truman, W. E., 1976, Geology of the Blue Ridge Front near Riner, Virginia (Masters Thesis): Blacksburg, Virginia Polytechnic Institute and State University, 102 p.

Verhoogen, J., Turner, F. J., and Weiss, L. E., 1970, The Earth; an introduction to physical geology: Holt, Rinehart and Winston, New York-London-Sydney, 748 p.

Vernon, R. H., 1974, Controls of mylonitic compositional layering during non-cataclastic ductile deformation: Geology Magazine, v. 111, no. 2, p. 121-123.

Vernon, R. H., 1975, Deformation and recrystallization of a plagioclase grain: American Mineralogist, v. 60, p. 884-888.

Vernon, R. H., 1976, Metamorphic processes, reactions and microstructure development: Allen and Unwin, London, 247 p.

Wakefield, John, 1977, Mylonitization in the Lethakane shear zone, eastern Botswana: Journal of the Geological Society of London, v. 133, p. 263-275.

White, S., 1975, Effect of polyphase deformation on the defect structures in quartz II: Neues. Jb. Miner. Abh., v. 123, p. 237-252.

White, S., 1976, The effects of strain on the microstructures, fabrics, and deformation mechanisms in quartzites: Philosophical Transactions of the Royal Society of London, v. A283, p. 69-86.

White, S. H., and Knipe, R. J., 1978, Transformation and reaction - enhanced ductility in rocks: Journal of the Geological Society of London, v. 135, p. 513-516.

Wilkinson, P., Soper, N. S., and Bell, A. M., 1975, Skolithos pipes as strain markers in mylonites: Tectonophysics, v. 28, p. 143-157.

Wilson, C. J. L., 1972, Preferred orientation of quartz in a prograde metamorphic sequence (abs.): EOS (American Geophysical Union Transactions), v. 53, no. 4, p. 514.

Wilson, C. J. L., 1973, The prograde microfabric in a deformed quartzite sequence, Mt. Isa, Australia: Tectonophysics, v. 19, p. 39-81.

Winkler, H. G., 1976, Petrogenesis of metamorphic rocks: New York, Springer-Verlag, 334 p.

Wintsch, R. P., 1975, Feldspathization as a result of deformation: Geological Society of America Bulletin, v. 86, p. 35-38.

Wood, D. S., 1973, Patterns and magnitudes of natural strain in rocks: Philosophical Transactions of the Royal Society of London, Ser. A, v. 274, p. 373-382.

Wood, D. S., Oertel, G., Singh, J., and Bennett, H. F., 1976, Strain and anisotropy in rocks: Philosophical Transactions of the Royal

Society of London, v. 283, no. 1312, p. 27-42.

APPENDIX I

SAMPLE LOCATIONS

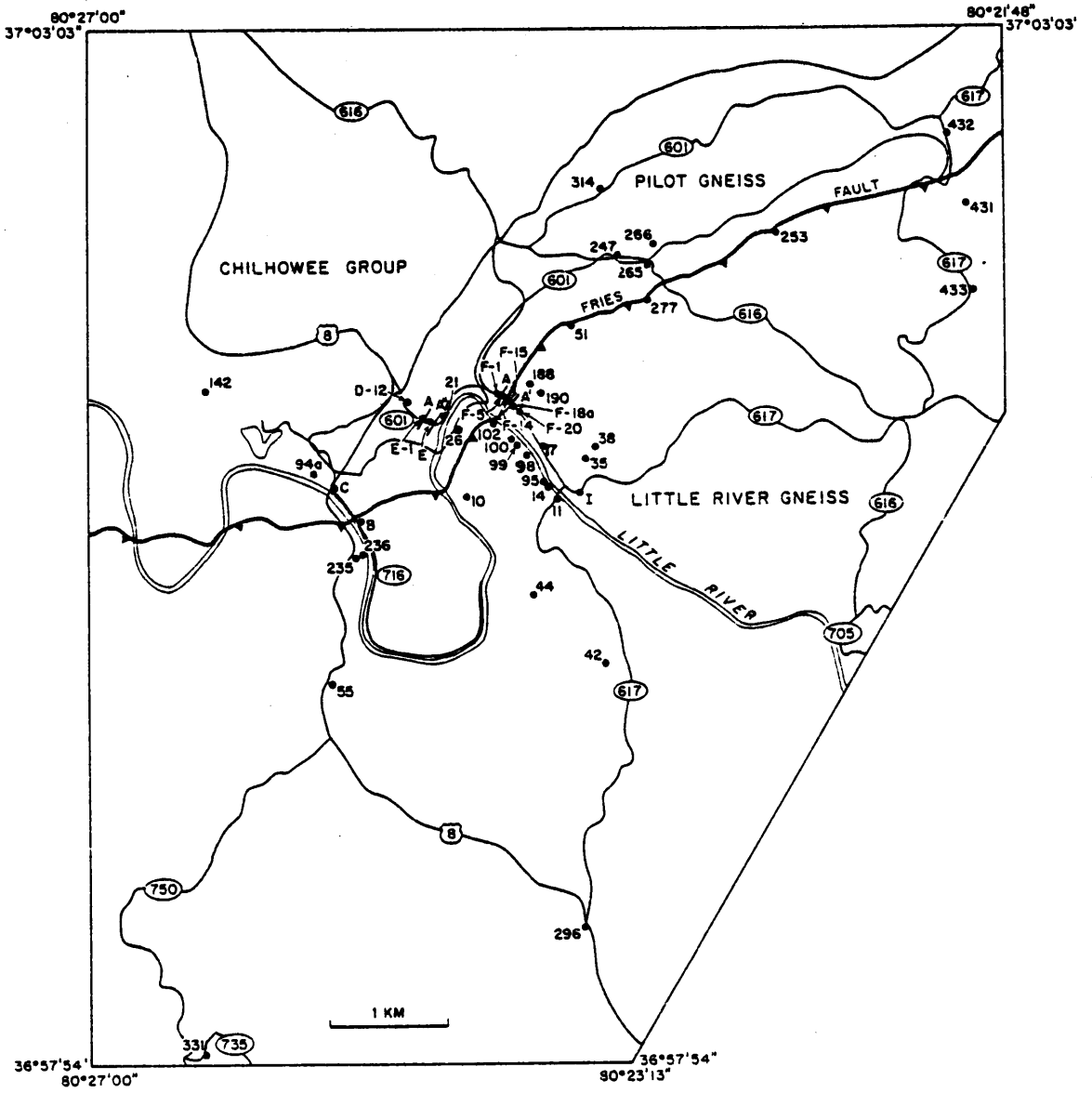

APPENDIX II: MICROPROBE DATA OF SELECTED SAMPLES ACROSS THE FRIES FAULT ZONE

MICROPROBE DATA

(weight percent of oxides)

Oxide	Plagioclase	Plagioclase	Alkali Feldspar	Alkali Feldspar	Biotite	Biotite	Muscovite
#331 - Nonmylonitized Little River Gneiss (see location map for all samples)							
MgO	0.000	0.011	0.000	0.000	6.763	6.859	2.279
Al_2O_3	19.070	19.201	18.010	18.010	14.469	14.999	24.617
SiO_2	68.601	67.819	62.735	62.735	35.717	34.492	47.323
Na_2O	11.607	11.371	0.498	0.498	0.064	0.070	0.167
K_2O	0.063	0.047	16.085	16.085	8.887	8.928	11.347
CaO	0.198	0.259	0.003	0.003	0.162	0.202	0.007
TiO_2	0.010	0.013	0.092	0.092	1.528	1.543	0.321
FeO	0.044	0.096	0.074	0.074	25.791	24.220	4.233
MnO	0.000	0.000	0.057	0.057	0.374	0.482	0.042
	99.591	98.818	97.554	97.554	93.755	91.796	90.336
#296 - Nonmylonitic Little River Gneiss							
MgO	0.000	0.005	0.032	0.000	8.412	8.329	
Al_2O_3	19.480	20.331	18.286	18.897	16.553	16.551	
SiO_2	69.301	67.696	63.939	67.866	37.021	36.801	
Na_2O	11.402	11.459	0.334	0.541	0.067	0.057	
K_2O	0.070	0.056	14.562	14.768	8.756	8.467	
CaO	0.276	0.125	0.000	0.032	0.086	0.088	
TiO_2	0.000	0.005	0.049	0.085	1.375	1.583	
FeO	0.000	0.000	0.034	0.030	23.880	22.728	
MnO	0.000	0.043	0.055	0.076	0.465	0.571	
	100.529	99.720	97.291	102.295	96.615	95.185	

MICROPROBE DATA

(weight percent of oxides)

Oxide	Plagioclase	Plagioclase	Alkali Feldspar	Alkali Feldspar	Biotite	Biotite	Biotite	Muscovite
#42 - Little River Gneiss - Protomylonite								
MgO	0.000	0.033	0.068	0.069	6.959			4.258
Al_2O_3	20.916	20.016	20.192	18.927	17.236			24.031
SiO_2	65.665	67.520	65.682	65.325	37.302			42.332
Na_2O	10.666	11.551	1.779	0.281	0.047			0.086
K_2O	0.061	0.102	12.632	13.941	7.604			8.916
CaO	1.810	0.139	0.022	0.073	0.103			0.016
TiO_2	0.009	0.000	0.033	0.130	1.529			0.643
FeO	0.355	0.005	0.000	0.082	21.355			11.527
MnO	0.000	0.030	0.034	0.031	0.397			0.295
	99.482	99.397	100.444	98.860	92.530			92.105
#11 - Little River Gneiss - Mylonite								
MgO	0.000	0.012	0.059	0.069	7.742	7.736	8.054	2.242
Al_2O_3	20.482	20.124	19.637	20.172	16.712	16.324	16.654	27.492
SiO_2	67.220	67.071	64.634	64.280	36.474	35.410	36.596	47.714
Na_2O	11.228	11.454	0.218	1.268	0.045	0.024	0.102	0.103
K_2O	0.042	0.217	13.392	11.740	8.334	7.645	7.882	9.135
CaO	0.121	0.099	0.050	0.373	0.038	0.072	0.109	0.000
TiO_2	0.000	0.000	0.018	0.060	1.736	1.511	1.258	0.229
FeO	0.055	0.029	0.052	0.006	25.560	25.171	25.423	4.991
MnO	0.075	0.000	0.095	0.018	0.530	0.409	0.473	0.144
	99.221	99.006	98.154	97.986	97.170	94.301	96.552	92.048

MICROPROBE DATA

(weight percent of oxides)

Oxide	Plagioclase	Plagioclase	Alkali Feldspar	Alkali Feldspar	Biotite	Biotite	Muscovite	Muscovite
#95 - Little River Gneiss, Mylonite								
MgO	0.000	0.000	0.081	0.083	7.776	7.587	2.199	2.654
Al_2O_3	18.963	21.356	18.615	18.997	16.294	15.806	26.326	25.828
SiO_2	70.214	67.892	64.403	64.926	37.139	37.453	48.770	47.934
Na_2O	11.885	11.578	0.507	0.302	0.023	0.070	0.145	0.104
K_2O	0.031	0.071	14.400	15.387	7.613	7.946	10.405	10.479
CaO	0.049	0.349	0.129	0.000	0.203	0.146	0.002	0.012
TiO_2	0.000	0.000	0.084	0.059	1.430	1.079	0.252	0.530
FeO	0.110	0.096	0.023	0.015	22.121	22.372	4.040	5.321
MnO	0.000	0.004	0.037	0.072	0.375	0.256	0.175	0.114
	101.252	101.345	98.280	99.840	92.973	92.715	92.316	92.975
#99a - Little River Gneiss - Mylonite								
MgO	0.000	0.028			7.601	7.020	2.500	
Al_2O_3	19.471	20.483			15.493	14.114	25.932	
SiO_2	68.221	67.991			37.793	36.438	48.655	
Na_2O	11.550	11.310			0.052	0.028	0.093	
K_2O	0.077	0.077			8.653	8.288	10.191	
CaO	0.235	0.457			0.129	0.073	0.033	
TiO_2	0.000	0.000			1.330	2.604	0.210	
FeO	0.044	0.061			22.134	22.496	4.408	
MnO	0.015	0.061			0.433	0.323	0.155	
	99.613	100.469			93.618	91.383	92.176	

MICROPROBE DATA

(weight percent of oxides)

Oxide	Plagioclase	Plagioclase	Alkali Feldspar	Alkali Feldspar	Biotite	Biotite	Muscovite
#B-22 - Little River Gneiss, intense part of mylonite zone (at fault trace)							
MgO	0.069	0.000	0.031	0.031	7.953	6.893	2.426
Al_2O_3	20.180	19.772	17.626	17.717	15.631	15.562	24.833
SiO_2	67.884	67.992	63.816	66.947	37.691	36.213	49.324
Na_2O	11.141	11.474	0.410	2.162	0.021	0.040	0.099
K_2O	0.605	0.075	15.775	14.035	9.701	9.588	11.139
CaO	0.503	0.207	0.012	0.198	0.048	0.091	0.000
TiO_2	0.013	0.005	0.061	0.068	0.898	1.591	0.230
FeO	0.205	0.035	0.000	0.000	25.248	25.167	5.326
MnO	0.031	0.000	0.000	0.129	0.384	0.361	0.055
	100.630	99.560	97.731	101.288	97.573	95.506	93.433
#38 - Granitic Phase of Little River Gneiss, Mylonite							
MgO	0.000	0.000	0.063	0.105	6.666	4.230	
Al_2O_3	20.725	20.547	19.106	19.238	14.615	19.919	
SiO_2	68.180	67.623	65.788	64.072	36.277	40.190	
Na_2O	11.694	11.554	0.360	0.250	0.022	0.067	
K_2O	0.061	0.039	14.723	14.800	7.922	8.730	
CaO	0.123	0.097	0.020	0.016	0.087	0.029	
TiO_2	0.007	0.000	0.032	0.036	1.258	1.236	
FeO	0.000	0.000	0.021	0.101	25.073	18.148	
MnO	0.005	0.004	0.082	0.077	0.497	0.325	
	100.795	99.864	100.195	98.696	92.419	92.874	

MICROPROBE DATA

(weight percent of oxides)

Oxide	Plagioclase	Plagioclase	Alkali Feldspar	Alkali Feldspar	Alkali Feldspar Lamellae	Garnet	Garnet
#10 - Granitic Phase of Little River Gneiss, Mylonite Zone							
MgO	0.000		0.004	0.071	0.000	2.598	2.937
Al_2O_3	19.909		18.532	18.752	19.603	17.174	17.575
SiO_2	68.013		65.190	65.677	67.868	37.652	38.524
Na_2O	11.620		0.577	0.220	11.081	0.004	0.011
K_2O	0.074		15.111	16.040	0.145	0.051	0.039
CaO	0.354		0.026	0.018	0.844	2.299	2.133
TiO_2	0.024		0.059	0.003	0.009	0.155	0.171
FeO	0.080		0.000	0.040	0.033	36.239	35.361
MnO	0.000		0.046	0.038	0.000	1.650	1.705
	100.073		99.545	100.860	99.583	97.822	98.638
#F-20 - Granitic Phase of Little River Gneiss, Ultramylonite Zone							
MgO	0.091	0.000	0.043	0.013	0.021		
Al_2O_3	18.996	21.488	17.526	17.371	20.791		
SiO_2	69.063	66.975	65.196	65.603	66.812		
Na_2O	11.341	10.156	0.346	0.260	11.166		
K_2O	0.133	0.755	15.641	16.276	0.144		
CaO	0.408	1.677	0.000	0.004	1.031		
TiO_2	0.000	0.003	0.095	0.072	0.001		
FeO	0.088	0.023	0.088	0.077	0.000		
MnO	0.000	0.000	0.111	0.000	0.010		
	100.122	101.078	99.046	99.675	99.977		

MICROPROBE DATA

(weight percent of oxides)

Oxide	Plagioclase	Plagioclase	Alkali Feldspar	Alkali Feldspar	Biotite	Biotite	Garnet	Garnet
#266 - Pilot Gneiss - Mylonite								
MgO	0.000	0.048	0.031	0.001				
Al_2O_3	18.984	19.350	17.971	17.541				
SiO_2	67.748	68.464	64.297	65.701				
Na_2O	11.360	11.631	0.886	0.389				
K_2O	0.058	0.058	15.062	16.245				
CaO	0.002	0.010	0.030	0.012				
TiO_2	0.003	0.000	0.065	0.067				
FeO	0.080	0.016	0.001	0.002				
MnO	0.000	0.034	0.062	0.000				
	98.185	99.610	98.406	99.958				
#314 - Pilot Gneiss (Porphyroblastic Phase) - Mylonite								
MgO			0.070	0.058	7.140	6.763	3.692	3.628
Al_2O_3			20.196	19.966	16.032	14.382	19.341	18.679
SiO_2			64.329	66.343	35.262	35.562	39.336	38.686
Na_2O			0.270	0.227	0.052	0.042	0.018	0.015
K_2O			13.513	13.450	6.732	9.267	0.027	0.028
CaO			0.051	0.045	1.306	0.109	3.682	3.802
TiO_2			0.077	0.097	4.132	3.668	0.159	0.143
FeO			0.080	0.054	21.171	23.080	34.444	34.330
MnO			0.047	0.137	0.283	0.281	1.175	1.209
			98.632	100.377	92.112	93.154	101.874	100.519

The vita has been removed from the scanned document

THE FRIES FAULT NEAR RINER, VIRGINIA
AN EXAMPLE OF A POLYDEFORMED, DUCTILE DEFORMATION ZONE

by

Patti Boyd Kaygi

(ABSTRACT)

The Fries Fault, a 1.2-2.3 km wide zone near Riner, is a major tectonic discontinuity in the Blue Ridge geologic province, characterized by progressive stages of continuous ductile deformation. Trending northeast with a shallow to moderate southeast dip, this fault juxtaposes Little River Gneiss on the southeast against Pilot Gneiss and the Chilhowee Formation to the northwest. A 0.8-1.2 km wide subzone of protomylonite within the Little River Gneiss grades into a 0.5-1.0 km wide mylonite subzone, the latter containing narrow bands of phyllonitic ultramylonite ranging in width from centimeters to tens of meters. Mylonitization is reflected by a marked reduction in grain size, elongation of quartz and fracturing of feldspar, all concomitant with the development of a mylonitic foliation (S_m). Ductile deformation processes involving grain elongation, recovery and recrystallization, combined with chemical processes (primarily pressure solution), are the dominant strain-accomodation mechanisms in the formation of S_m. Rocks within the fault zone have undergone four phases of Paleozoic deformation. An early S_1 foliation has been nearly completely transposed by $S_m(S_2)$, which dominates across most of the area. The development of S_m was accompanied by a retrogressive metamorphism that altered basement rocks from lower amphibolite to greenschist facies. Chilhowee

Group rocks remained at lower greenschist facies. Post-faulting deformation produced an S_3 crenulation cleavage associated with northeast trending, overturned F_3 folds. Subsequent refolding produced open, northwest trending F_4 folds. Although the bulk deformation is progressive simple shear, flattening is increasingly dominant during the later stages of deformation.

80°27'
37°03'03"

80°21'48"
37°03'03"

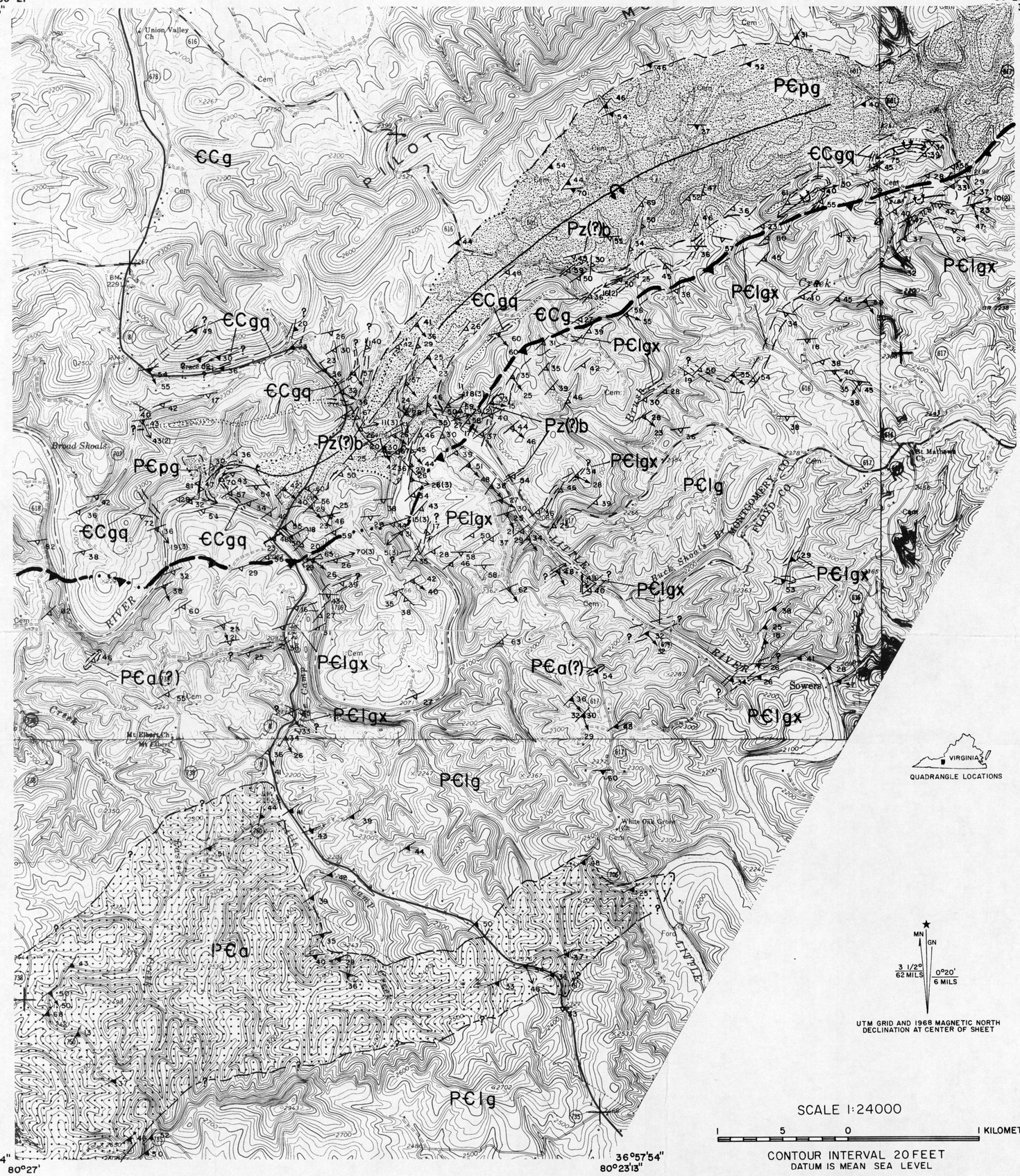

EXPLANATION

PALEOZOIC — CAMBRIAN

€Cg / €Cgq — Chilhowee Group metagraywackes, phyllites, and quartzites (€Cgq)

PRECAMBRIAN? AND/OR PALEOZOIC? — LATE PRECAMBRIAN TO MID PALEOZOIC

Pz(?)b — mafic dikes and sills

PRECAMBRIAN — LATE PRECAMBRIAN

P€a — Ashe Formation phyllites and biotite-muscovite schists

P€lg / P€lgx — Little River Gneiss medium to fine grained, biotite-rich, augen gneiss with lenses of a leucocratic gneiss (P€lgx)

GRENVILLE

P€pg — Pilot Gneiss medium grained, granitic gneiss; hornblende and hornblende-free phases undifferentiated

VIRGINIA

QUADRANGLE LOCATIONS

MN GN

3 1/2° 62 MILS — 0°20' 6 MILS

UTM GRID AND 1968 MAGNETIC NORTH DECLINATION AT CENTER OF SHEET

CONTACTS

- exposed
- approximate
- questionable
- covered
- Thrust fault

ATTITUDE OF ROCKS

- 65 / 62 — Strike and dip of foliation (S_1) and lineations (I_1)
- 50 / 45 — Strike and dip of foliation (S_2/S_m) and lineations (L_2/L_m)
- 25 — Strike and dip of foliations (S_3)
- 50(x) — Bearing and plunge of minor fold axis (fold generation x=2 or 3)
- Major fold axis, overturned anticline
- Major fold axis, overturned syncline

SCALE 1:24000

1 5 0 1 KILOMETER

CONTOUR INTERVAL 20 FEET
DATUM IS MEAN SEA LEVEL

Topographic Bases From U.S. Geological Survey; 1967, ALUM RIDGE Quadrangle, 1963, PILOT And RINER Quadrangles, All 7 1/2-Minute Series

36°57'54"
80°27'

36°57'54"
80°23'13"

GEOLOGIC MAP OF THE FRIES FAULT ZONE NEAR RINER, VIRGINIA

Geology by Patti Boyd Kaygi

1980